T.3.7 Structural Analysis (Accidents)

The design basis accident events specified by ANSI/ANS 57.9-1984, and other credible accidents postulated to affect the normal safe operation of the standardized NUHOMS® system are addressed in this section. Analyses are provided for a range of hypothetical accidents, including those with the potential to result in an annual dose greater than 25 mrem outside the owner controlled area in accordance with 10CFR72. The postulated accidents considered in the analysis and the associated NUHOMS® components affected by each accident condition are the same as those shown in Table 8.2-1, reproduced in this Appendix as Table T.3.7-1.

In the following sections, each accident condition is analyzed to demonstrate that the requirements of 10CFR72.122 are met and that adequate safety margins exist for the standardized NUHOMS® system design. The resulting accident condition stresses in the NUHOMS® system components are evaluated and compared with the applicable code limits set forth in Section 3.2 and chapter T.2, as applicable. Where appropriate, these accident condition stresses are combined with those of normal operating loads in accordance with the load combination definitions in Tables 3.2-5, 3.2-6, 3.2-7 and 3.2-8. Load combination results for the HSM, DSC, and transfer cask and the evaluation for fatigue effects are presented in Section T.3.7.12.

The evaluations in Chapter 8.2 for the HSM Models 80/102 and in their respective appendices for HSM Models 152 and 202 are not changed since the maximum heat load of a 61BTH allowed in an HSM is limited to 24 kW, the evaluated heat load for the DSCs allowed for storage in these HSM models. In addition the HSM Models 80/102/152/202 have been evaluated in the UFSAR for weights that bound the 61BTH DSC weights.

The TC evaluations in Section 8.2 do not change. The thickness and openings dimensions of the OS197FC-B TC top lid have not changed relative to those of the OS197FC. Thus, the top lid stress evaluation in Appendix P for the OS197FC remains applicable to the OS197FC-B. The results of the standardized TC presented in Section 8.2 do not change.

The postulated accident conditions addressed in this section include:

A. Tornado winds and tornado generated missiles. (T.3.7.1)

B. Design basis earthquake. (T.3.7.2)

C. Design basis flood. (T.3.7.3)

D. Accidental transfer cask drop with loss of neutron shield. (T.3.7.4)

E. Lightning effects. (T.3.7.6)

F. Debris blockage of HSM and HSM-H air inlet and outlet opening. (T.3.7.7)

G. Postulated DSC leakage. (T.3.7.8)

H. Pressurization due to fuel cladding failure within the DSC. (T.3.7.9)

I. Reduced HSM Air Inlet and Outlet Shielding (T.3.7.10), and

J. Fire and Explosion (T.3.7.11)

T.3.7.1 Tornado Winds/Tornado Missile

HSM

The applicable design parameters for the design basis tornado (DBT) are specified in Section 3.2.1 for Models 80/102 and in their respective appendices for Models 152/202. The determination of the tornado wind and tornado missile loads acting on the HSM are detailed in Section 3.2.1.2 for Models 80/102 and in their respective appendices for Models 152/202. The end modules of an array utilize shield walls to resist tornado wind and missile loads. For the conservative generic analysis, the tornado loads are assumed to act on a single free-standing HSM (with two end shield walls and a rear shield wall). This case conservatively envelopes the effects of wind on an HSM array.

For DBT wind and missile effects, the HSM is more stable when loaded with a heavier NUHOMS®-61BTH DSC since the overturning moment is not a function of the DSC weight while the resisting moment increases with the increased payload. The increased DSC weight does not have any effect on HSM sliding stability, since the weight terms on either side of the sliding equation presented in Section 8.2.2 cancel out. Thus, the analyses presented in Section 8.2.2 for DBT winds and missile effects remains bounding.

HSM-H

Results presented in Section P.3.7.1 are bounding.

T.3.7.2 Earthquake

HSM

Results for HSM Models 80/102 presented in Section M.3.7.3 are bounding. The seismic evaluations for HSM Models 152/202, as described in their respective appendices, are applicable for these HSM models when loaded with a 61BTH DSC.

HSM-H

Results presented in Section P.3.7.2 are bounding.

T.3.7.2.1 DSC Seismic Evaluation

For the DSC inside the HSM, the results presented in Section M.3.7.3 are bounding. For the DSC inside the HSM-H, the results presented in Section P.3.7.2.1 are bounding.

T.3.7.2.2 Basket Seismic Evaluation

The basket seismic analysis is performed using the models which were developed for normal and off-normal evaluations. A description of the seismic models, applied loads and associated results

is presented in Section T.3.6.1.3.4 B. The basket natural frequency is also calculated in Section T.3.6.1.3.4 D.

T.3.7.2.3 HSM and HSM-H Seismic Evaluation

The seismic results of 61BTH stored in an HSM are bounded by results presented in Section M.3.7.3.3 for HSM Models 80/102 and in their respective appendices for HSM Models 152/202. The seismic results of 61BTH stored in an HSM-H are bounded by results presented in Section P.3.7.2.3.

T.3.7.2.4 DSC Support Structure Seismic Evaluation

The seismic results of 61BTH DSC support structure inside the HSM are bounded by those presented in Section M.3.7.3.4 for HSM Models 80/102 and in their respective appendices for HSM Models 152/202. The seismic results of 61BTH DSC support structure inside the HSM-H are bounded by those presented in Section P.3.7.11.6.4.

T.3.7.2.5 DSC Axial Retainer Seismic Evaluation

The HSM axial retainer is qualified for a maximum DSC weight of 102 kips in Appendix M. The maximum DSC weight is 93 kips for the 61BTH, Type 2 DSC. Therefore, Appendix M, Section M.3.7.3.5 results for the HSM axial retainer are bounding.

The HSM-H axial retainer is qualified for a maximum DSC weight of 110 kips in Appendix P, whereas maximum DSC weight is 93 kips for the 61BTH, Type 2 DSC. Therefore, Appendix P, Section P.3.7.11.6.7 results for the HSM-H axial retainer are bounding.

T.3.7.2.6 TC Seismic Evaluation

The seismic evaluation for the OS197/OS197H in Chapter 8, Section 8.2.3.2(D), is based on very conservatively derived seismic accelerations of 1.31g horizontal and 0.84g vertical. These amplified accelerations were obtained by applying amplification factors of 3.5 and 3.3 for the horizontal and vertical directions, respectively, and, furthermore, applying a "multimode" factor of 1.5 to the base seismic criteria values of 0.25g and 0.17g for the horizontal and vertical directions, respectively.

The frequency analysis for a similar NUHOMS® TC documented in Reference [3.38] showed that the TC can be considered a rigid component (the first mode frequency of the TC in [3.38] is on the order of 69 Hz. This frequency content is well in the rigid range relative to the frequency content of the seismic input motion (33 Hz). Therefore, no significant response amplification is expected due to seismic load for the OS197 type cask, and, thus, the maximum accelerations used in the seismic evaluation of the OS197/OS197H as discussed above are deemed to be more than adequate to meet the increased seismic criteria of 0.3g horizontal and 0.20g vertical. Consequently, the seismic stress evaluations and results as described in the UFSAR are applicable and no further evaluation is required.

The seismic stability evaluation described in Section 8.2.3.2(D) for the TC mounted horizontally in the transfer trailer and subjected to the 0.25g and 0.17g seismic accelerations shows a factor of

safety of 2.0 against overturning. For the increased accelerations, the factor of safety is approximately 1.7. Thus, there is sufficient margin to accommodate the increased seismic accelerations.

T.3.7.3 Flood

Since the source of flooding is site specific, the source, or quantity of flood water should be established by the licensee. As described in Section 3.3.2, the design basis flooding load is specified as a 50 foot static load of water and a maximum flow velocity of 15 feet per second. Each licensee should confirm that this represents a bounding design for their specific ISFSI site.

T.3.7.3.1 HSM and HSM-H Flooding Analysis

The evaluation in Section M.3.7 is bounding for the 61BTH in the HSM for HSM Models 80/102. Similarly, the evaluations for HSM Models 152/202 as contained in their respective appendices in the UFSAR. The evaluation in P.3.7.3.1 is bounding for the 61BTH in the HSM-H.

T.3.7.3.2 DSC Flooding Analyses

The DSC is evaluated for the design basis fifty foot hydrostatic head of water producing external pressure on the DSC shell and outer cover plates. To conservatively determine design margin which exists for this condition, the maximum allowable external pressure on the DSC shell is calculated for Service Level A stresses using the methodology presented in NB-3133.3 of the ASME Code [3.1] for both DSC types. The resulting limiting allowable pressure of 34.0 psi (at a conservatively evaluated temperature of 700°F) is 1.57 times the maximum external pressure of 21.7 psi due to the postulated fifty foot flood height. Therefore, buckling of the DSC shell will not occur under the worst case external pressure due to flooding.

The DSC Type 1 and Type 2 shell stresses for the postulated flood condition are determined using ANSYS analytical models similar to those shown in Figure 8.1-14a and Figure 8.1-14b. The 21.7 psig external pressure is applied to each model as a uniform pressure on the outer surfaces of the top cover plate, DSC shell and bottom cover plate. The maximum DSC shell primary membrane stress intensity for the 21.7 psi external pressure is 1.67 ksi which is considerably less than the Service Level C allowable primary membrane stress of 21.7 ksi (at 450°F). The maximum membrane plus bending stress in the flat heads of the DSCs occurs in the inner top cover plate (Type 1 DSC). The maximum membrane plus bending stress in the inner top cover plate is 0.63 ksi. This value is considerably less than the ASME Service Level C allowable of 32.6 ksi (at 450°F) for primary membrane plus bending stress. These stresses are combined with the appropriate loads to formulate load combinations. The resulting total stresses for the DSCs are bounded by those reported in Section T.3.7.12.1.

T.3.7.4 Accidental Cask Drop

This section addresses the structural integrity of the standardized NUHOMS® on-site transfer cask, the DSC and its internal basket assembly when subjected to postulated cask drop accident conditions.

Cask drop evaluations include the following:

- DSC Shell Assembly (T.3.7.4.2),
- Basket Assembly (T.3.7.4.3),
- On-Site TC (T.3.7.4.5), and
- Loss of the TC Neutron Shield (T.3.7.5).

The DSC shell assembly, transfer cask, and loss of neutron shield evaluations are based on the approaches and results presented in Section 8.2. The basket assembly cask drop evaluation is presented in more detail since the basket assembly is a new design and uses slightly different analytical approaches for qualification.

A short discussion of the effect of the NUHOMS®-61BTH DSC on the transfer operation, accident scenario and load definition is presented in Section T.3.7.4.1.

T.3.7.4.1 General Discussion

Cask Handling and Transfer Operation

Various transfer cask drop scenarios have been evaluated in Section 8.2.5. The NUHOMS®-61BTH DSC is heavier than the NUHOMS®-52B DSC. Therefore, the expected g loads for the postulated drop accidents would be lower. However, for conservatism, the g loads used for the NUHOMS®-52B analyses are also used for the NUHOMS®-61BTH DSC analyses. See Section 8.2.5.

Cask Drop Accident Scenarios

In spite of the incredible nature of any scenario that could lead to a drop accident for the transfer cask, a conservative range of drop scenarios are developed and evaluated. These bounding scenarios assure that the integrity of the DSC and spent fuel cladding is not compromised. Analyses of these scenarios demonstrate that the transfer cask will maintain the structural integrity of the DSC confinement boundary. Therefore, there is no potential for a release of radioactive materials to the environment due to a cask drop. The range of drop scenarios conservatively selected for design are:

1. A horizontal side drop or slap down from a height of 80 inches.
2. A vertical end drop from a height of 80 inches onto the top or bottom of the transfer cask (two cases). Note that vertical end drop is not a credible event but only considered to show that corner drop is enveloped by the side drop and end drop.
3. An oblique corner drop from a height of 80 inches at an angle of 30° to the horizontal, onto the top or bottom corner of the transfer cask. This case is not specifically evaluated. The side drop and end drop cases envelope the corner drop.

Cask Drop Accident Load Definitions

Same as Section 8.2.5.1(D).

Cask Drop Surface Conditions

Same as Section 8.2.5.1(D).

T.3.7.4.2 DSC Shell Assembly Drop Evaluation

The shell assembly consists of the DSC shell, the shield plugs, and the top and bottom inner and outer cover plates. The shell assembly drop evaluation is presented in three parts:

1. DSC shell assembly horizontal drop analysis,

2. DSC shell assembly vertical drop analysis, and

3. DSC shell stability analysis.

T.3.7.4.2.1 DSC Shell Assembly Horizontal Drop Analysis

The DSC shell assembly is analyzed for the postulated horizontal side drop using the ANSYS 3-D models of the DSC shell assembly discussed in Section 3.6.1.2. Half-symmetry (180°) models of the top end and bottom end sections of the DSC shell assembly are developed based on the models developed for the end drops shown in Figure 8.1-14a and Figure 8.1-14b. Each model includes one-half of the height of the cylindrical shell. Each of the DSC shell assembly components is modeled using ANSYS solid 3-D elements. The full weight of the DSC is conservatively assumed to drop directly onto a single rail. Elastic-plastic analyses are performed and stresses are determined for each DSC shell assembly component. The NUHOMS®-61BTH DSC shell stresses in the region of the basket assembly are also analyzed for the postulated horizontal side drop conditions. This analysis and results are presented in Section T.3.7.4.2.3.

T.3.7.4.2.2 DSC Shell Assembly Vertical Drop Analysis

For this drop accident case, the transfer cask is assumed to be oriented vertically and dropped onto a uniform unyielding surface. The vertical cask drop evaluation conservatively assumes that the transfer cask could be dropped onto either the top or bottom surfaces. No credit is taken for the energy absorbing capacity of the cask top or bottom cover plate assemblies during the drop. Therefore, the DSC is analyzed as though it is dropped on to an unyielding surface. The principal components of the DSC and internals affected by the vertical drop are the DSC shell, the inner and outer top cover plates, the shield plugs, and the inner and outer bottom cover plates.

The end drop with the bottom end of the DSC oriented downward is the more credible of the two possible vertical orientations. Nevertheless, an analysis for the DSC top end drop accident is also performed. For a postulated vertical drop, membrane stresses in the DSC shell and local stresses at the cover plate weld region discontinuities are evaluated.

T.3.7.4.2.3 DSC Shell Assembly Stress Analysis

The ANSYS analytical models of the DSC shell assembly as described in Section T.3.6.1.2 and shown in Figure 8.1-14a and Figure 8.1-14b are used to determine the vertical end drop accident stresses in the DSC shell, the inner cover plates, the outer cover plates, and the shield plugs. The models consist of 90° quarter symmetry models and include one-half of the height of the cylindrical shell. To capture the maximum stress state in the DSC assembly components, each model was analyzed for end drop loading on the opposite end (i.e., the bottom end model was analyzed for top end drop, and the top end model was analyzed for bottom end drop). In these drop orientations, the end plates are supported at the perimeter by the shell. For the top and bottom end drops, the nodal locations on the impacted end are restrained in the vertical direction. An equivalent static linear elastic analysis is conservatively used for the vertical end drop analyses. Inertia loadings based on forces associated with the 75g deceleration are statically applied to the models. Analyses show that the stresses in the DSC cover plates and shield plugs are low. These low stresses occur since for the bottom end drop, the inner and outer top cover plates are supported by the top shield plug. During a top end drop, the outer top cover plate is assumed to be supported by the unyielding impacted surface and is subjected to a uniform bearing load imposed by the DSC internals. The same is true for the DSC bottom outer cover plate and shield plug for the bottom end drop. The highest stresses occur in the DSC shell and bottom inner cover plate. The maximum stresses in the bottom inner cover plate result from the top end vertical drop condition, in which the bottom inner cover plate is supported only at the edges. The maximum DSC shell membrane stresses, which occur near the top end of the DSC shell area, result from the accelerated weight of the DSC shell and the bottom end (for top end drop case) or top end (for the bottom end drop case) assemblies.

A summary of the calculated stresses for the main components of the DSC and associated welds is provided in Table T.3.7-2 and Table T.3.7-3.

T.3.7.4.2.4 DSC Shell Stability Analysis

The stability of the DSC shell for a postulated vertical drop impact is also evaluated. For Level D conditions, the allowable axial stress in the DSC shell is based on Appendix F of the ASME Code. The maximum axial stress in the DSC shell obtained from the 65g end drop analyses is 10.31 ksi for the Type 1 DSC. The allowable axial stress is 12.0 ksi. The maximum axial stress in the DSC shell obtained from the 65g end drop analyses is 9.85 ksi for the Type 2 DSC. The allowable axial stress is 11.3 ksi. Therefore, buckling of the DSC shell for a 65g vertical deceleration load does not occur.

T.3.7.4.3 Basket Assembly Drop Evaluation

As discussed in previous chapters, the primary structural components of the basket assembly include:

- Holddown ring/top grid,
- Fuel compartments,

- Outer wrappers,
- Basket rails,
- Basket rail to fuel compartment rail studs, and
- Poison plate support insert welds.

The DSC resides in the transfer cask for all drop conditions. The DSC is supported horizontally in the transfer cask by two cask rails that are integral to the cask wall. The effect of these cask rails are included in the horizontal drop evaluations.

The evaluation is presented in three parts:

1. Basket assembly horizontal drop analysis which includes a stress evaluation of the basket, basket rails, and basket rail studs.
2. Basket assembly vertical drop analysis which includes a stress evaluation of the basket (fuel compartment tubes and outer wrappers), basket rail, insert welds, and the holddown ring/top grid assembly. Holddown ring/top grid assembly stability is also demonstrated for the vertical loading condition.
3. Basket assembly stability which includes a buckling evaluation of the basket using the finite element models developed for the horizontal drop stress analysis of the basket and basket rails.

T.3.7.4.3.1 Basket Assembly Horizontal Drop Analysis

T.3.7.4.3.1.1 Basket and Basket Rail Stress Analysis

The basket and DSC are analyzed for two modes of side drops using the ANSYS finite element model described in Section T.3.6.1.3.1. First, the cask is assumed to drop away from the transfer cask support rails. Under this condition, 45, 60 and 90 degree orientation side drops are assumed to bound the possible maximum stress cases. Second, the side drop occurs on the transfer cask support rails at 161.5 and 180 degree orientations. The lateral load orientation angles are defined in Figure T.3.6-7. The load resulting from the fuel assembly weight was applied as pressure on the plates. At 90 and 180 degree orientations, the pressure acted only on the horizontal plates while at other orientations, it was divided in components to act on horizontal and vertical plates. The pressures for different orientations are summarized in the Table T.3.7-4 for 1g acceleration.

The inertia load due to basket, rails and DSC dead weight is simulated using the density and appropriate acceleration. The poison plate weight is included by increasing the basket plate density.

The pressure distribution for 90, 180 , 45, 60 and 161.5 degree analyses are shown on Figure T.3.7-1 to Figure T.3.7-4.

Analysis and Results

A nonlinear stress analysis of the structural basket is conducted for computing the stresses for the 45, 60, 90, 161.5 and 180 degree drop orientations. A maximum load of 100g was applied in each analysis. The automatic time stepping program option "Autots" was activated. This option lets the program decide the actual size of the load-substep for a converged solution. Displacements, stresses and forces for each converged substep load were written on ANSYS result files. The program stops at the load substep when it fails to result in a converged solution. In all side drop cases the program gave converged solutions up to 100g load. Results were extracted at the load sub-step nearest to the maximum drop load of 75g. Maximum nodal stress intensities in the Type 1 basket, rails and DSC are shown on Figure T.3.7-5 to Figure T.3.7-34 and summarized in Table T.3.7-5 for Type 1 DSC. Maximum nodal stress intensities in the Type 2 basket rails and DSC are shown in Figure T.3.7-35 to Figure T.3.7-64 and summarized in Table T.3.7-6 for Type 2 DSC.

T.3.7.4.3.1.2 Basket Rail Stud Stress Analysis

It was observed from the side drop basket stress summary table that the maximum membrane stresses in the rail and basket occurred during 90-degree drop orientation. In other side drop orientations, membrane stresses were somewhat lower. Accordingly, the maximum shear stress in the rail stud are expected to occur due to the a 90 degree drop orientation. This seems reasonable since during this basket orientation, the fuel weight sits squarely on the largest number of basket panels. The rail stud stresses are therefore computed for a 90-degree side drop orientation. These stresses bound the stud stresses for other basket drop orientations.

The load resulting from the fuel assembly weight was applied as pressure on the basket panels. At the 90° orientation, the pressure acted only on the horizontal plates.

Finite Element Model Description

A three-dimensional finite element model of the basket, rails and DSC were constructed with the following modifications using the finite element model described in Section T.3.6.1.3.

- The couplings at the rail stud locations were replaced with ANSYS Pipe Elements.
- Shear stresses were considered critical in the rail stud weld (O.D. = 0.5" and I.D. = 0.3"). Therefore, the pipe real constant (equivalent thickness) was calculated based on the weld area. The solid stud area is greater than the weld area. Stresses will be lower in the solid area of the stud.
- All material properties, real constants and couplings of the remainder of the model are the same as used for the previous 90° side drop analysis.

The calculated maximum rail stud shear stress for the 90° side drop orientation (75g) is 17.43 ksi. Maximum rail stresses are included in the summary of stresses in Table T.3.7-5 for Type 1 DSC and Table T.3.7-6 for Type 2 DSC.

T.3.7.4.3.2 Basket Assembly Vertical Drop Analysis

During an end drop, the fuel assemblies and fuel compartments are forced against the bottom of the DSC/cask. It is important to note that, for any vertical or near vertical loading, the fuel assemblies react directly against the bottom or top end of the DSC/cask and not through the basket structure as in lateral loading. It is the dead weight of the basket only that causes axial compressive stress during an end drop. Axial compressive stresses are conservatively computed assuming all the weight will be taken by the compartment tubes and wrappers only. A conservative basket weight of 23.5 kips is used in end drop stress calculations for Type 1 Basket and 28 kips for Type 2 Basket.

T.3.7.4.3.2.1 Component Stress Analysis

Compressive Stress at Fuel Compartment Tubes and Outer Wrappers

Type 1:
Total weight = 23.5 kips (includes top grid)

Weight excluding top grid, poison plates, aluminum plates, and rails,
23.5 – 1.55 – 3.17 – 0.88 – 3.68 – 1.98 = 12.24 kips

Section area = 12,240 /(164 x 0.284) = 262.80 in^2
Stress due to 1g = -23.5 / 262.80 = - 0.089 ksi
At 60g = - 0.089 ksi × 60 = - 5.34 ksi

Type 2:
Total weight = 28.0 kips

Weight excluding top grid, poison plates, aluminum plates, and rails,
28.0 – 1.55 – 3.17 – 6.29 – 3.68 – 0.92 =12.39 kips

Section area = 12,390 /(164 x 0.284) = 266.02 in^2
Stress due to 1g = -28.0 / 266.02 = - 0.105 ksi
At 60g = - 0.105 ksi × 60 = - 6.30 ksi

Shear Stress in Insert Plate Weld

The insert plates maintain the position of the poison during an end drop. The weight per insert plate weld is calculated by taking the total poison weight divided by 64 (the number of insert plates that support the total poison plate weight of 3.17 kips).

Load/insert = 3.17 / 64 = 0.050 kips
Weld Shear Area = 0.707 x 3 x 0.125 = 0.2651 in^2
Shear stress (1g) = 0.050 / 0.2651 = 0.19 ksi
At 60g = 0.19 ksi × 60 = 11.40 ksi

Shear Stress in Rail Stud

During the 60g end drop, the basket support rail will support its own weight. However, the evaluation below conservatively assumes that the weight of the stainless steel portion of the rail will be supported by the rail studs attached to compartment outer boxes. The aluminum portions of the rails are slotted to allow for thermal expansion and will not load the rail studs.

Type 1-R45 (168 studs):
Weight of SST portion of rails = 3.68 kips
Weld Shear Area = $\pi/4\ (0.5^2 - 0.3^2) = 0.126\ in^2$

Shear stress (1g) = 3.68 / (0.126 × 168) = 0.17 ksi
At 60g = 0.17 ksi × 60 = 10.2 ksi

Type 1-R90 (56 studs):
Weight of SST portion of rails = 1.98 kips
Weld Shear Area = $\pi/4\ (0.5^2 - 0.3^2) = 0.126\ in^2$
Shear stress (1g) = 1.98 / (0.126 × 56) = 0.28 ksi
At 60g = 0.28 ksi × 60 = 16.8 ksi

Type 2-R45 (168 studs):
Weight of SST portion of rails = 3.68 kips
Weld Shear Area = $\pi/4\ (0.5^2 - 0.3^2) = 0.126\ in^2$
Shear stress (1g) = 3.68 / (0.126 × 168) = 0.17 ksi
At 60g = 0.17 ksi × 60 = 10.4 ksi

Type 2-R90 (56 studs):
Weight of SST portion of rails = 0.92 kips
Weld Shear Area = $\pi/4\ (0.5^2 - 0.3^2) = 0.126\ in^2$
Shear stress (1g) = 0.92 / (0.126 × 56) = 0.13 ksi
At 60g = 0.13 ksi × 60 = 7.8 ksi

Compressive Stress On Holddown Ring / Top Grid

Type 1: (holddown ring is bounding)
Weight of holddown ring = 0.940 kips
Section area = 940/(14.5 x 0.284) = 228.3 in^2
Stress due to 1g = -24.0 / 228.3 = - 0.105 ksi
At 60g = - 0.105 ksi × 60 = -6.3 ksi

Type 2:
Weight of top grid = 1.341 kips (excluding gusset plates, wt. = 1546 – 205)
Section area = 1,341/(14.5 x 0.284) = 325.64 in^2
Stress due to 1g = -28.0 / 325.64 = - 0.086 ksi
At 60g = - 0.086 ksi × 60 = -5.2 ksi

Results of Basket End Drop Analysis

Table T.3.7-7 and Table T.3.7-8 summarize the Type 1 and Type 2 basket structural analysis results due to the 60g vertical end drop accident condition.

T.3.7.4.3.2.2 Holddown Rings/Top Grid Buckling Analysis

The buckling of the holddown ring 6.20" x 6.20" box and 12.96" x 12.96" box and the top grid 6.33" x 6.33" box (minimum) are evaluated below for 6.3 ksi axial compressive stress.

6.20" x 6.20" Box (Type 1 Basket Holddown Ring)

As given in ASME Code, Subsection NF, Paragraph NF-3322-1(c)(2)(a)(Level A Condition) and modified as per Appendix F, Paragraph F-1334 (Level D Condition), the compressive stress limit for the accident condition (Level D) when KL/r is less than 120 and $S_u > 1.2\ S_y$ is:
$F_a = 2 \times S_y\ [0.47 - (KL/r)/444]$

Where:

K = 2.1 as recommended by AISC (9th Edition [3.18], Table C-C2.1). The box is conservatively assumed free at one end and fixed on the other end.
Plate thickness, h = 0.375 in.
Box outer width = 6.20 + 2 x 0.375 = 6.95"
S_y = 18,400 psi (at 600°F)
$I = (1/12)[\ 6.95^4 - 6.20^4] = 71.29$ in.^{4}
$A = 6.95^2 - 6.20^2 = 9.86$ in.^{2}
$r = (I/A)^{1/2} = 2.69$ in.
$KL/r = 2.1 \times 14.5 / 2.69 = 11.32$

Substituting the values given above,

$F_a = 2 \times 18{,}400\ [0.47 - (11.32)/444] = 16{,}358$ psi $\approx$ 16.36 ksi

The allowable buckling stress (16.36 ksi) is higher than the actual compressive stress (6.3 ksi), therefore, buckling will not occur.

12.96" x 12.96" Box (Type 1 Basket Holddown Ring)

Box outer width = 12.96 + 2 x 0.375 = 13.71 in.
$I = (1/12)[13.71^4 - 12.96^4] = 593.28$ in.^{4}
$A = 13.71^2 - 12.96^2 = 20.0$ in.^{2}
$r = (I/A)^{1/2} = 5.446$ in.
$KL/r = 2.1 \times 14.5 / 5.446 = 5.591$

$F_a = 2 \times 18{,}400\ [0.47 - (5.591)/444] = 16{,}832$ psi $\approx$ 16.83 ksi

The allowable buckling stress (16.83 ksi) is higher than the actual compressive stress (6.3 ksi), therefore, buckling will not occur.

6.33" x 6.33" Box (Type 1 and Type 2 Top Grid, 14.5" long option is bounding)

Plate thickness, h = 0.25 in.
Box outer width = 6.33 + 2 x 0.25 = 6.83"
S_y = 18,400 psi (at 600°F)
$I = (1/12)[6.83^4 - 6.33^4] = 47.55$ in.^{4}
$A = 6.83^2 - 6.33^2 = 6.58$ in.^{2}
$r = (I/A)^{1/2} = 2.69$ in.
$KL/r = 2.1 \times 14.5 / 2.69 = 11.32$

Substituting the values given above,

$F_a = 2 \times 18{,}400\ [0.47 - (11.32)/444] = 16{,}358$ psi $\approx$ 16.36 ksi

The allowable buckling stress (16.36 ksi) is higher than the actual compressive stress (6.3 ksi), therefore, buckling will not occur.

T.3.7.4.3.3 Basket Assembly Stability Analysis

Basket assembly stability which includes a buckling evaluation of the wall between the fuel compartments and support rails is determined in this section.

The three drop orientations analyzed for the basket and basket rails for buckling evaluation are:

- 0° (load applied in the direction parallel to the basket plates)
- 30° (load applied at 30° relative to the basket plate direction)
- 45° (load applied at 45° relative to the basket plate direction)

In order to calculate the buckling load, the finite element model is constructed using SHELL43 plastic large strain shell elements. A maximum load of 100g was applied in each analysis. The automatic time stepping option AUTOTS was activated. This option lets the program decide the actual size of the load sub-step for a converged solution. The program stops at the load sub-step that fails to result in a converged solution. The g-load for the last load step with a converged solution is considered to be the buckling load. The safety factor against buckling is calculated as the acceleration at the buckling load divided by 75g.

Finite Element Model Description

A three-dimensional finite element model of the Type 1 and Type 2 basket, rails and canister is constructed using SHELL 43 elements. The overall finite element models of the Type 1 and Type 2 basket, rails and canister are shown in Figure T.3.7-66 through Figure T.3.7-71. For conservatism, the strength of aluminum poison plates was neglected by excluding these from the finite element model. However, their weight was accounted for by increasing the density of the stainless steel basket plates. In addition, no credit is taken for the aluminum at the R45 rails, but the density of the associated stainless steel rails is increased to account for the additional aluminum weight. Because of the large number of plates in the basket and large size of the basket, certain modeling approximations were necessary. In view of continuous support of the basket plates by rails along the entire length during a side drop, only a 3" long slice of the basket,

rails and canister was modeled. At the two cut faces of the model, symmetry boundary conditions were applied (UZ = ROTX = ROTY= 0).

The gap elements (CONTACT 52) are used to simulate the interface between the basket rails and the inner side of the canister as well as between the outer side of the canister and the inside of the cask. Each gap element contains two nodes; one on each surface of the structure. The gap nodes specified at the inner side of the cask are restrained in the x, y and z directions. The gap size at each gap element is determined by the difference between the basket rails radius and the inside radius of the cask inner shell; and by the difference between the outer side of the canister radius and the inside radius of the cask. The gap sizes between rails and canister; and canister and cask (over 5° interval up to 90° and 10° interval beyond) are shown in Figure T.3.6-8 and Figure T.3.6-9. The finite element model of the canister and gaps is shown in Figure T.3.7-72 and Figure T.3.7-73.

The connections between stainless steel fuel compartment square tubes (with intermediate aluminum poison plates), between the tubes and outer stainless steel boxes, and between outer boxes and stainless steel rails are made with node couplings. The nodes of various plates are coupled together in the out-of-plane directions so that they will bend in unison under surface pressure or other lateral loading and to simulate through-the-thickness support provided by the poison plates. The bolt connections between the rail members and outer boxes are also simulated by node couplings. During each side drop orientation, some fuel boxes and rails may have a tendency to separate or slide. Gap elements were used to model the connections at such locations. During 0 degree side drops, the basket is symmetric about the drop axis. Thus, only one-half of the entire model is used in these analyses.

To consider the case of fuel assemblies with channel plates, Zircaloy channel plates (0.08" thick) were added at tube walls loaded by the equivalent fuel load pressure (based on 705 lbs per assembly). The fuel assembly channel plates are modeled only at the most highly loaded tube walls near the perimeter of the basket, and are shown in Figure T.3.7-74.

Material Nonlinearities

The modeled components of the basket, canisters and fuel assembly channels are based on lower bound material properties. A bilinear stress-strain curve with a 5% tangent modulus is used for the Type 304 stainless steel. A bilinear stress-strain curve with a 1% tangent modulus is used for the aluminum R90 basket rails (Type 2 only). A bilinear stress-strain curve with a 1% tangent modulus is used for the Zircaloy fuel assembly channel plates for load cases where the Zircaloy did not remain elastic. Conservatively, credit is taken for an increase in effective yield strength due to strain rate effects (conservative).

The basket, rails, canister and fuel channel material properties are dependent on temperature. A bounding temperature profile is used that envelops the 100°F ambient temperature profile for both the Type 1 and Type 2 transfer conditions. The use of a higher temperature for material properties gives lower E and S_y values and therefore, gives a conservative, lower buckling capacity. The material properties used in the analysis are provided in Table T.3.7-9.

Gap Element Nonlinearities

Gap elements (Contact 52) are used to model the actual surface clearance between the basket rails and canister inside surface as well as between the canister outside surface and the cask inside surface. The gap elements introduce nonlinearities in the analysis depending on whether they are open or closed.

Loadings

Due to symmetry, the basket drop orientations of 0, 30, and 45 degrees are assumed to bound the possible drop orientations. The lateral load orientation angles are defined in Figure T.3.7-65. The load resulting from the fuel assembly weight was applied as pressure on the plates. At the 0 degree orientation, the pressure acted only on the horizontal plates. While at other orientations, it was divided into components to act on horizontal and vertical plates.

The applied pressures due to the 705 lb fuel assemblies (with channels) for different orientations are calculated below for a 1g acceleration:

- At 0 degrees; Pressure, p = Fuel assembly wt. / (Panel span x Panel length)
  = 705 lb / (6.22" x 164") = 0.6911 psi
- At 30 degrees; p_v on horizontal plates = p Cos 30° = 0.6911 x 0.866 = 0.5985 psi
  P_h on vertical plates = p Sin 30° = 0.6911 x 0.5 = 0.3456 psi
- At 45 degrees; p_v on horizontal plates = p Sin 45° = 0.6911 x 0.7071 = 0.4887 psi
  P_h on vertical plates = p Cos 45° = 0.6911 x 0.7071 = 0.4887 psi

The applied pressures due to the 640 lb fuel assemblies (without channels) are applied by scaling the above values by the factor 640 lb / 705 lb = 0.908.

The ANSYS 1g accelerations, indicating direction of load, are:

- 0 - degree acel, 0, 1, 0
- 30-degree acel, -0.5, 0.866, 0
- 45-degree acel, -0.707, 0.707, 0

For 100g loading, the ANSYS acceleration values are 100 times the above values.

The load distribution conditions for the 0, 30, and 45 degree analyses are shown in Figure T.3.7-78 through Figure T.3.7-80. The node coupling at different orientations are shown in Figure T.3.7-75 through Figure T.3.7-77. A summary of pressure loads used for different drop orientations is provided in Table T.3.7-10.

A nonlinear analysis of the structural basket is conducted for computing the buckling load for the 0, 30, and 45 degree drop orientations. A maximum load of 100g was applied in each analysis. The automatic time stepping program option "AUTOTS" was activated. This option lets the program decide the actual size of the load-substep for a converged solution. Results for each converged substep load were written to ANSYS result files. The program stops at the load

substep which fails to result in a converged solution. In all cases, the program gave converged solutions greater than the 75g load.

T.3.7.4.3.4 Results of Basket Buckling Analysis

The results of the analysis indicate the allowable collapse g loads for the NUHOMS®-61BTH basket are higher than the applied 75g side drop impact load.

A summary of the buckling analysis results for Type 1 and Type 2 baskets is presented in Table T.3.7-11. Figure T.3.7-81 to Figure T.3.7-83 show the deformed shape of the Type 1 basket for the last converged time step. Figure T.3.7-84 to Figure T.3.7-86 show the deformed shape of the Type 2 basket for the last converged time step. In each case, the last converged time step determines the buckling load.

T.3.7.4.4 Confirmatory Analysis of 61BTH Basket Using LS DYNA

The 61BTH basket model described in Section T.3.7.4.3.3 was used to perform a confirmatory stability analysis using LS-DYNA. The LS-DYNA model is shown in Figure T.3.7-87. A dynamic time history analysis is performed for the accident side drop condition. The input history is taken from the response time history of the OS187H transfer cask accident drop analysis documented in Reference [3.38]. The maximum acceleration obtained from the TC accident drop analyses in [3.38] is 67g. The input time history (scaled to 1g amplitude) is shown in Figure T.3.7-88. This response time history is considered representative of an accident drop response time history and adequate for this confirmatory analysis. However, for these analyses, the amplitude of the time history is scaled to 75g, 85g and 95g in order to examine the buckling capacity of the 61BTH basket assembly. The time scale is unchanged.

A non-linear elastic-plastic analysis is performed. Both material and geometric non-linearities are considered. Surface-to-surface contacts definitions are used to model the contact between the components of the basket and DSC shell and between the DSC shell and the transfer cask inner shell and support rails. A bounding temperature profile was used to define material properties (S_y and E). For purposes of this confirmatory analysis a 45° drop orientation is analyzed.

The LS-DYNA confirmatory analysis show that the basket has significant margin against buckling collapse relative to the 75g postulated accident side drop acceleration. Although the basket experiences some localized plastic deformation it does not collapse for the maximum amplitude of the scaled time history (95g) used in this confirmatory analysis. Figure T.3.7-89, Figure T.3.7-90 and Figure T.3.7-91 show the results of the confirmatory analysis for load amplitudes scaled to 75g, 85g and 95g, respectively.

T.3.7.4.5 On-site TC Horizontal and Vertical Drop Evaluation

An analysis has been performed (Section 8.2.5.2) to evaluate the transfer cask when loaded with the NUHOMS®-52B DSC for postulated horizontal and vertical drop accidents with a static equivalent deceleration of 75g's.

The weight of the NUHOMS®-61BTH Type 2 DSC is 93,120 lbs compared to the 80,000 lbs used for the NUHOMS®-52B DSC. The minimum margin of safety for the NUHOMS®-52B DSC analysis for this accident has been scaled by a factor of [80,000/93,120 = 0.859] to establish the minimum factor of safety applicable to the NUHOMS®-61BTH DSC. See Section T.3.7.12.3.

T.3.7.5 Loss of Neutron Shield

No change.

T.3.7.6 Lightning

No change.

T.3.7.7 Blockage of Air Inlet and Outlet Openings

This accident conservatively postulates the complete blockage of the HSM-H ventilation air inlet and outlet openings on the HSM-H side walls.

Since the NUHOMS® HSM-Hs are located outdoors, there is a remote probability that the ventilation air inlet and outlet openings could become blocked by debris from such unlikely events as floods and tornadoes. The NUHOMS® design features such as the perimeter security fence and the redundant protected location of the air inlet and outlet openings reduces the probability of occurrence of such an accident. Nevertheless, for this conservative generic analysis, such an accident is postulated to occur and is analyzed.

The structural consequences due to the weight of the debris blocking the air inlet and outlet openings are negligible and are bounded by the HSM-H loads induced for a postulated tornado (Section 8.2.2) or earthquake (Section 8.2.3).

The thermal effects for this accident for NUHOMS®-61BTH DSC are described in Section T.4 and T.11. The blocked vent accident condition stress evaluation is described in Section T.3.7.12.5.

T.3.7.8 DSC Leakage

The 61BTH DSC is leak tested to meet the leaktight criteria ($1x10^{-7}$ std. cm^3/sec) of ANSI N14.5 [3.37]. The analysis of the 61BTH demonstrate that the pressure boundary is not breached since its meets the applicable stress limits for normal, off-normal and postulated accident conditions.

T.3.7.9 Accident Pressurization of DSC

The NUHOMS® 61BTH is evaluated and designed for DSC internal pressure which bounds the maximum accident pressure calculated in Chapter T.4. The pressure boundary stresses due to this pressure load are bounded by the results presented in Table T.3.7-16 and Table T.3.7-17. Therefore, the 61BTH DSC is acceptable for this postulated accident condition.

T.3.7.10 Reduced HSM Air Inlet and outlet Shielding

This accident condition is addressed in Section T.11.2.1.

T.3.7.11 Fire and Explosion

This accident condition is addressed in Section T.11.2.10.

T.3.7.12 Load Combinations

The load categories associated with normal operating conditions, off-normal conditions and postulated accident conditions are described and analyzed in previous sections. The load combination results for the NUHOMS® components important to safety are presented in this section. Fatigue effects on the transfer cask and the DSC are also addressed in this section.

T.3.7.12.1 DSC Load Combination Evaluation

As described in Section 3.2, the stress intensities in the DSC at various critical locations for the appropriate normal operating condition loads are combined with the stress intensities experienced by the DSC during postulated accident conditions. It is assumed that only one postulated accident event occurs at any one time. The DSC load combinations summarized in Table 3.2-6 are expanded in Table T.2.-11. Since the postulated cask drop accidents are by far the most critical, the load combinations for these events envelope all other accident event combinations. Table T.3.7-12 through Table T.3.7-18 tabulate the maximum stress intensity for each component of the DSC (shell and basket assemblies) calculated for the enveloping normal operating, off-normal, and accident load combinations. For comparison, the appropriate ASME Code allowables are also presented in these tables.

T.3.7.12.2 DSC Fatigue Evaluation

Although the normal and off-normal internal pressures for the NUHOMS®-61BTH DSC are slightly higher relative to the NUHOMS®-52B DSC, the range of pressure fluctuations due to seasonal temperature changes are essentially the same as those evaluated for the NUHOMS®-52B DSC. Similarly, the normal and off-normal temperature fluctuations for the NUHOMS®-61BTH DSC due to seasonal fluctuations are essentially the same as those calculated for the NUHOMS®-52B DSC. Therefore, the fatigue evaluation presented in Section 8.2.10.2 remains applicable to the NUHOMS®-61BTH DSC.

T.3.7.12.3 TC Load Combination Evaluation

As described in Section 3.2, the transfer cask calculated stresses due to normal operating loads are combined with the appropriate calculated stresses from postulated accident conditions at critical stress locations. It is assumed that only one postulated accident can occur at a time. Also, since the postulated drop accidents produce the highest calculated stresses, the load combination of dead load plus drop accident envelopes the stresses induced by other postulated accident scenarios. The limiting (minimum) factor of safety for membrane plus bending stress intensity in the Cask Bottom Support Ring under the dead weight plus thermal plus earthquake

load combination has been updated to reflect the increased deadweight of 93,120 lbs for the NUHOMS®-61BTH DSC. This updated limiting factor of safety is conservatively established as 1.22. Hence, the resulting stresses for the OS197 TC when handling the NUHOMS®-61BTH DSC remain well below the code allowables

T.3.7.12.4 TC Fatigue Evaluation

No change.

T.3.7.12.5 HSM-H Load Combination Evaluation

The HSM-H evaluations in P.3.7.11.5 are bounding. The evaluated loads for the HSM-H bound those associated with the 61BTH DSC.

T.3.7.12.6 Thermal Cycling of the HSM

No change.

T.3.7.12.7 DSC Support Structure Load Combination Evaluation

See Section T.3.7.12.5 above.

Table T.3.7-1
Postulated Accident Loading Identification

Accident Load Type	Section Reference	NUHOMS® Component Affected				
		DSC Shell Assembly	DSC Basket	DSC Support Structure	HSM	On-Site Transfer Cask
Loss of Adjacent HSM Shielding Effects	8.2.1	(radiological consequence only)				
Tornado Wind	8.2.2				X	X
Tornado Missiles	8.2.2				X	X
Earthquake	8.2.3	X	X	X	X	X
Flood	8.2.4	X			X	
Accident Cask Drop	8.2.5	X	X			X
Loss of Cask Neutron Shield	8.2.5					X
Lightning	8.2.6				X	
Blockage of HSM Air Inlets and Outlets	8.2.7	X	X	X	X	
DSC Leakage	8.2.8	(radiological consequence only)				
DSC Accident Internal Pressure	8.2.9	X				
Load Combinations	8.2.10	X	X	X	X	X

Table T.3.7-2
Maximum NUHOMS®-61BTH Type 1 DSC Stresses for Drop Accident Loads(2)

DSC Components	Stress Type	Calculated Stress (ksi)(1)	
		Vertical	Horizontal
DSC Shell	Primary Membrane	11.93	35.85
	Membrane + Bending	31.78	58.98
Inner Top Cover Plate	Primary Membrane	0.49	32.34
	Membrane + Bending	1.90	43.52
Outer Top Cover Plate	Primary Membrane	0.85	36.06
	Membrane + Bending	2.25	51.45
Inner Bottom Cover Plate	Primary Membrane	6.37	22.25
	Membrane + Bending	23.78	55.40
Outer Bottom Cover Plate	Primary Membrane	1.40	31.56
	Membrane + Bending	3.07	45.54
Top Cover Plate Weld(2)	Primary	0.36	11.40
Bottom Cover Plate Weld	Primary	0.67	9.13

Notes:
(1) Values shown are maximums irrespective of location.
(2) Stress values are the envelope of drop loads with and without 20 psig internal pressure.

Table T.3.7-3
Maximum NUHOMS®-61BTH Type 2 DSC Stresses for Drop Accident Loads(2)

DSC Components	Stress Type	Calculated Stress (ksi)(1)	
		Vertical	Horizontal
DSC Shell	Primary Membrane	14.54	36.47
	Membrane + Bending	39.64	55.83
Inner Top Cover Plate	Primary Membrane	2.41	25.08
	Membrane + Bending	5.87	46.30
Outer Top Cover Plate	Primary Membrane	2.22	36.85
	Membrane + Bending	5.12	55.86
Inner Bottom Cover Plate	Primary Membrane	7.61	38.36
	Membrane + Bending	25.27	56.65
Outer Bottom Cover Plate	Primary Membrane	2.00	32.74
	Membrane + Bending	3.67	51.31
Top Cover Plate Weld(2)	Primary	0.68	11.53
Bottom Cover Plate Weld	Primary	0.61	8.24

Notes:
(1) Values shown are maximums irrespective of location.
(2) Stress values are the envelope of drop loads with and without 20 psig internal pressure.

Table T.3.7-4
Fuel Assembly Weight Simulation Based on 1g Load

Drop Orientations	Pressure Applied to Horizontal Plates $P \times \sin\theta$ (psi)	Pressure Applied to Vertical Plates $P \times \cos\theta$ (psi)
90° and 180°	0.6911	-
45°	0.4887	0.4887
60°	0.5985	0.3456
161.5°	0.6554	0.2193

Table T.3.7-5
Stress Summary of the Type 1 Basket Due to Side Drop Loads – 75g

Drop Orientation	Component[1]	Stress Category	Max. Stress (ksi)	Allowable Stress (ksi)[2]	Reference Figures
45° Side Drop	Basket	P_m	14.54	44.38	Figure T.3.7-5
		$P_m + P_b$	27.12	57.06	Figure T.3.7-6
	Rails	P_m	16.52	44.38	Figure T.3.7-7
		$P_m + P_b$	25.27	57.06	Figure T.3.7-8
	Canister	P_m	2.01	44.38	Figure T.3.7-9
		$P_m + P_b$	19.60	57.06	Figure T.3.7-10
60° Side Drop	Basket	P_m	14.43	44.38	Figure T.3.7-11
		$P_m + P_b$	27.30	57.06	Figure T.3.7-12
	Rails	P_m	20.85	44.38	Figure T.3.7-13
		$P_m + P_b$	28.72	57.06	Figure T.3.7-14
	Canister[3]	P_m	2.44	44.38	Figure T.3.7-15
		$P_m + P_b$	19.57	57.06	Figure T.3.7-16
90° Side Drop	Basket	P_m	18.02	44.38	Figure T.3.7-17
		$P_m + P_b$	22.78	57.06	Figure T.3.7-18
	Rails	P_m	29.03	44.38	Figure T.3.7-19
		$P_m + P_b$	32.79	57.06	Figure T.3.7-20
	Canister[3]	P_m	3.17	44.38	Figure T.3.7-21
		$P_m + P_b$	16.83	57.06	Figure T.3.7-22
161.5° Side Drop Impact on one Transfer cask Support rail	Basket	P_m	13.47	44.38	Figure T.3.7-23
		$P_m + P_b$	25.76	57.06	Figure T.3.7-24
	Rails	P_m	19.71	44.38	Figure T.3.7-25
		$P_m + P_b$	44.37	57.06	Figure T.3.7-26
	Canister[3]	P_m	3.27	44.38	Figure T.3.7-27
		$P_m + P_b$	23.12	57.06	Figure T.3.7-28
180° Side Drop Impact on two Transfer cask Support rails	Basket	P_m	16.22	44.38	Figure T.3.7-29
		$P_m + P_b$	23.55	57.06	Figure T.3.7-30
	Rails	P_m	28.09	44.38	Figure T.3.7-31
		$P_m + P_b$	34.71	57.06	Figure T.3.7-32
	Canister[3]	P_m	4.72	44.38	Figure T.3.7-33
		$P_m + P_b$	26.13	57.06	Figure T.3.7-34

Notes:
1. Reported rails are stainless steel rails only.
2. Based on elastic/plastic analyses and allowable at 750°F.
   $P_m \leq \max(0.7\ S_U, S_Y + 1/3\ (S_U - S_Y))$
   $P_m + P_b \leq 0.9\ S_U$
3. Canister stresses excluded pressure.

Table T.3.7-6
Stress Summary of the Type 2 Basket Due to Side Drop Loads – 75g

Drop Orientation	Component[1]	Stress Category	Max. Stress (ksi)[2]	Allowable Stress (ksi)[3]	Reference Figures
45° Side Drop	Basket	P_m	17.47	44.38	Figure T.3.7-35
		$P_m + P_b$	28.35	57.06	Figure T.3.7-36
	Rails	P_m	19.43	44.38	Figure T.3.7-37
		$P_m + P_b$	38.65	57.06	Figure T.3.7-38
	Canister	P_m	2.34	44.38	Figure T.3.7-39
		$P_m + P_b$	20.08	57.06	Figure T.3.7-40
60° Side Drop	Basket	P_m	15.43	44.38	Figure T.3.7-41
		$P_m + P_b$	27.87	57.06	Figure T.3.7-42
	Rails	P_m	21.88	44.38	Figure T.3.7-43
		$P_m + P_b$	44.77	57.06	Figure T.3.7-44
	Canister[4]	P_m	2.79	44.38	Figure T.3.7-45
		$P_m + P_b$	21.42	57.06	Figure T.3.7-46
90° Side Drop	Basket	P_m	20.42	44.38	Figure T.3.7-47
		$P_m + P_b$	25.75	57.06	Figure T.3.7-48
	Rails	P_m	19.61	44.38	Figure T.3.7-49
		$P_m + P_b$	42.16	57.06	Figure T.3.7-50
	Canister[4]	P_m	1.66	44.38	Figure T.3.7-51
		$P_m + P_b$	14.12	57.06	Figure T.3.7-52
161.5° Side Drop Impact on one Transfer cask Support rail	Basket	P_m	18.72	44.38	Figure T.3.7-53
		$P_m + P_b$	32.85	57.06	Figure T.3.7-54
	Rails	P_m	20.95	44.38	Figure T.3.7-55
		$P_m + P_b$	45.95	57.06	Figure T.3.7-56
	Canister[4]	P_m	4.00	44.38	Figure T.3.7-57
		$P_m + P_b$	25.09	57.06	Figure T.3.7-58
180° Side Drop Impact on two Transfer cask Support rails	Basket	P_m	18.96	44.38	Figure T.3.7-59
		$P_m + P_b$	27.85	57.06	Figure T.3.7-60
	Rails	P_m	20.34	44.38	Figure T.3.7-61
		$P_m + P_b$	45.34	57.06	Figure T.3.7-62
	Canister[4]	P_m	3.75	44.38	Figure T.3.7-63
		$P_m + P_b$	25.13	57.06	Figure T.3.7-64

Notes:

1. Reported rails are stainless steel rails only. The function of the solid aluminum R90 basket support rails is to support the fuel compartment tube structure such that stresses and displacements in the compartment tube structure are acceptable. Since the solid aluminum rails are entrapped between the fuel compartment tube structure and DSC shell, no additional checks of the aluminum are required for accident loading.
2. ANSYS results are conservatively increased by 8% to account for any missing weight.
3. Based on elastic/plastic analyses and allowable at 750°F.
   $P_m \leq \max(0.7\ S_U, S_Y + 1/3\ (S_U - S_Y))$
   $P_m + P_b \leq 0.9\ S_U$
4. Canister stresses excluded pressure.

Table T.3.7-7
Stress Summary of the Type 1 Basket due to 60g End Drop Load

Drop Orientation	Component	Stress Category	Max. Stress (ksi)	Allowable Stress (ksi)[5]
End Drop	Holddown Ring / Top Grid	P_m	6.3	39.36 [1]
End Drop	Basket	P_m	5.34	37.44 [1]
	Rail Stud	Shear[4]	16.8	26.6 [2]
	Plate Insert Weld	Shear	11.4	19.7 [3]

Notes:
1. MIN(2.4 S_m, 0.7 S_u)
2. Minimum of weld shear allowable of 0.55 MIN(3.6 S_m, 1.0 S_u) or pure stud shear allowable of 0.42 S_u. Weld quality factor of 0.55 is based on progressive inspection of weld.
3. 0.35 MIN(3.6 S_m, 1.0 S_u). Weld quality factor of 0.35 is based on fillet weld visual inspection.
4. Envelope of weld or stud shear stress (weld is controlling for stress).
5. Allowables at 750°F for the basket rail studs and plate insert welds and 600°F for the holddown ring / top grid.

Table T.3.7-8
Stress Summary of the Type 2 Basket due to 60g End Drop Load

Drop Orientation	Component	Stress Category	Max. Stress (ksi)	Allowable Stress (ksi)(5)
End Drop	Top Grid	P_m	5.2	39.36 (1)
	Basket	P_m	6.3	37.44 (1)
	Rail Stud	Shear(4)	10.4	26.6 (2)
	Plate Insert Weld	Shear	11.4	19.7 (3)

Notes:
1. MIN(2.4 S_m, 0.7 S_u)
2. Minimum of weld shear allowable of 0.55 MIN(3.6 S_m, 1.0 S_u) or pure stud shear allowable of 0.42 S_u. Weld quality factor of 0.55 is based on progressive inspection of weld.
3. 0.35 MIN(3.6 S_m, 1.0 S_u). Weld quality factor of 0.35 is based on fillet weld visual inspection.
4. Envelope of weld or stud shear stress (weld is controlling for stress).
5. Allowables at 750°F for the basket rail studs and plate insert welds and 600°F for the top grid.

Table T.3.7-9
Mechanical Properties of Materials

	SA-240, Type 304 Stainless Steel at 500°F	**6061-O Aluminum (Anneled) at 500°F**
Modulus of Elasticity (psi)	25.8×10^6	7.9×10^6
Yield Strength (psi)	19,400	5,500
Tangent Modulus (psi)	1.29×10^6	7.9×104

Table T.3.7-10
Summary of Pressure Loads Used for Different Drop Orientations

Drop Orientation (Degree)	1g Load		100g Load	
	Horizontal Plate Pressure (psi)	Vertical Plate Pressure (psi)	Horizontal Plate Pressure (psi)	Vertical Plate Pressure (psi)
Vertical	0.6911	0	69.11	0
30	0.5985	0.3456	59.85	34.56
45	0.4887	0.4877	48.87	48.87

Table T.3.7-11
Summary of Basket Buckling Analysis

Type 1 Basket:

Basket Orientation	Last Converged Load (g)	Safety Factor [3]	Figure #
0°	79.3 g	1.057	Figure T.3.7-81
30° [1]	80.9 g	1.079	Figure T.3.7-82
30° [2]	84.1 g	1.121	Note 4
45° [1]	80.4 g	1.072	Figure T.3.7-83
45° [2]	82.8 g	1.104	Note 4

Notes:

1. With 0.08" thick fuel channels modeled at loaded tube walls, 705 lb per fuel assembly weight.
2. Without Zircaloy fuel channels, 640 lb per fuel assembly weight.
3. Last converged load divided by 75g.
4. Not the governing case.

Type 2 Basket:

Basket Orientation	Last Converged Load (g)	Safety Factor [3]	Figure #
0°	90.1 g	1.201	Figure T.3.7-84
30° [1]	87.6 g	1.168	Figure T.3.7-85
30° [2]	87.9 g	1.172	Note 4
45° [1]	81.0 g	1.080	Figure T.3.7-86
45° [2]	90.1 g	1.201	Note 4

Notes:

1. With 0.08" thick Zircaloy fuel channels modeled at loaded tube walls, 705 lb per fuel assembly weight.
2. Without Zircaloy fuel channels, 640 lb per fuel assembly weight.
3. Last converged load divided by 75g.
4. Not the governing case.

Table T.3.7-12
NUHOMS®-61BTH Type 1 DSC Enveloping Load Combination Results for Normal and Off-Normal Loads
(ASME Service Levels A and B)

DSC Components	Stress Type	Controlling Load Combination (1)	Stress (ksi)	
			Calculated	Allowable (2)
DSC Shell	Primary Membrane	TR-7	7.17	17.2
	Membrane + Bending	NO-1	19.39	26.3
	Primary + Secondary	LD-5	44.34	60.0
Inner Bottom Cover Plate	Primary Membrane	LD-4	4.71	17.5
	Membrane + Bending	NO-1	18.84	40.5
	Primary + Secondary	LD-5	39.37	52.5
Outer Bottom Cover Plate	Primary Membrane	LD-4, LD-5	6.28	17.5
	Membrane + Bending	UL-5, UL-6	25.44	29.1
	Primary + Secondary	LD-5	38.81	52.5
Inner Top Cover Plate	Primary Membrane	TR-5	3.75	17.5
	Membrane + Bending	TR-5	9.14	26.3
	Primary + Secondary	TR-5	33.35	52.5
Outer Top Cover Plate	Primary Membrane	TR-7	4.39	17.5
	Membrane + Bending	TR-7	10.68	26.3
	Primary + Secondary	TR-7	28.77	52.5
Basket	Primary Membrane	TR-8	3.21	15.6
	Membrane + Bending	TR-8	18.62	23.4
	Primary + Secondary	HSM-3	38.25	46.80
Rail	Primary Membrane	TR-8	2.66	15.60
	Membrane + Bending	TR-8	11.93	23.40
	Primary + Secondary	HSM-3	13.33	46.80
Rail Stud	Shear	TR-1	5.44	9.36

See Table T.3.7-18 for notes.

Table T.3.7-13
NUHOMS®-61BTH Type 2 DSC Enveloping Load Combination Results for Normal and Off-Normal Loads
(ASME Service Levels A and B)

DSC Components	Stress Type	Controlling Load Combination (1)	Stress (ksi)	
			Calculated	Allowable (2)
DSC Shell	Primary Membrane	DD-1	9.09	17.2
	Membrane + Bending	TR-7	21.66	26.3
	Primary + Secondary	HSM-1	59.44	60.0
Inner Bottom Cover Plate	Primary Membrane	LD-5	4.49	17.0
	Membrane + Bending	NO-1	23.07	40.5
	Primary + Secondary	LD-4	49.26	53.7
Outer Bottom Cover Plate	Primary Membrane	UL-6	6.83	18.1
	Membrane + Bending	UL-5	25.53	25.53
	Primary + Secondary	LD-4	39.97	53.7
Inner Top Cover Plate	Primary Membrane	TR-5	2.65	17.2
	Membrane + Bending	DD-1	16.83	25.8
	Primary + Secondary	DD-1	30.45	51.6
Outer Top Cover Plate	Primary Membrane	TR-7	4.21	17.2
	Membrane + Bending	TR-7	8.83	25.8
	Primary + Secondary	TR-7	27.38	51.6
Basket	Primary Membrane	TR-8	4.11	15.6
	Membrane + Bending	TR-8	18.55	23.4
	Primary + Secondary	HSM-3	38.76	46.80
Rail	Primary Membrane	TR-8	3.28	15.60
	Membrane + Bending	TR-8	20.77	23.40
	Primary + Secondary	HSM-3	22.17	46.80
Rail Stud	Shear	TR-1	5.44	9.36

See Table T.3.7-18 for notes.

Table T.3.7-14
NUHOMS®-61BTH Type 1 DSC Enveloping Load Combination Results for Accident Loads
(ASME Service Level C)

DSC Components	Stress Type	Controlling Load Combination[1]	Stress (ksi)	
			Calculated	Allowable[2]
DSC Shell	Primary Membrane	HSM-8	16.85	22.4
	Membrane + Bending	HSM-8	25.73	33.7
Inner Bottom Cover Plate	Primary Membrane	HSM-8	9.72	23.2
	Membrane + Bending	HSM-8	16.36	34.8
Outer Bottom Cover Plate	Primary Membrane	UL-7	7.87	23.2
	Membrane + Bending	UL-7	33.01	34.8
Inner Top Cover Plate	Primary Membrane	HSM-8	8.61	22.4
	Membrane + Bending	HSM-8	21.38	33.7
Outer Top Cover Plate	Primary Membrane	HSM-8	8.08	22.4
	Membrane + Bending	HSM-8	21.80	33.7
Basket	Primary Membrane	HSM-8	3.0	23.40
	Membrane + Bending	HSM-8	19.67	35.0
Rail	Primary Membrane	HSM-8	2.66	23.40
	Membrane + Bending	HSM-8	15.22	35.10
Rail Stud	Shear	HSM-8	5.44	9.36

See Table T.3.7-18 for notes.

Table T.3.7-15
NUHOMS®-61BTH Type 2 DSC Enveloping Load Combination Results for Accident Loads
(ASME Service Level C)

DSC Components	Stress Type	Controlling Load Combination[1]	Stress (ksi)	
			Calculated	Allowable[2]
DSC Shell	Primary Membrane	HSM-8	13.74	21.7
	Membrane + Bending	HSM-8	32.83	34.9
Inner Bottom Cover Plate	Primary Membrane	HSM-8	5.16	22.1
	Membrane + Bending	HSM-8	6.65	33.1
Outer Bottom Cover Plate	Primary Membrane	UL-7	8.59	22.1
	Membrane + Bending	UL-7	33.06	34.0
Inner Top Cover Plate	Primary Membrane	HSM-8	4.42	21.6
	Membrane + Bending	HSM-8	13.83	32.4
Outer Top Cover Plate	Primary Membrane	HSM-8	9.17	21.6
	Membrane + Bending	HSM-8	17.42	32.4
Basket	Primary Membrane	HSM-8	6.17	23.40
	Membrane + Bending	HSM-8	26.61	35.10
Rail	Primary Membrane	HSM-8	3.88	23.40
	Membrane + Bending	HSM-8	24.95	35.10
Rail Stud	Shear	HSM-8	5.44	9.36

See Table T.3.7-18 for notes.

Table T.3.7-16
NUHOMS®-61BTH Type 1 DSC Enveloping Load Combination Results for Accident Loads
(ASME Service Level D)[3]

DSC Components	Stress Types	Controlling Load Combination[1]	Stress (ksi)	
			Calculated	Allowable[2]
DSC	Primary Membrane	TR-10	35.85	44.1
Shell	Membrane + Bending	TR-10	58.98	59.6[2]
Inner Bottom	Primary Membrane	TR-10	22.80	44.4
Cover Plate	Membrane + Bending	TR-10	56.77	59.6[6]
Outer Bottom	Primary Membrane	TR-10	32.39	44.4
Cover Plate	Membrane + Bending	UL-8	62.54	65.1
Inner Top	Primary Membrane	TR-10	32.34	46.3
Cover Plate	Membrane + Bending	TR-10	55.21	59.6
Outer Top	Primary Membrane	TR-10	39.84	46.3
Cover Plate	Membrane + Bending	TR-10	54.89	59.6
Basket	Primary Membrane	TR-10	18.02	44.31
	Membrane + Bending	TR-10	27.30	56.97
Rail	Primary Membrane Membrane + Bending	TR-10 TR-10	29.03 44.37	44.31 56.97
Rail Stud	Shear	TR10	17.43	26.59

See Table T.3.7-18 for notes.

Table T.3.7-17
NUHOMS®-61BTH Type 2 DSC Enveloping Load Combination Results for Accident Loads
(ASME Service Level D)[3]

DSC Components	Stress Types	Controlling Load Combination[1]	Stress (ksi)	
			Calculated	Allowable[2]
DSC	Primary Membrane	TR-10	36.47	44.4
Shell	Membrane + Bending	TR-10	55.83	59.3
Inner Bottom	Primary Membrane	TR-10	38.36	44.4
Cover Plate	Membrane + Bending	TR-10	56.65	58.6
Outer Bottom	Primary Membrane	TR-10	32.74	44.4
Cover Plate	Membrane + Bending	TR-10	51.31	57.1
Inner Top	Primary Membrane	TR-10	25.08	44.4
Cover Plate	Membrane + Bending	TR-10	46.30	57.1
Outer Top	Primary Membrane	TR-10	36.85	44.4
Cover Plate	Membrane + Bending	TR-10	55.86	57.6
Basket	Primary Membrane	TR-10	20.42	44.31
	Membrane + Bending	TR-10	32.85	56.97
Rail	Primary Membrane Membrane + Bending	TR-10 TR-10	21.88 45.95	44.31 56.97
Rail Stud	Shear	TR10	14.77	26.59

See Table T.3.7-18 for notes.

Table T.3.7-18
DSC Enveloping Load Combination Table Notes

(1) See Table T.2-6 for load combination nomenclature.

(2) See Table T.2-9 for allowable stress criteria. Material properties were obtained from Table 8.1-3 at a design temperature of 750°F or as noted.

(3) In accordance with the ASME Code, thermal stresses need not be included in Service Level D load combinations.

(4) Not used.

(5) The maximum side drop membrane + bending stress is highly localized near the cask rail, at the outer bottom cover plate. The maximum temperature in this region is less than 240°F (temperature case 2).

(6) The maximum side drop membrane + bending stress is highly localized over the cask rail. The maximum temperature in this region is less than 300°F.

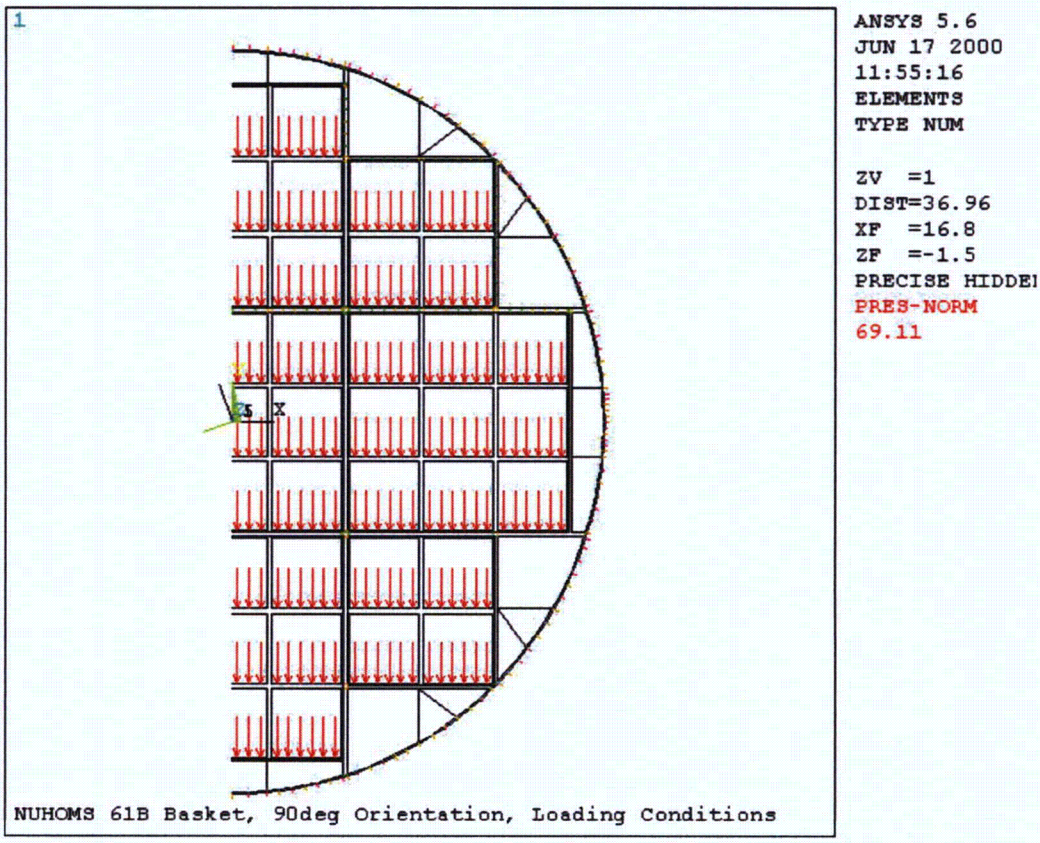

Figure T.3.7-1
90° and 180° Orientation Side Drop – Pressure Distribution

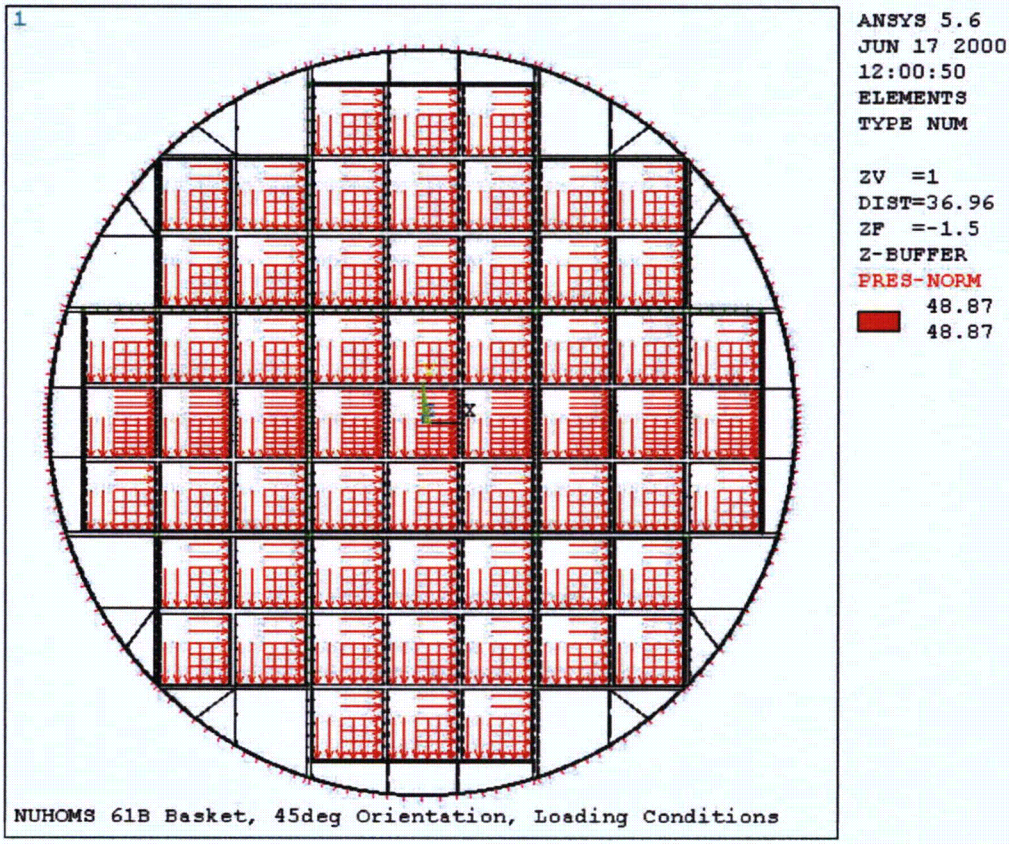

Figure T.3.7-2
45° Orientation Side Drop – Pressure Distribution

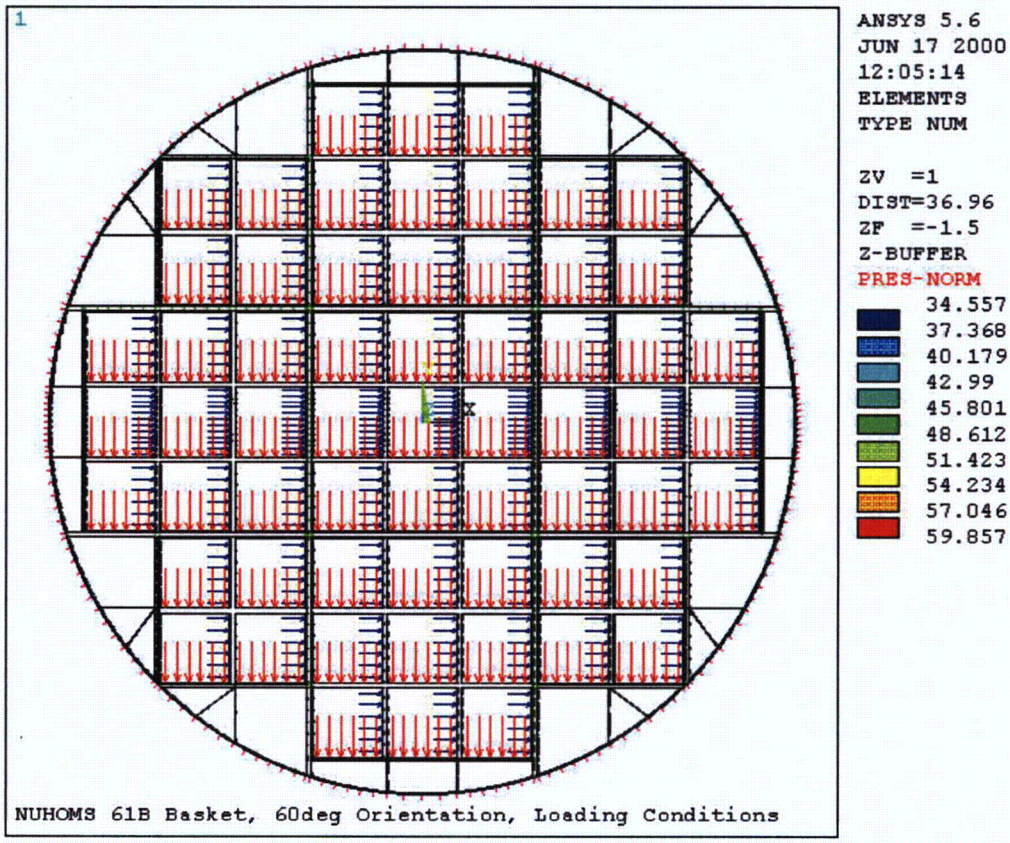

Figure T.3.7-3
60° Orientation Side Drop – Pressure Distribution

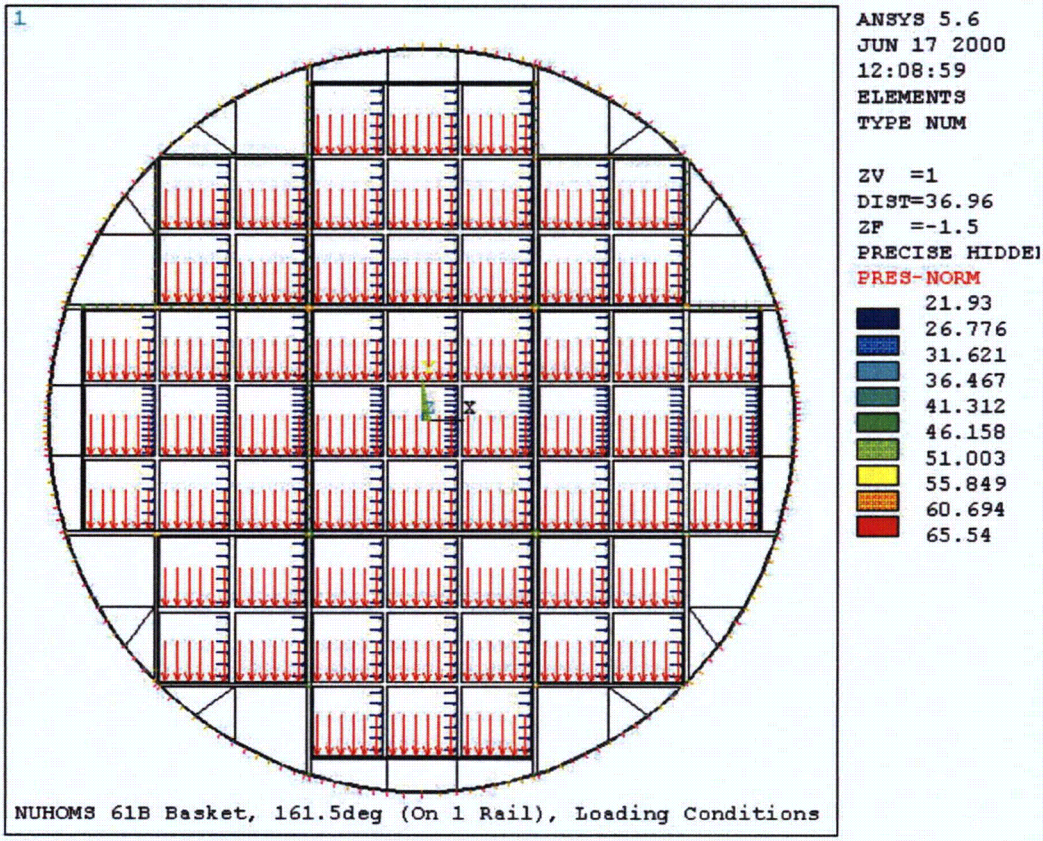

Figure T.3.7-4
161.5° Orientation Side Drop – Pressure Distribution

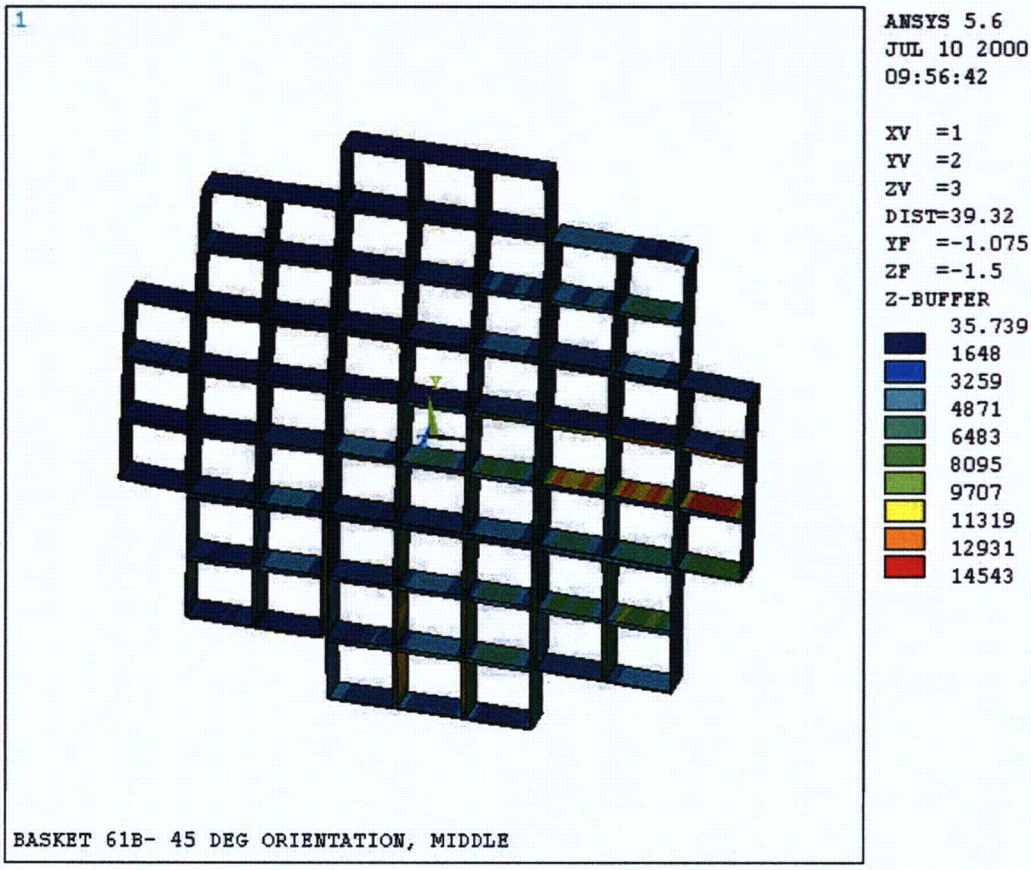

Figure T.3.7-5
45° Orientation Side Drop – Type 1 Basket, P_m (76.25g)

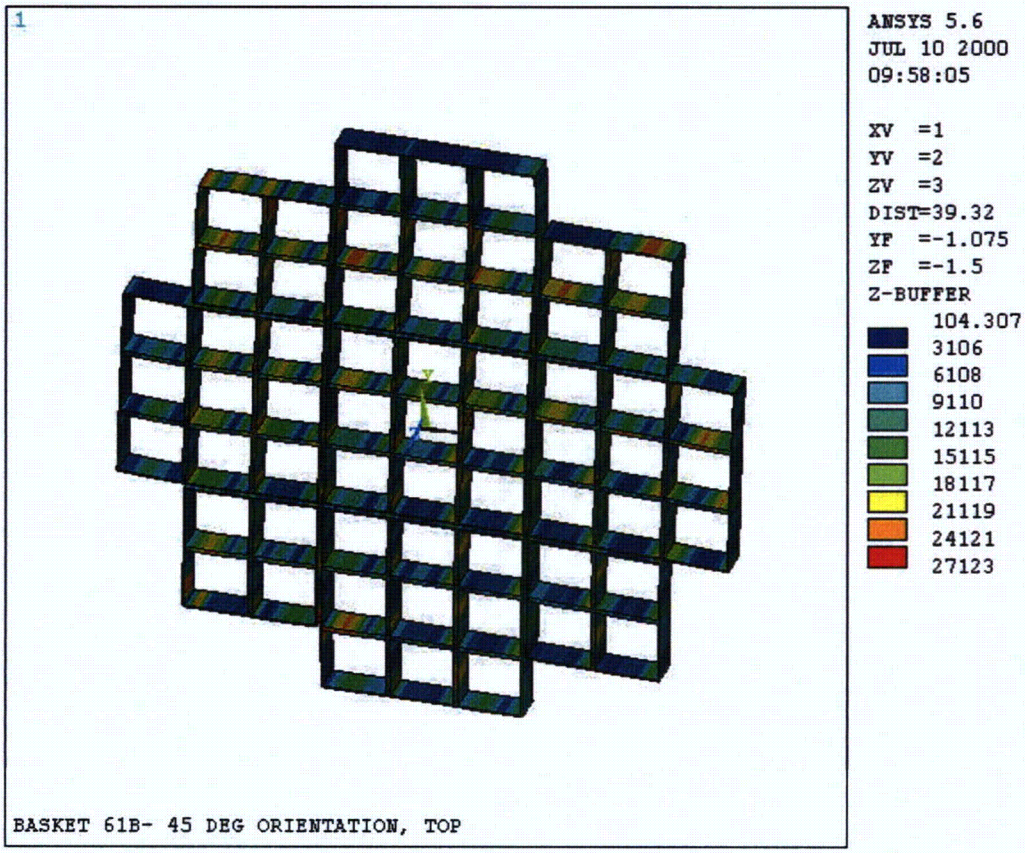

Figure T.3.7-6
45° Orientation Side Drop – Type 1 Basket, $P_m + P_b$ (76.25g)

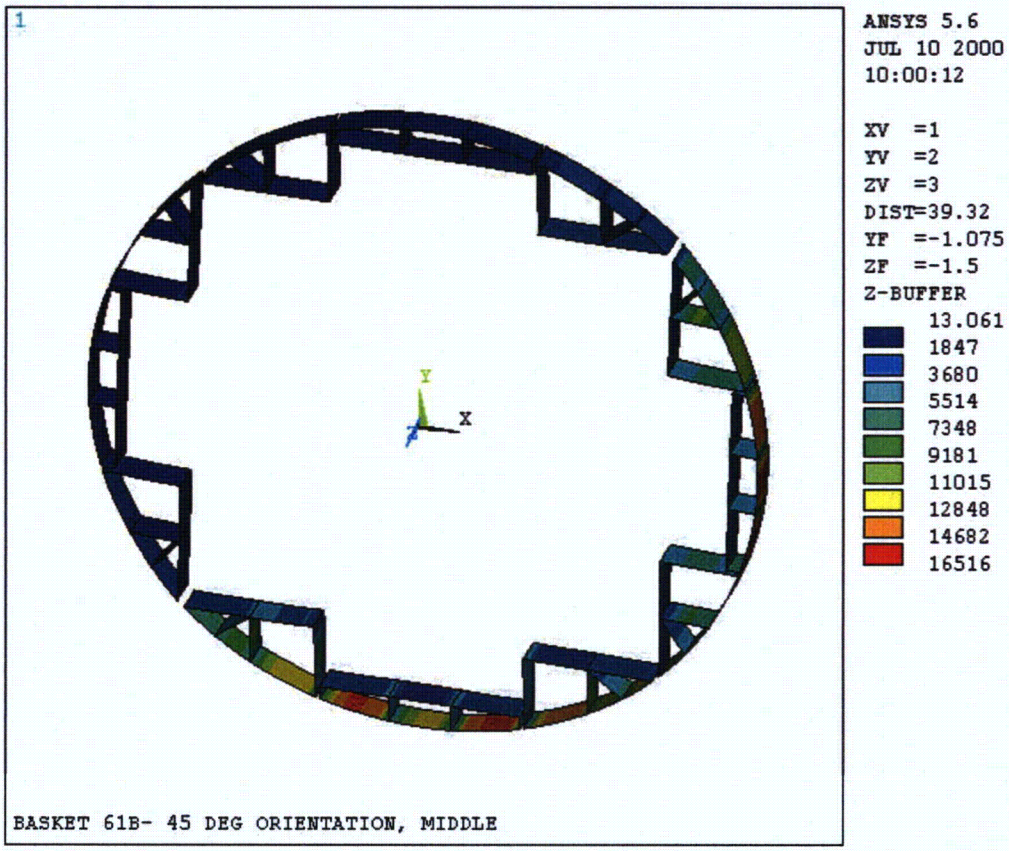

Figure T.3.7-7
45° Orientation Side Drop – Type 1 Rails, P_m (76.2g)

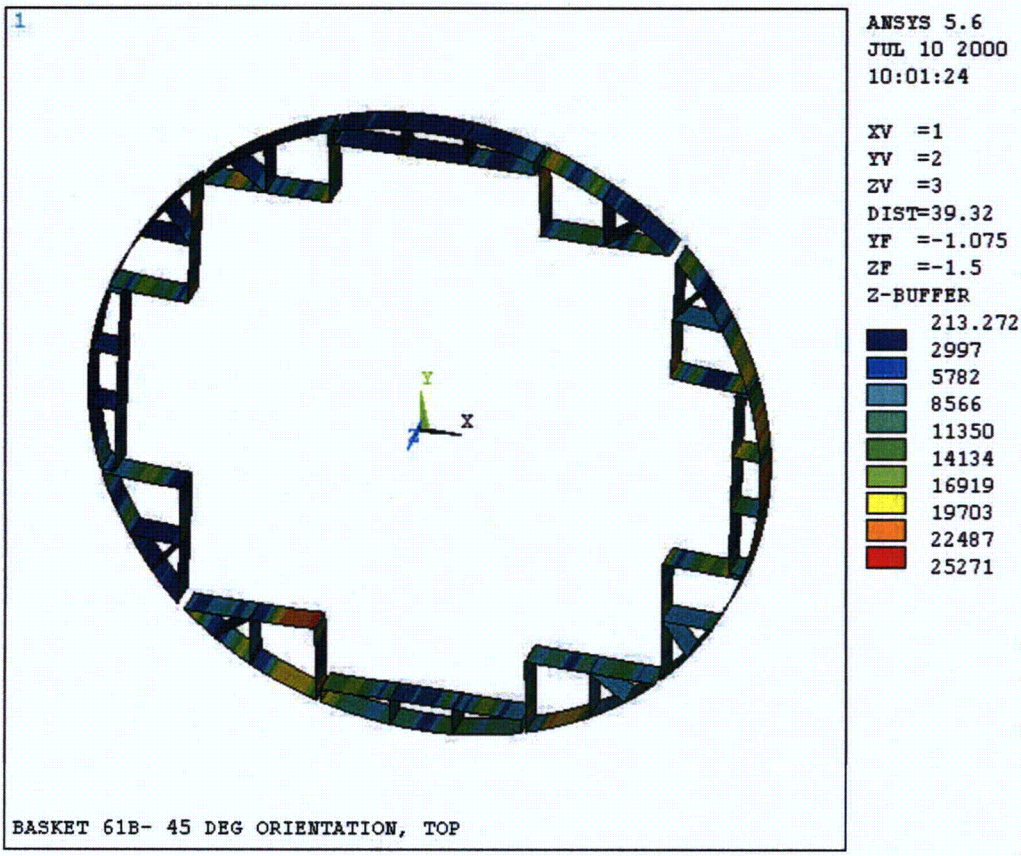

Figure T.3.7-8
45° Orientation Side Drop – Type 1 Rails, $P_m + P_b$ (75.5g)

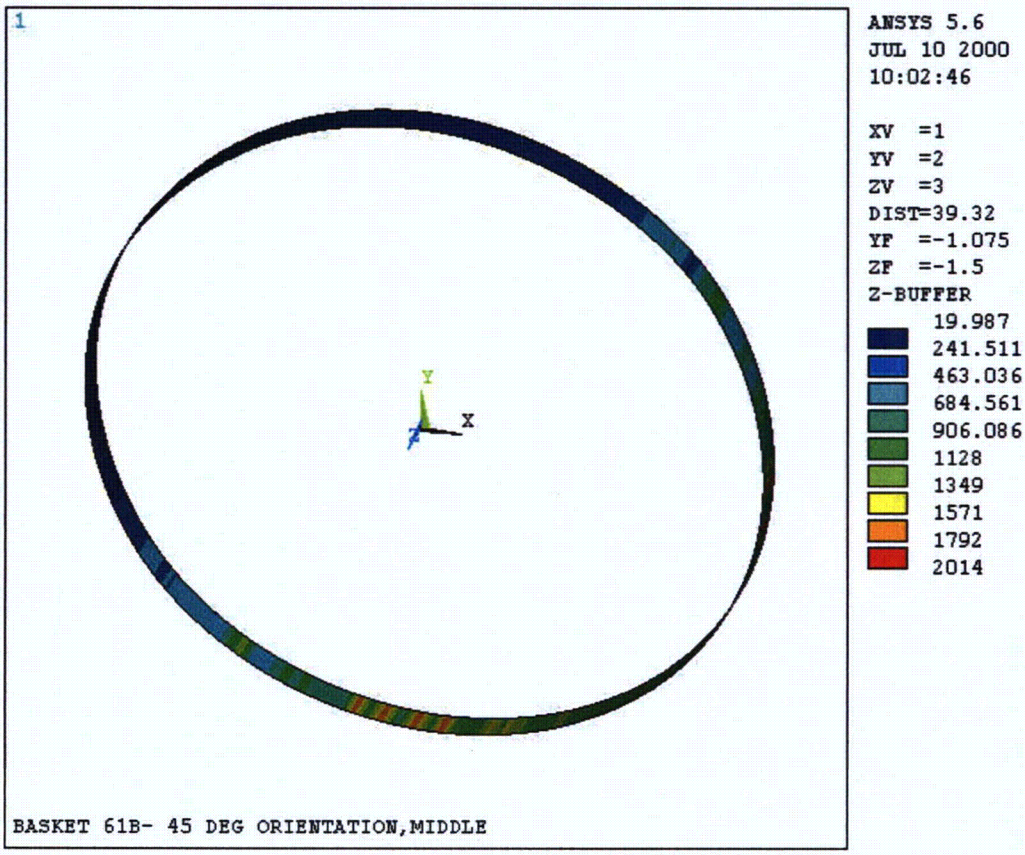

Figure T.3.7-9
45° Orientation Side Drop – Type 1 Canister, P_m (76.25g)

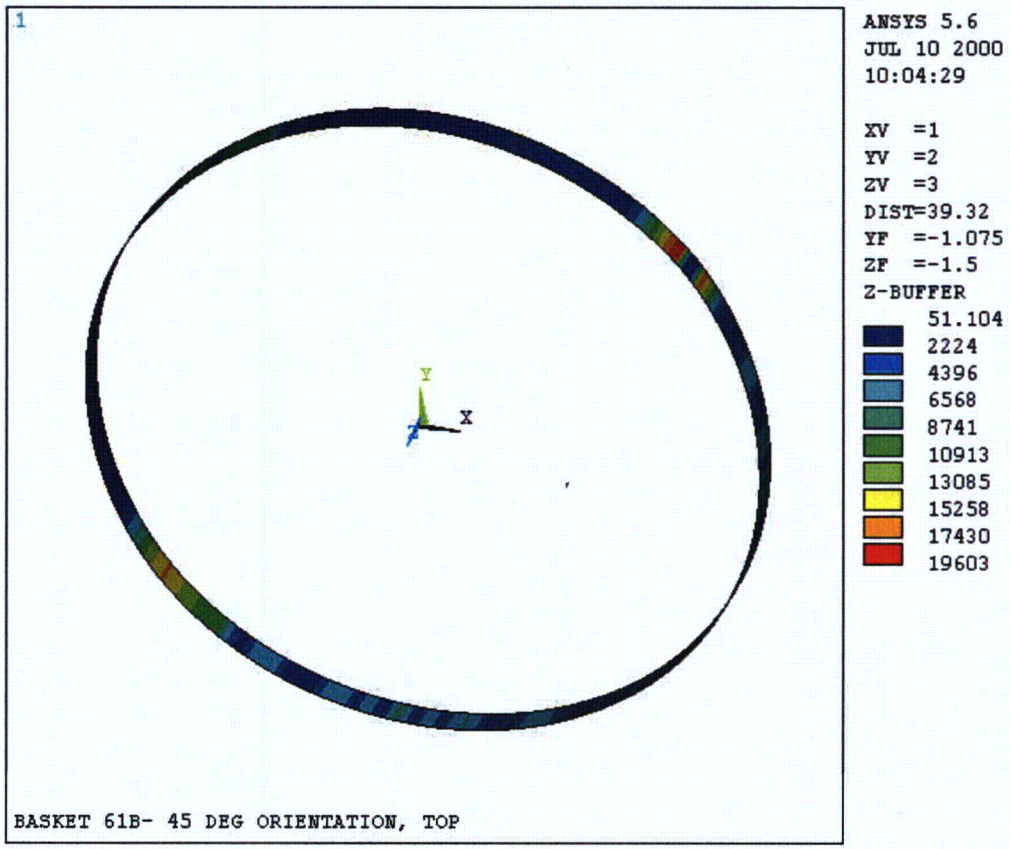

Figure T.3.7-10
45° Orientation Side Drop – Type 1 Canister, $P_m + P_b$ (76.25g)

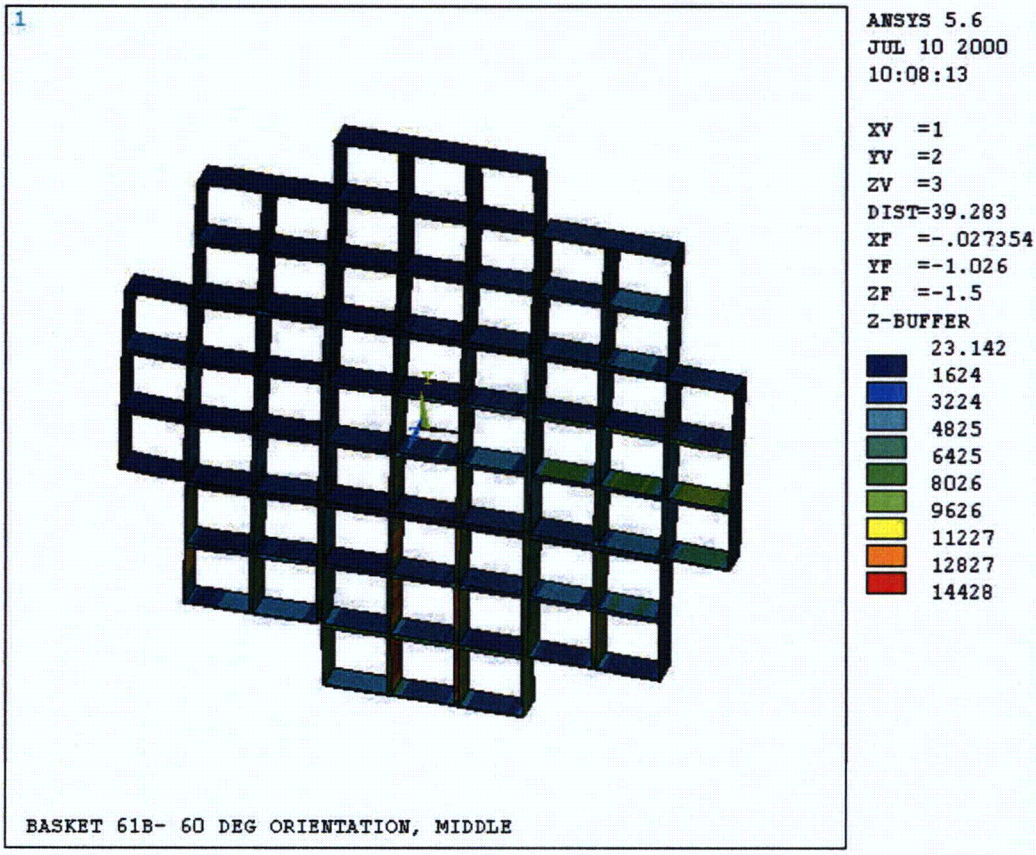

Figure T.3.7-11
60° Orientation Side Drop – Type 1 Basket, P_m (75.5g)

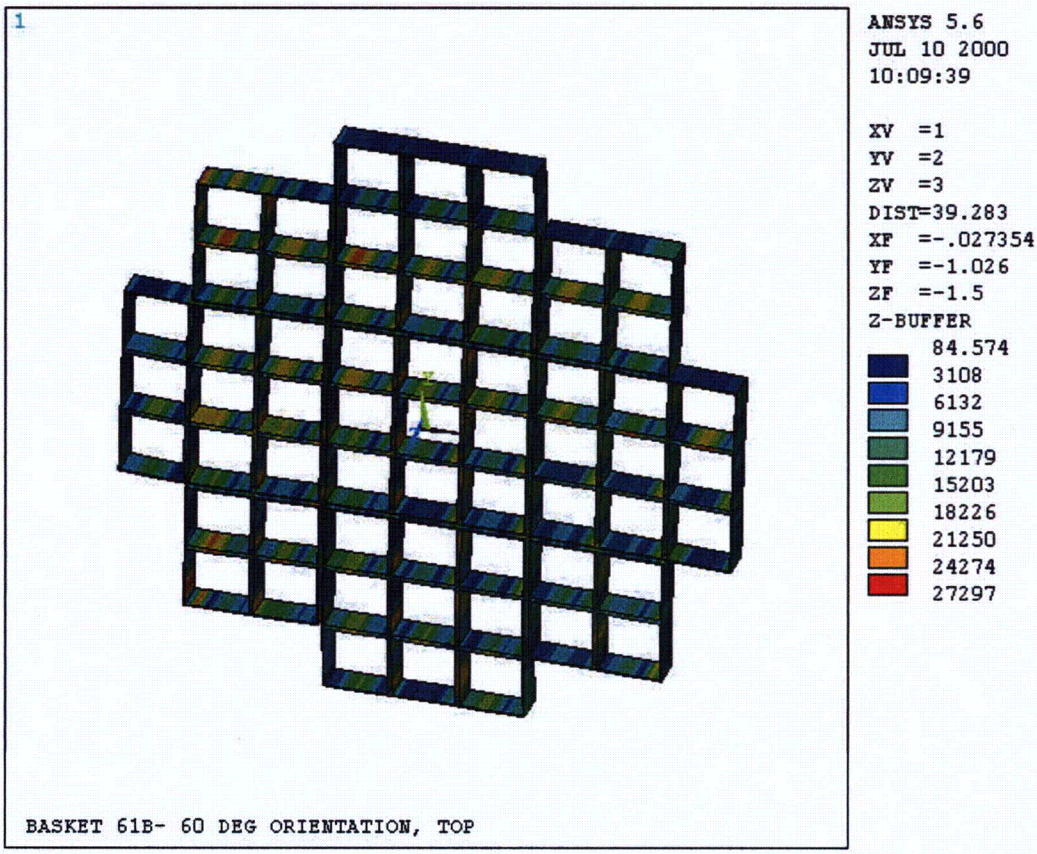

Figure T.3.7-12
60° Orientation Side Drop – Type 1 Basket, $P_m + P_b$ (75.5g)

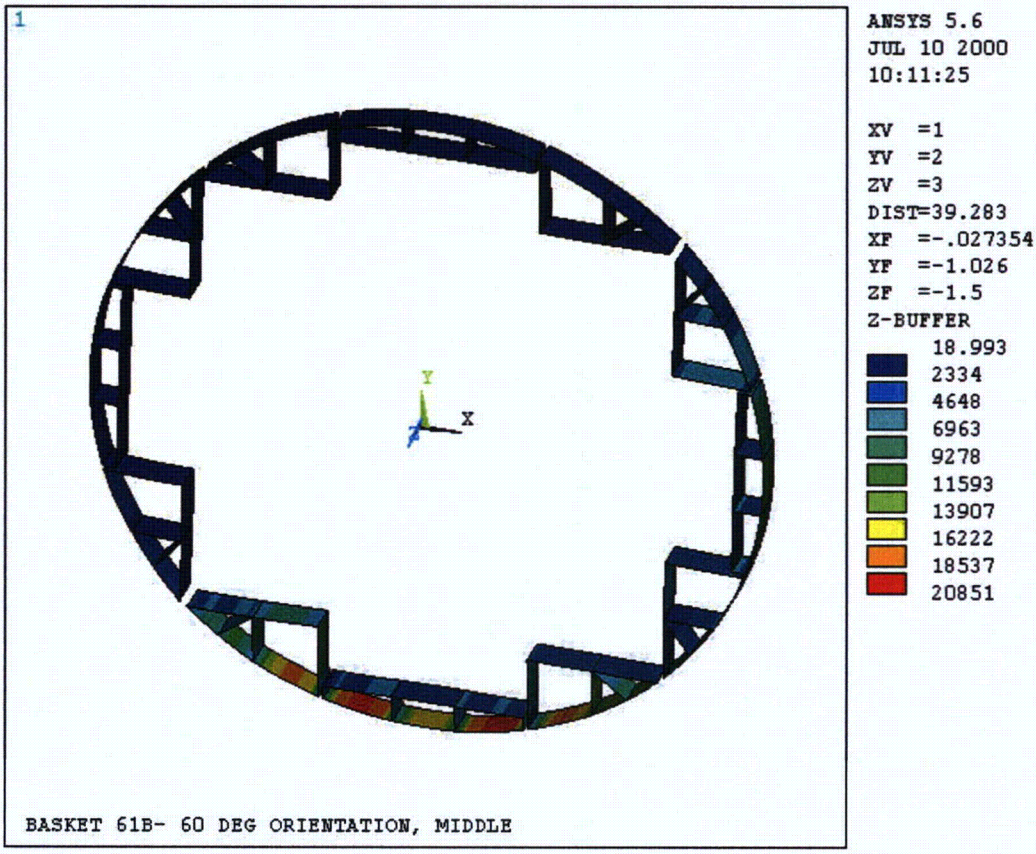

Figure T.3.7-13
60° Orientation Side Drop – Type 1 Rails, P_m (75.5g)

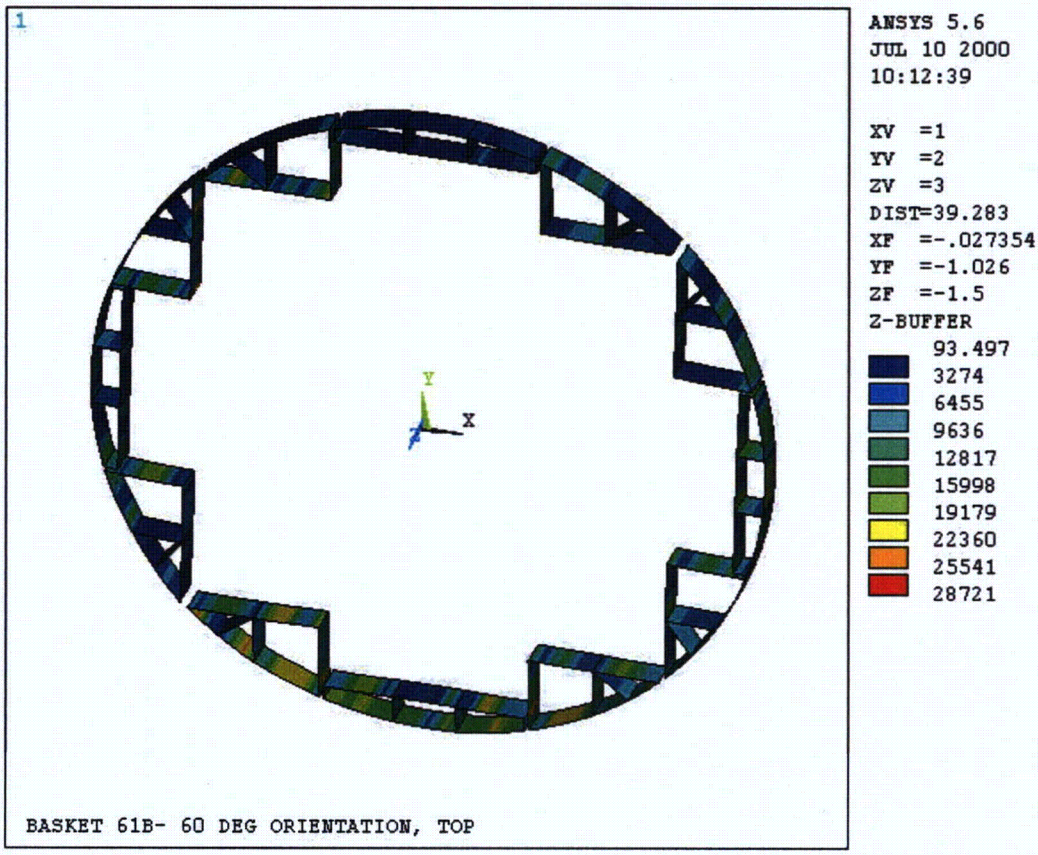

Figure T.3.7-14
60° Orientation Side Drop – Type 1 Rails, $P_m + P_b$ (75.5g)

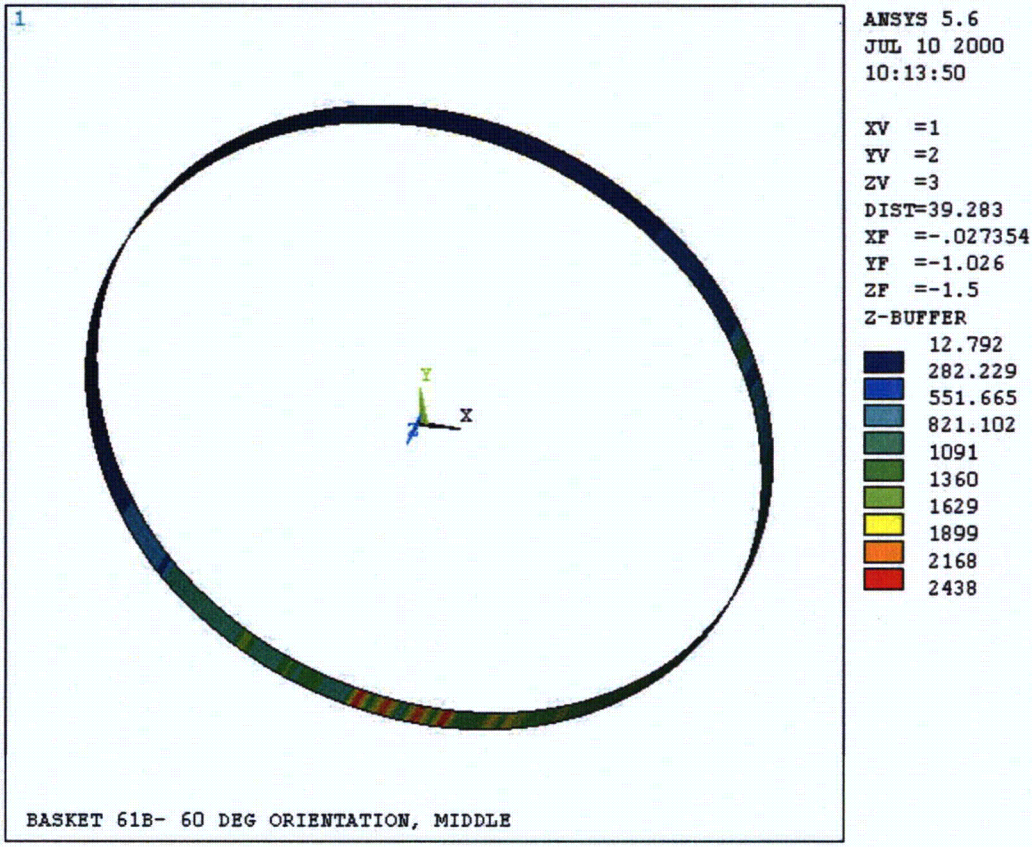

Figure T.3.7-15
60° Orientation Side Drop – Type 1 Canister, P_m (75.5g)

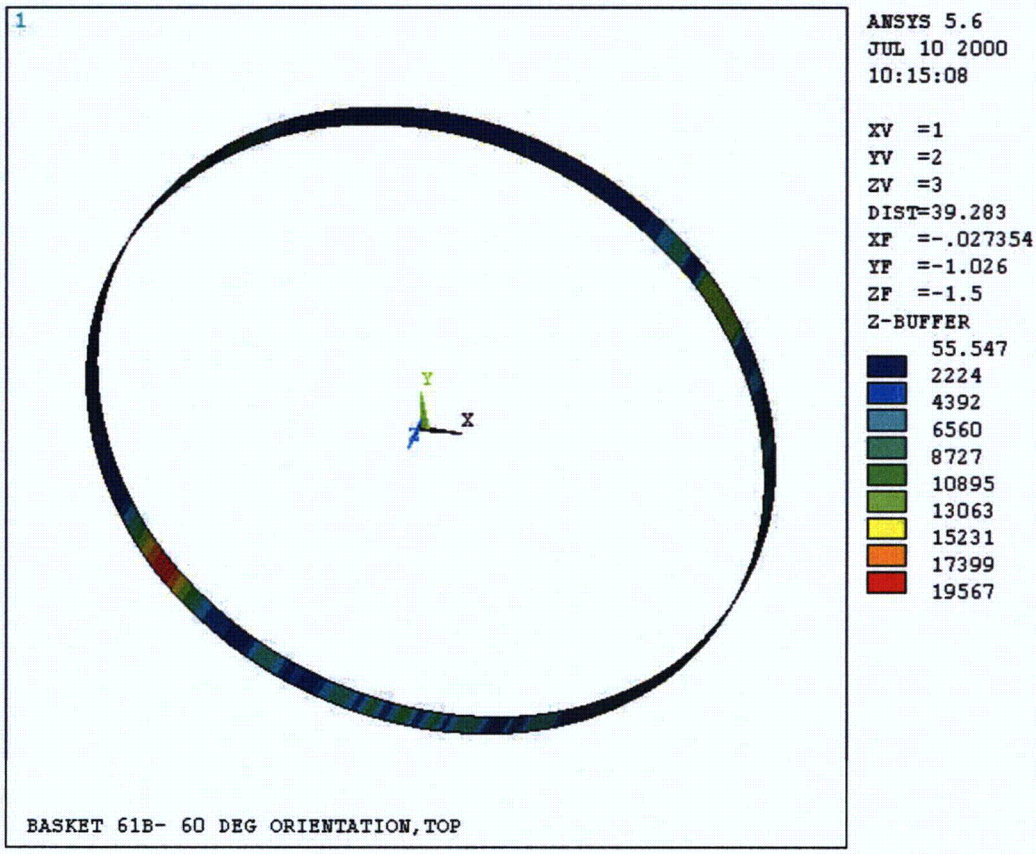

Figure T.3.7-16
60° Orientation Side Drop – Type 1 Canister, $P_m + P_b$ (75.5g)

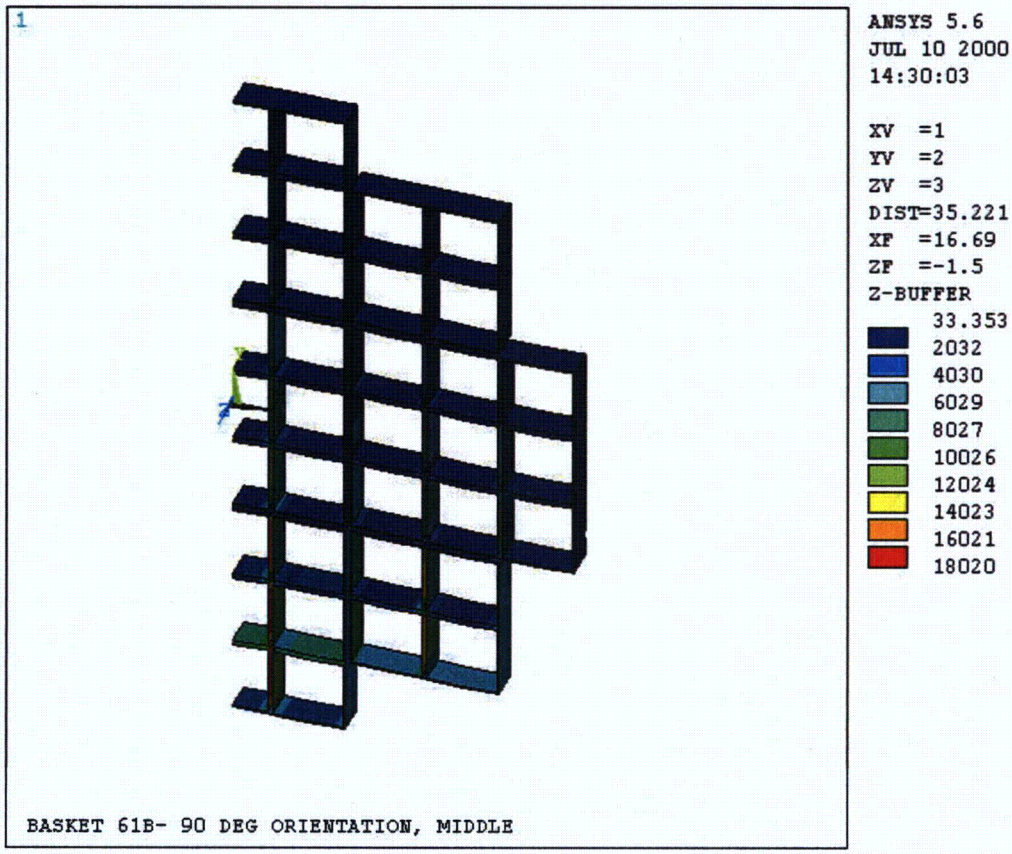

Figure T.3.7-17
90° Orientation Side Drop – Type 1 Basket, P_m (75.5g)

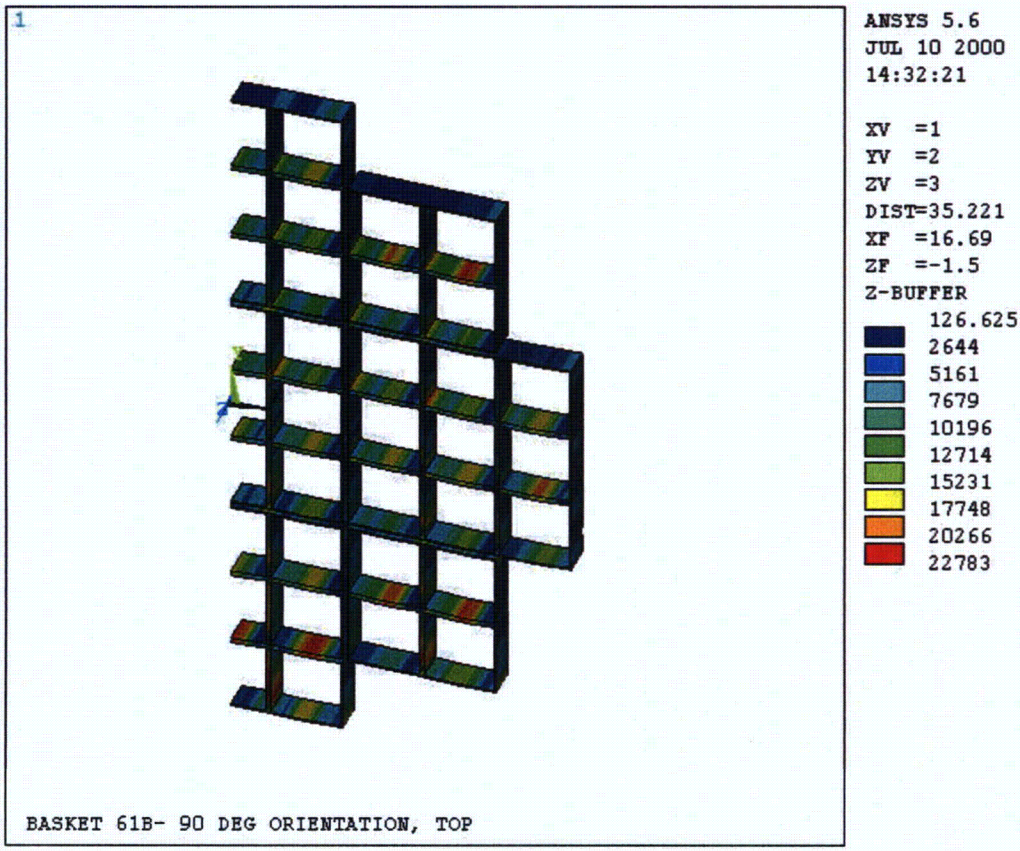

Figure T.3.7-18
90° Orientation Side Drop – Type 1 Basket, $P_m + P_b$ (75.5g)

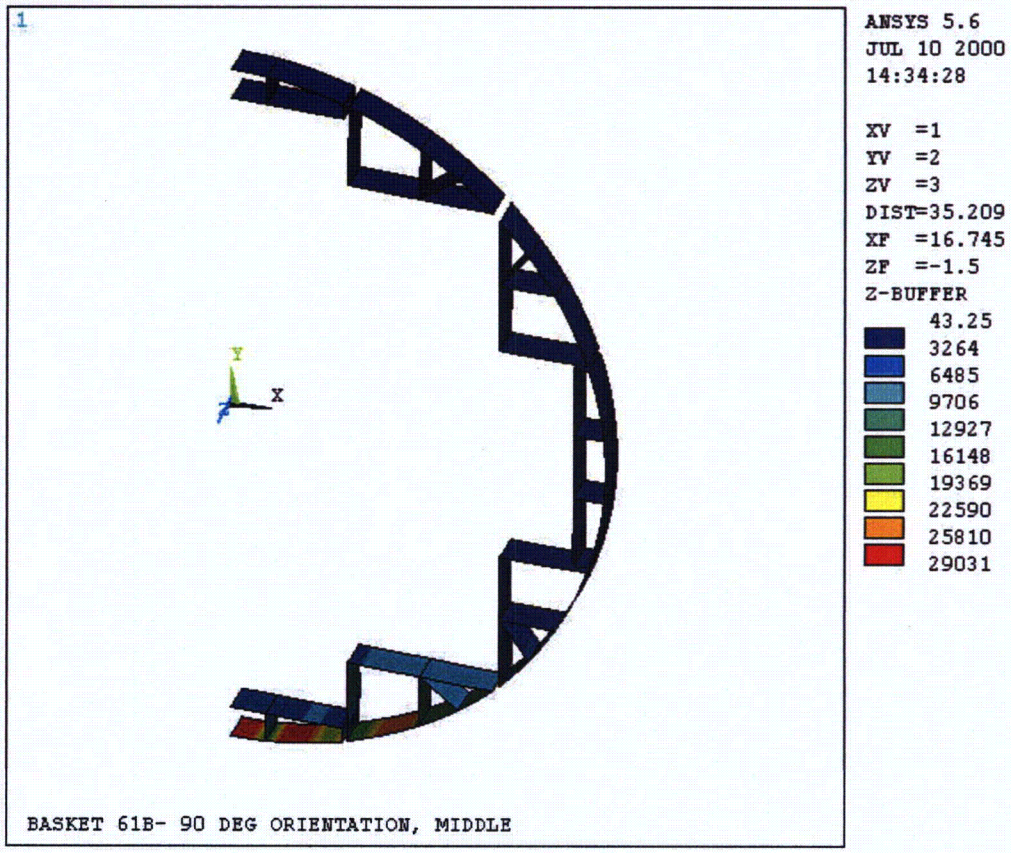

Figure T.3.7-19
90° Orientation Side Drop – Type 1 Rails, P_m (75.5g)

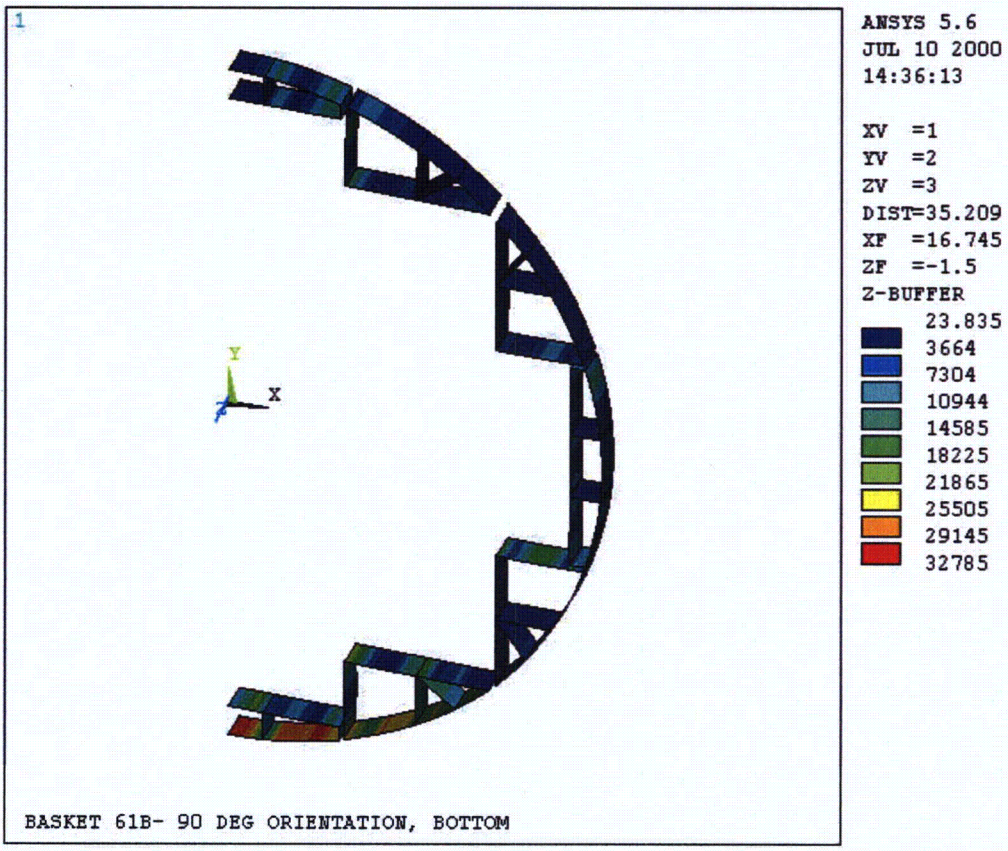

Figure T.3.7-20
90° Orientation Side Drop – Type 1 Rails, $P_m + P_b$ (75.5g)

Figure T.3.7-21
90° Orientation Drop – Type 1 Canister, P_m (75.5g)

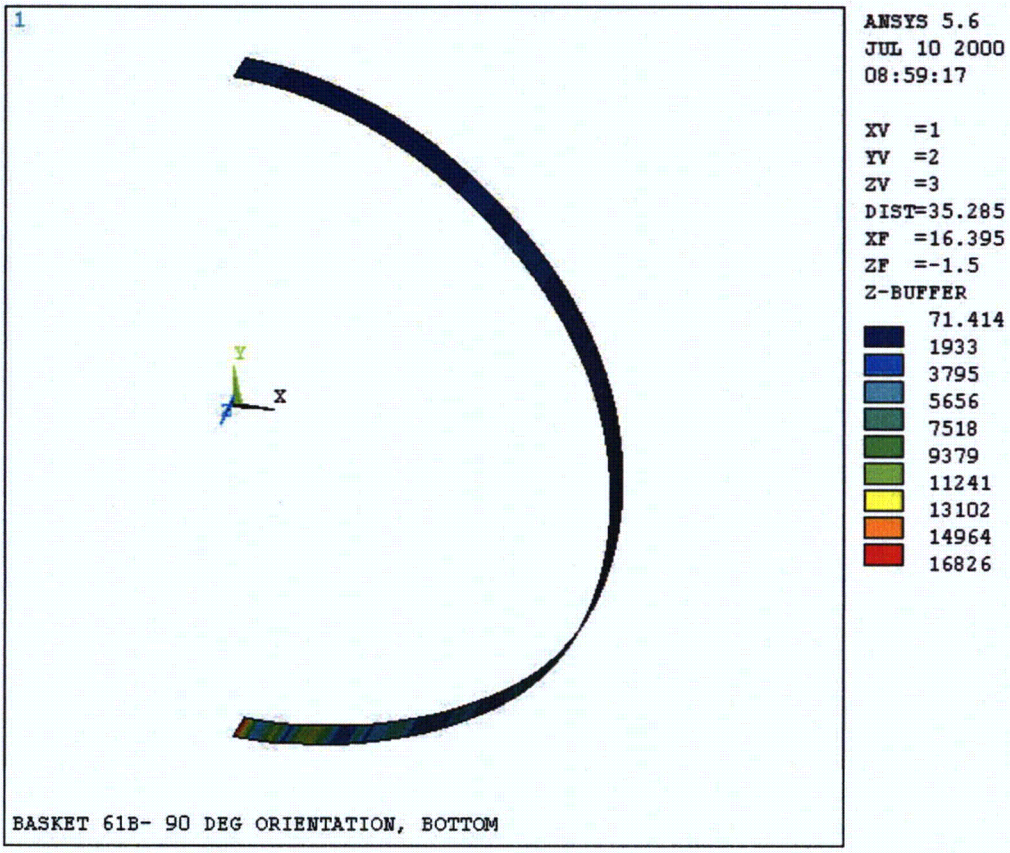

Figure T.3.7-22
90° Orientation Side Drop– Type 1 Canister, $P_m + P_b$ (75.5g)

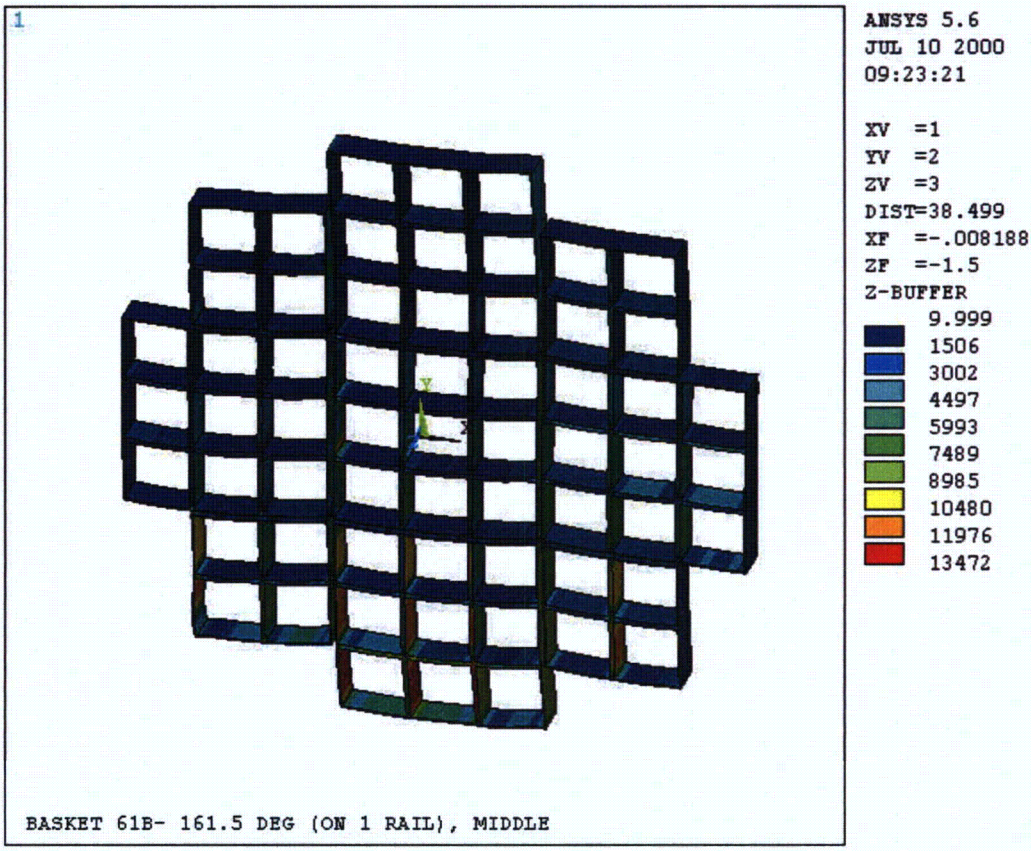

Figure T.3.7-23
161.5° Orientation Side Drop – Type 1 Basket, P_m (76.0g)

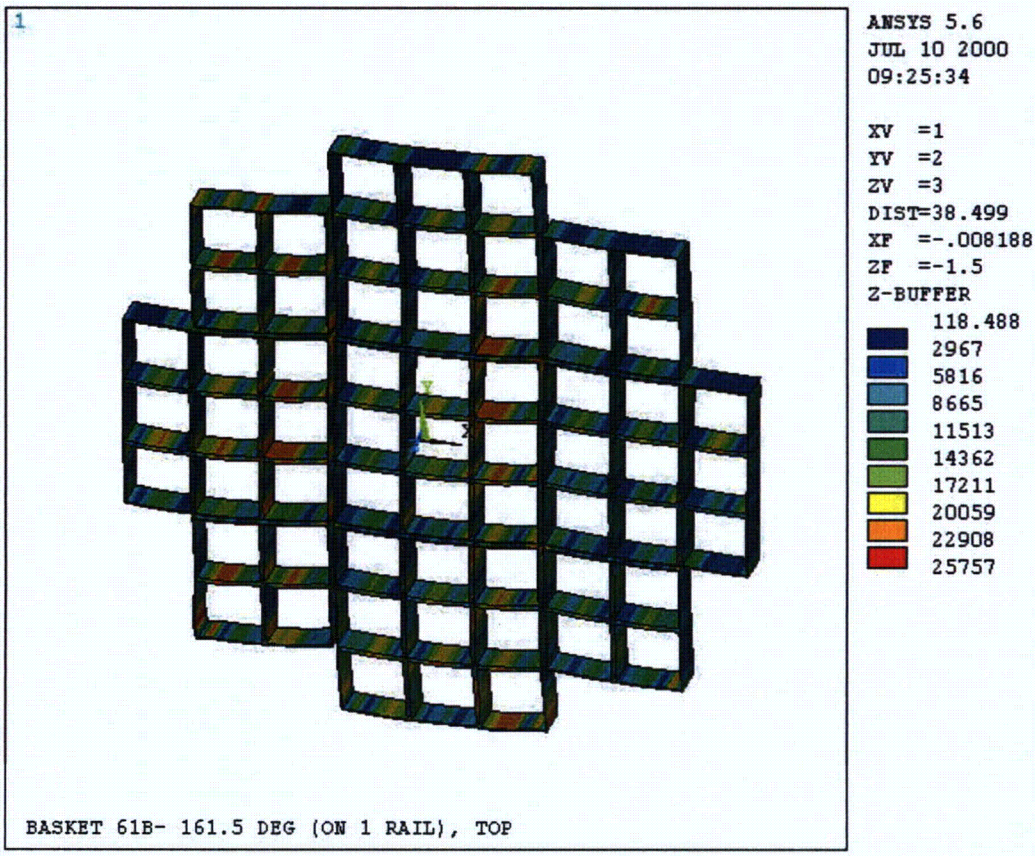

Figure T.3.7-24
161.5° Orientation Side Drop – Type 1 Basket, $P_m + P_b$ (76.0g)

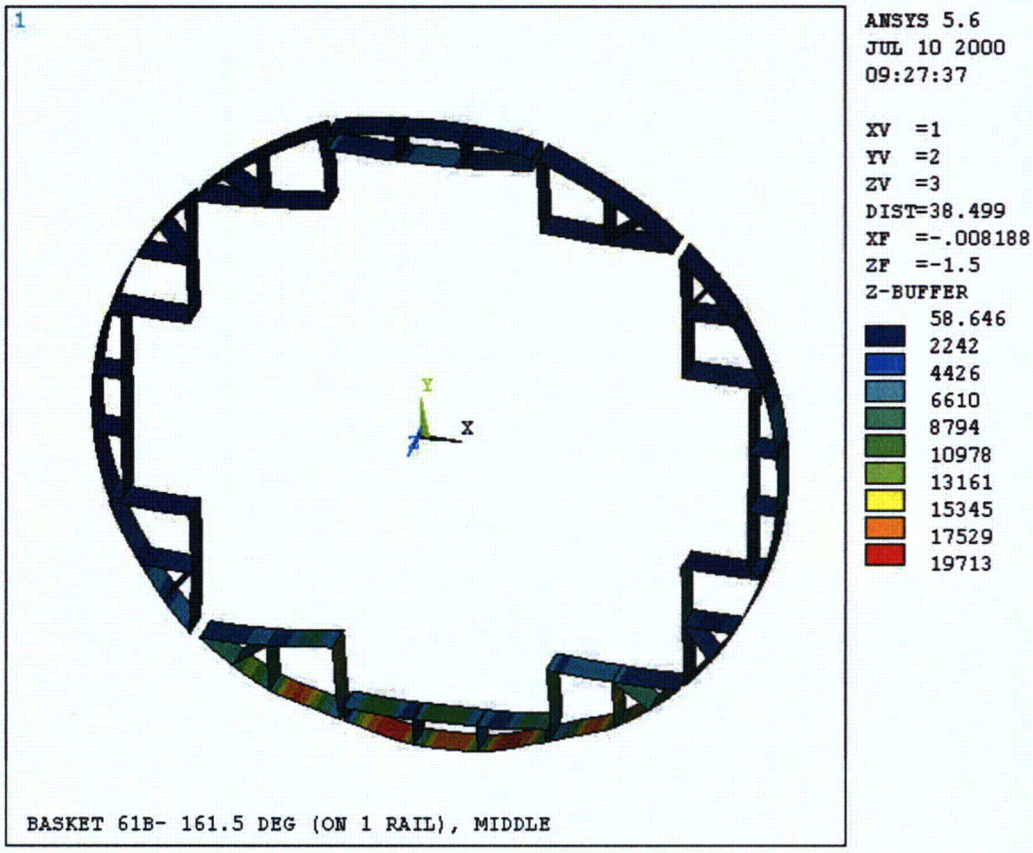

Figure T.3.7-25
161.5° Orientation Side Drop – Type 1 Rails, P_m (76.0g)

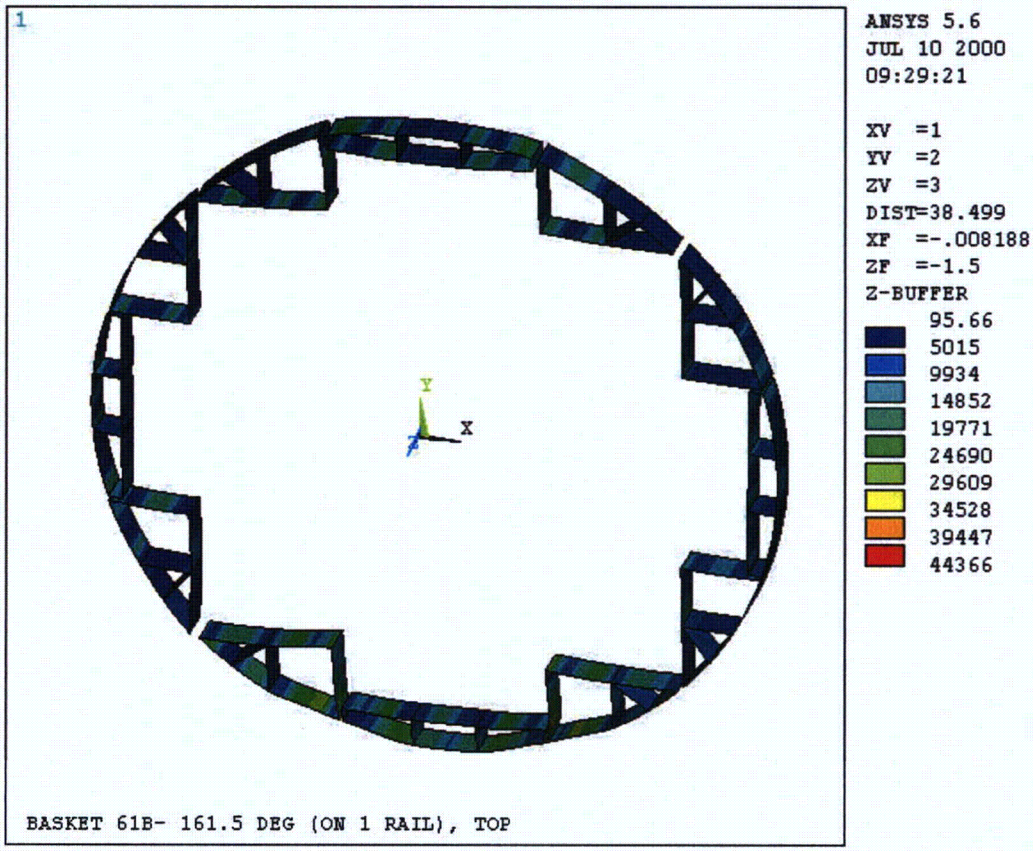

Figure T.3.7-26
161.5° Orientation Side Drop – Type 1 Rails, $P_m + P_b$ (76.0g)

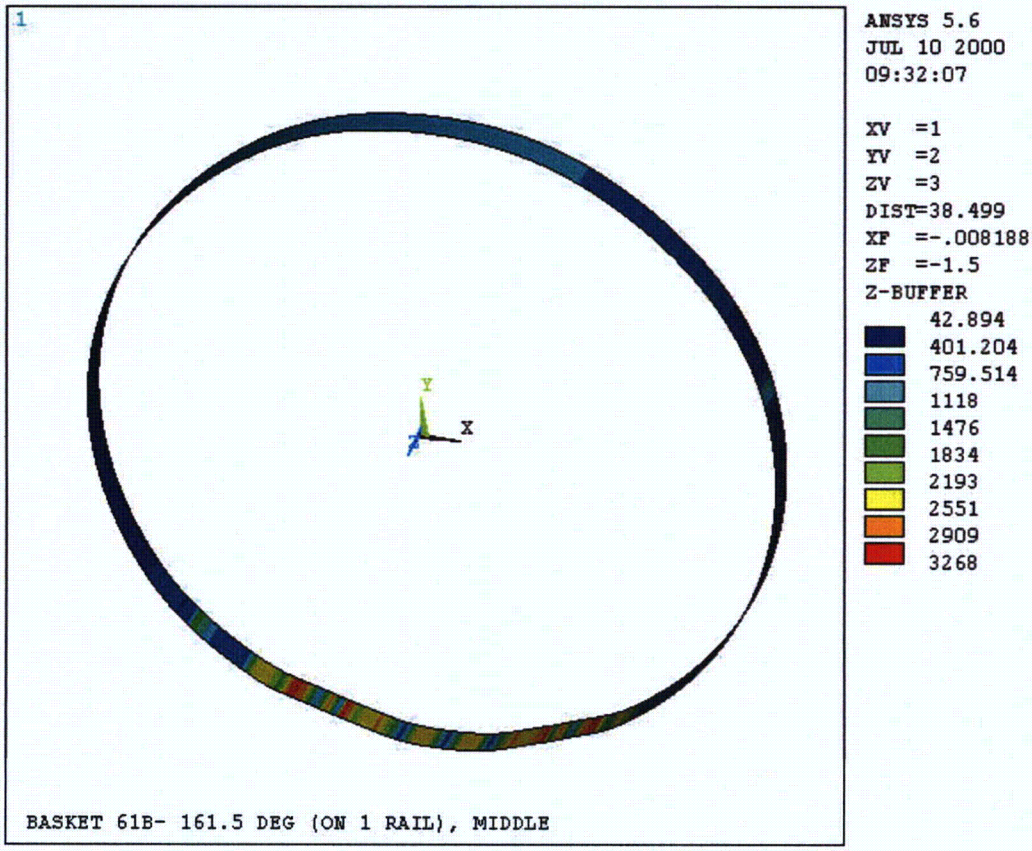

Figure T.3.7-27
161.5° Orientation Side Drop – Type 1 Canister, P_m (76.0g)

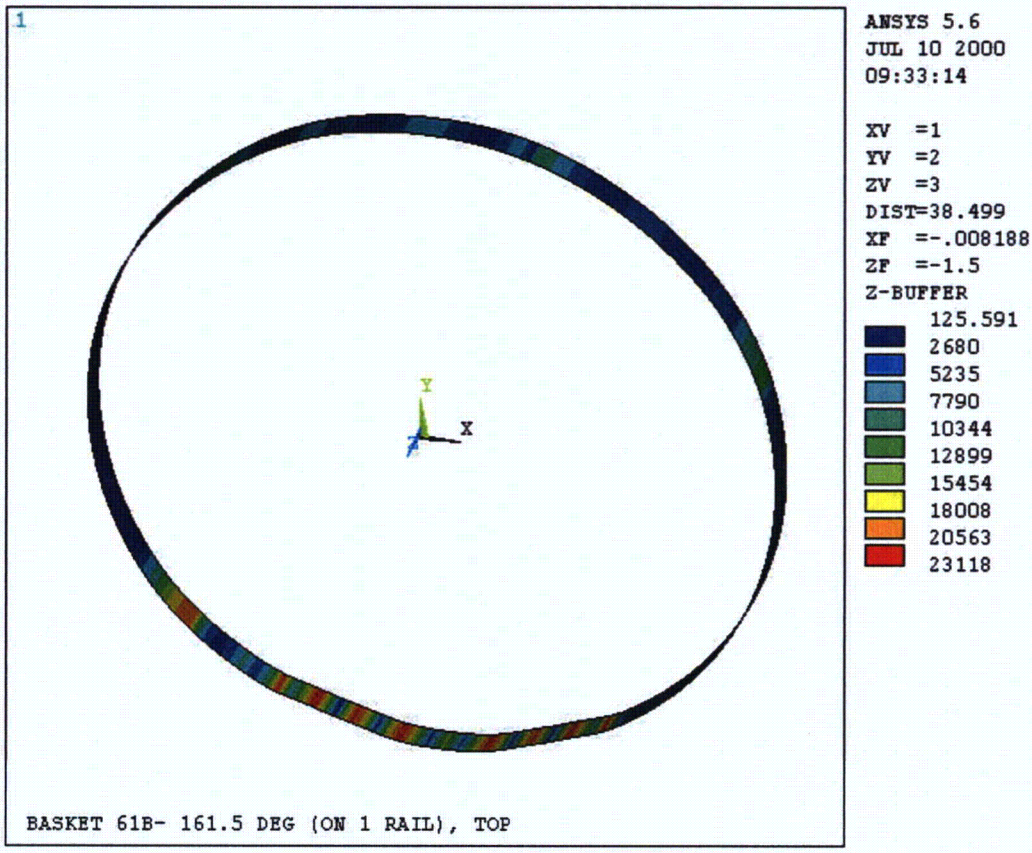

Figure T.3.7-28
161.5° Orientation Side Drop – Type 1 Canister, $P_m + P_b$ (76.0g)

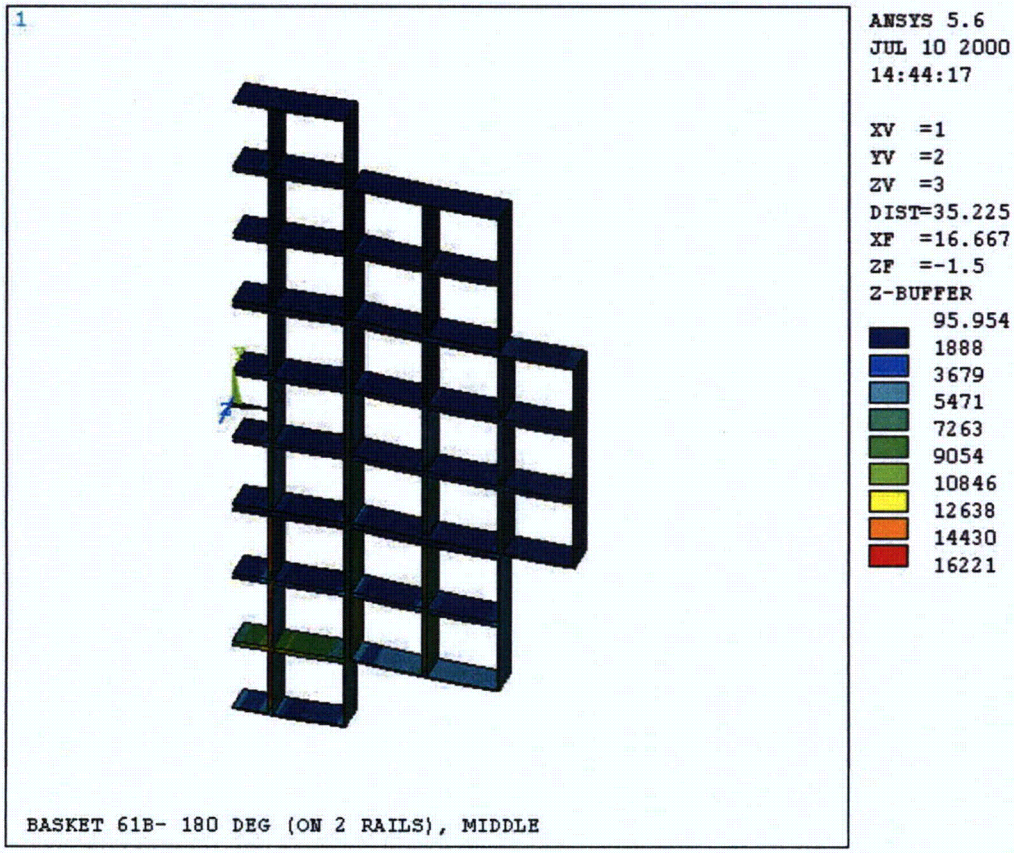

Figure T.3.7-29
180° Orientation Side Drop – Type 1 Basket, P_m (75.5g)

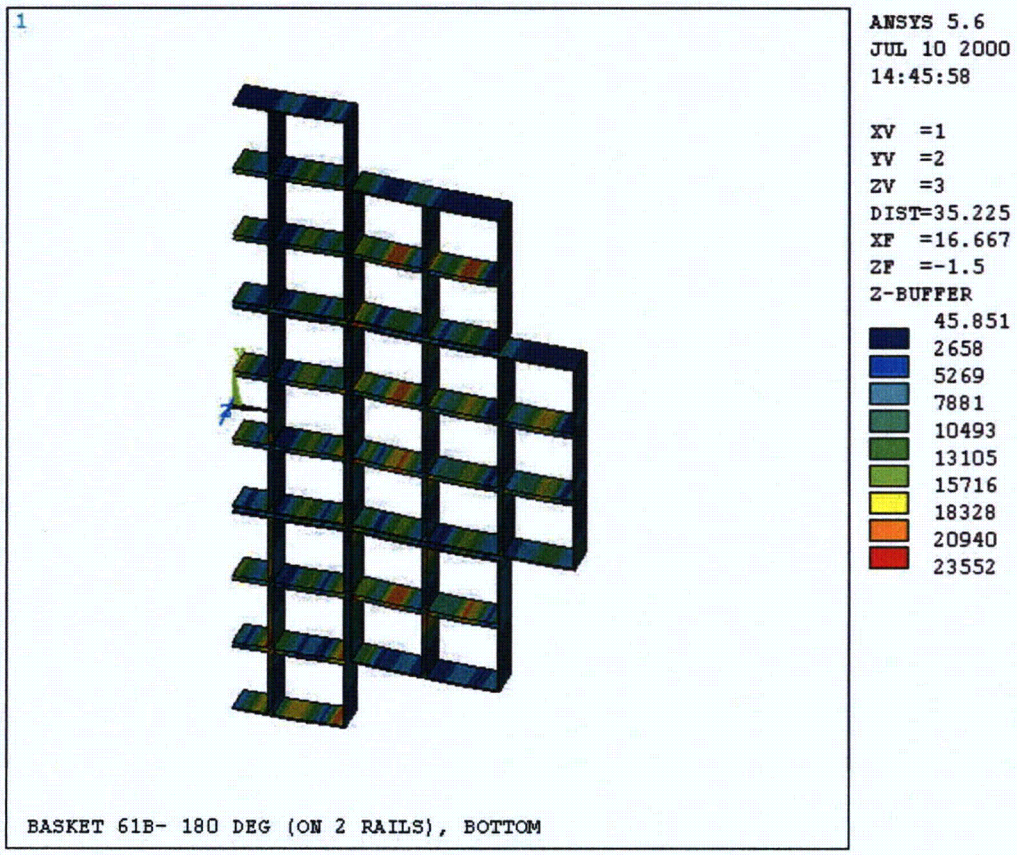

Figure T.3.7-30
180° Orientation Side Drop – Type 1 Basket, $P_m + P_b$ (75.5g)

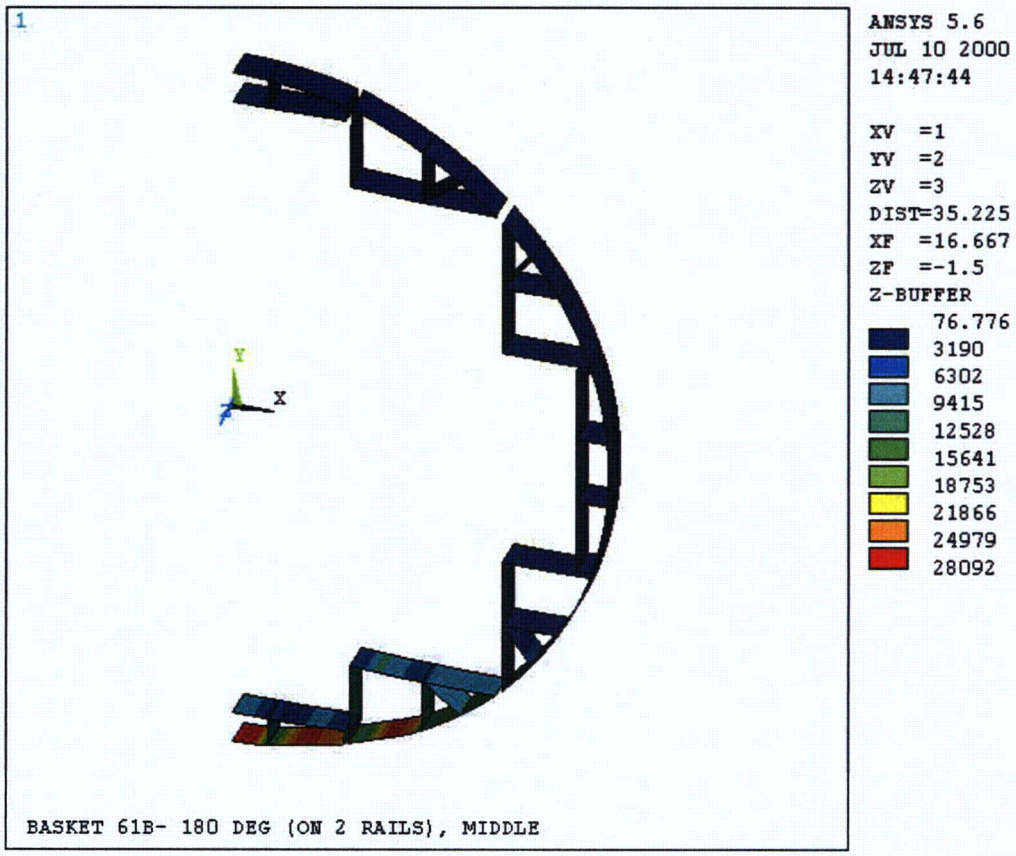

Figure T.3.7-31
180° Orientation Side Drop – Type 1 Rails, P_m (75.5g)

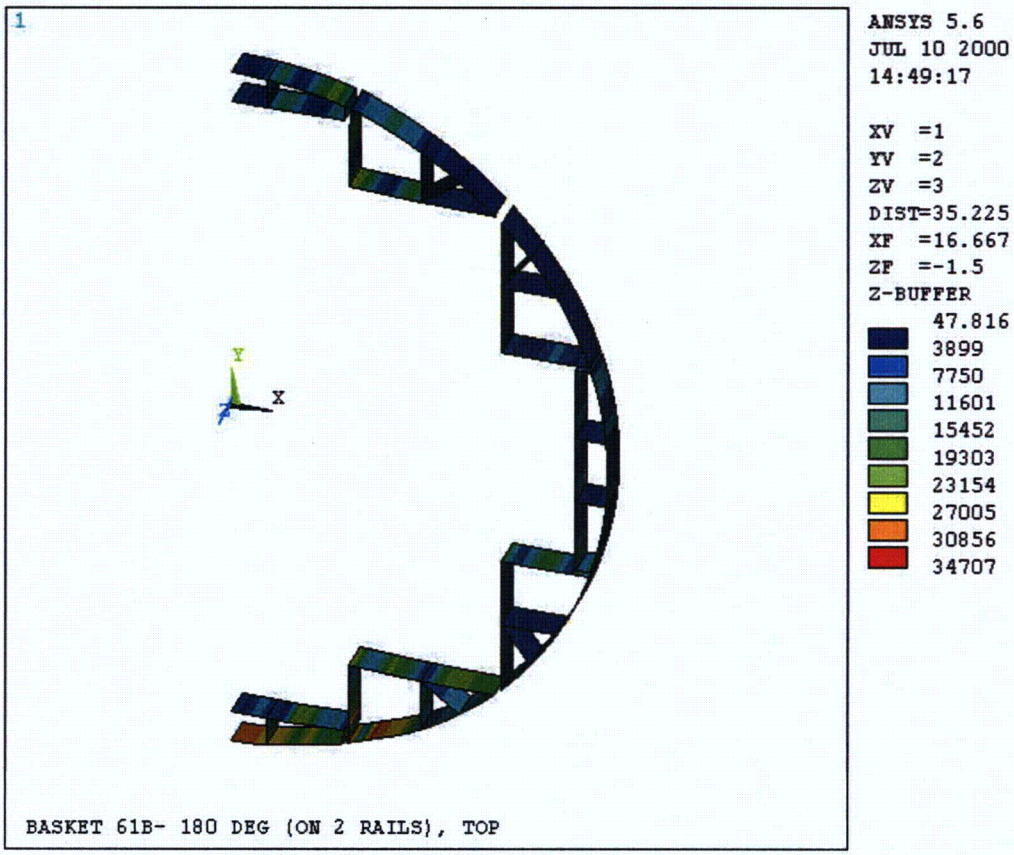

Figure T.3.7-32
180° Orientation Side Drop – Type 1 Rails, $P_m + P_b$ (75.5g)

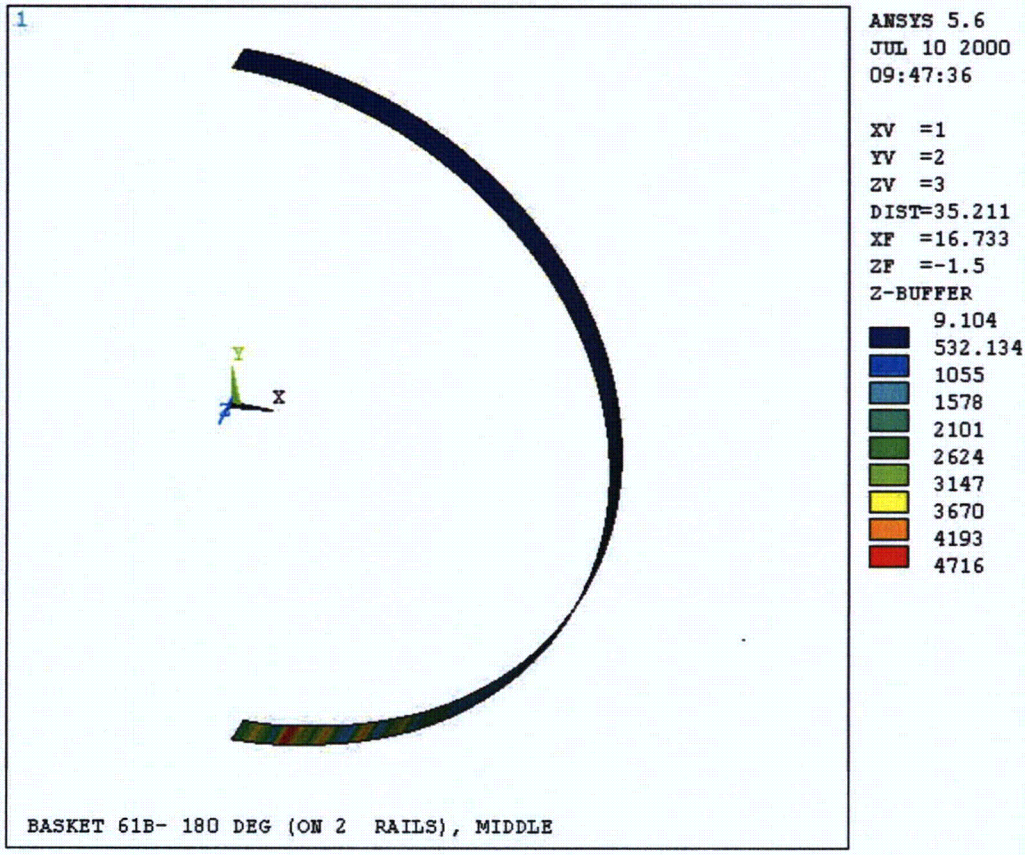

Figure T.3.7-33
180° Orientation side Drop – Type 1 Canister, P_m (75.5g)

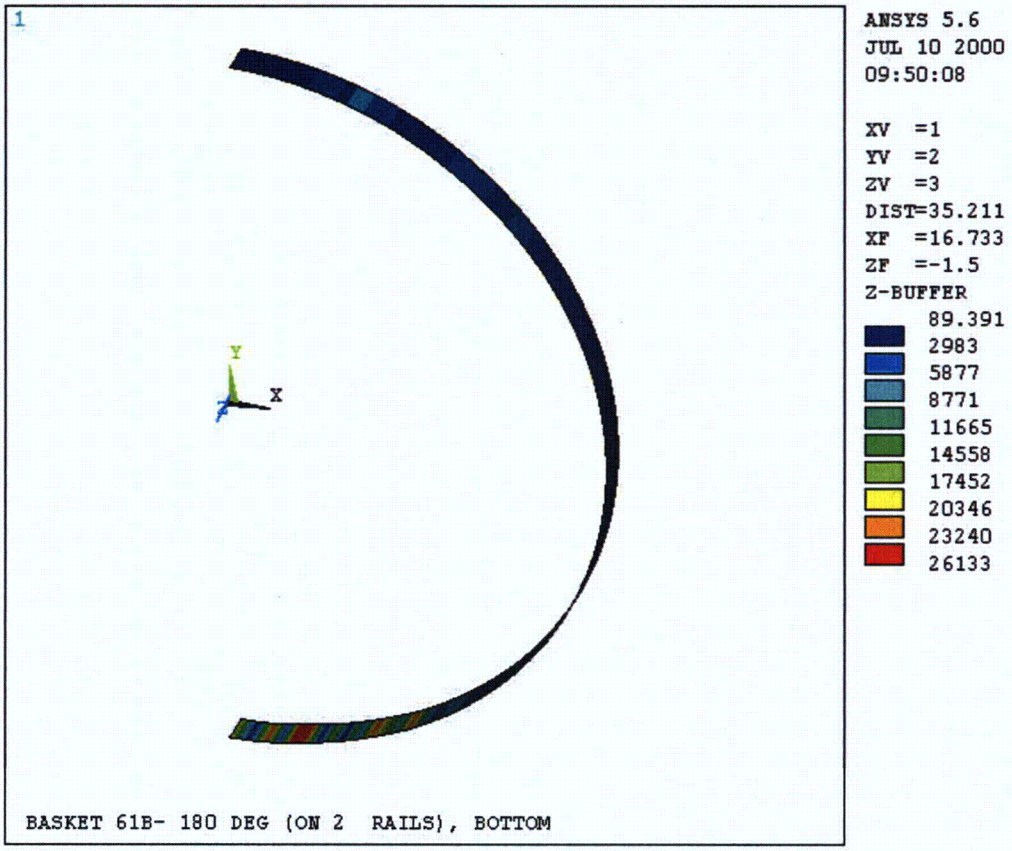

Figure T.3.7-34
180° Orientation Side Drop – Type 1 Canister, $P_m + P_b$ (75.5g)

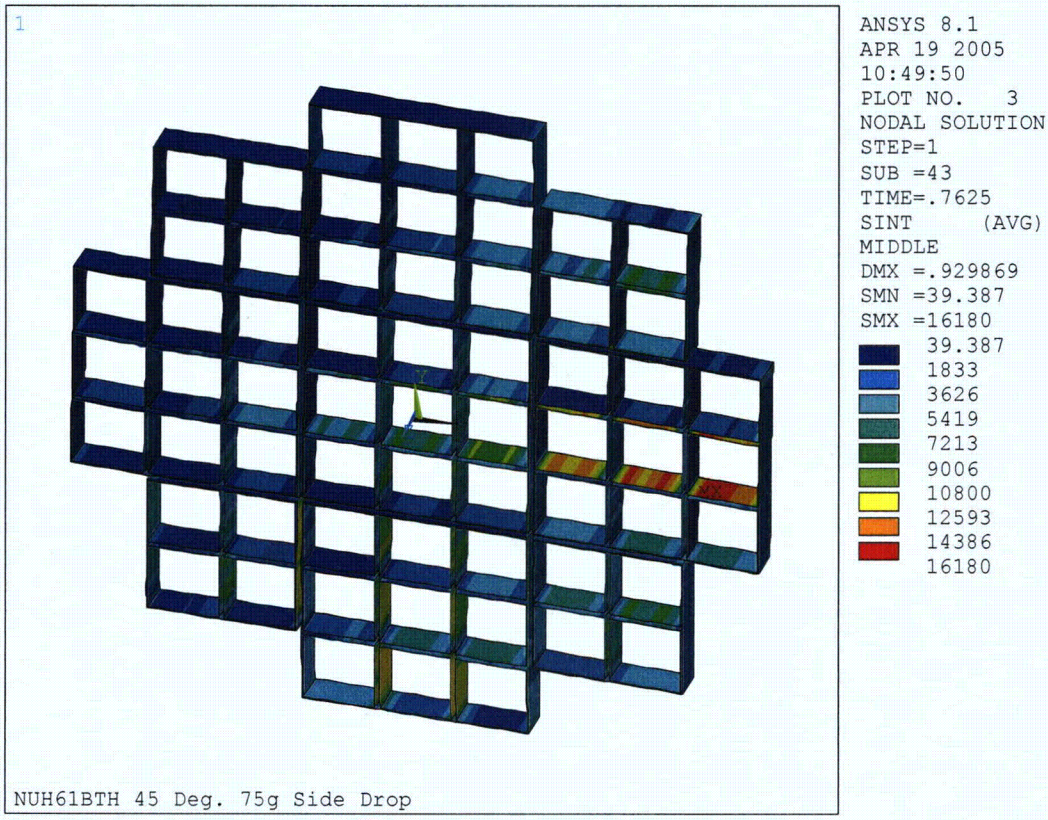

Figure T.3.7-35
45° Orientation – Type 2 Basket, P_m (76.25G)

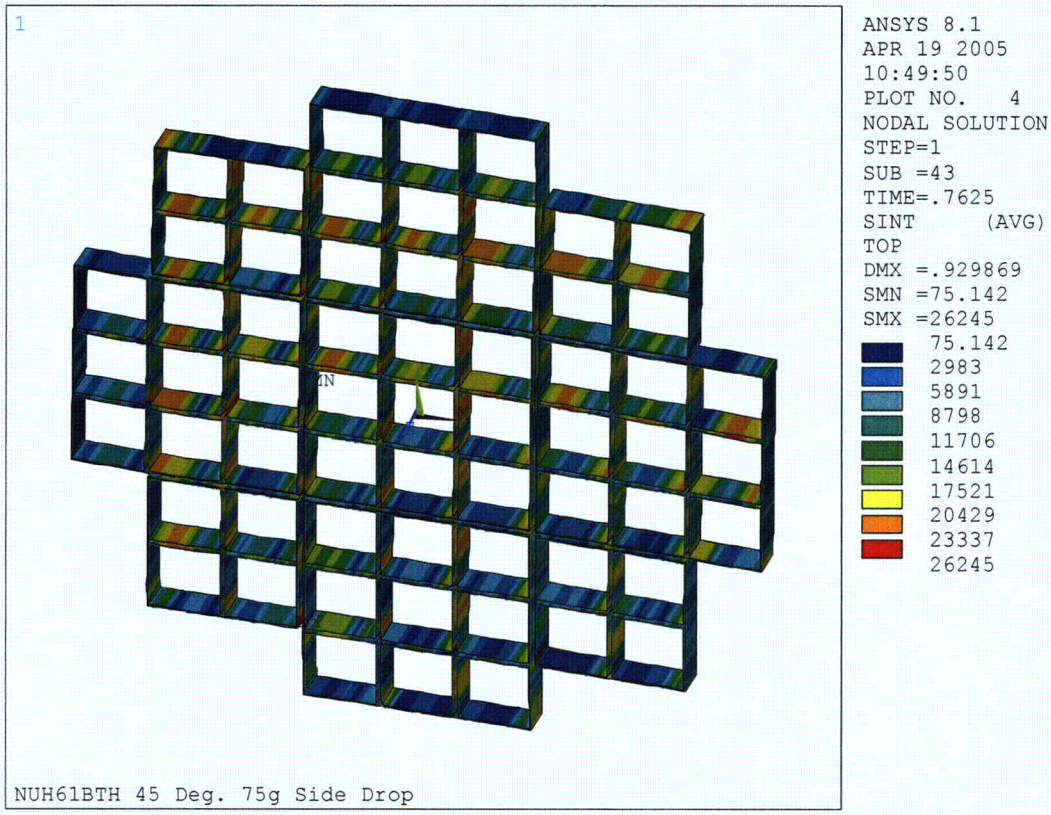

Figure T.3.7-36
45° Orientation – Type 2 Basket, $P_m + P_b$, Top (76.25G)

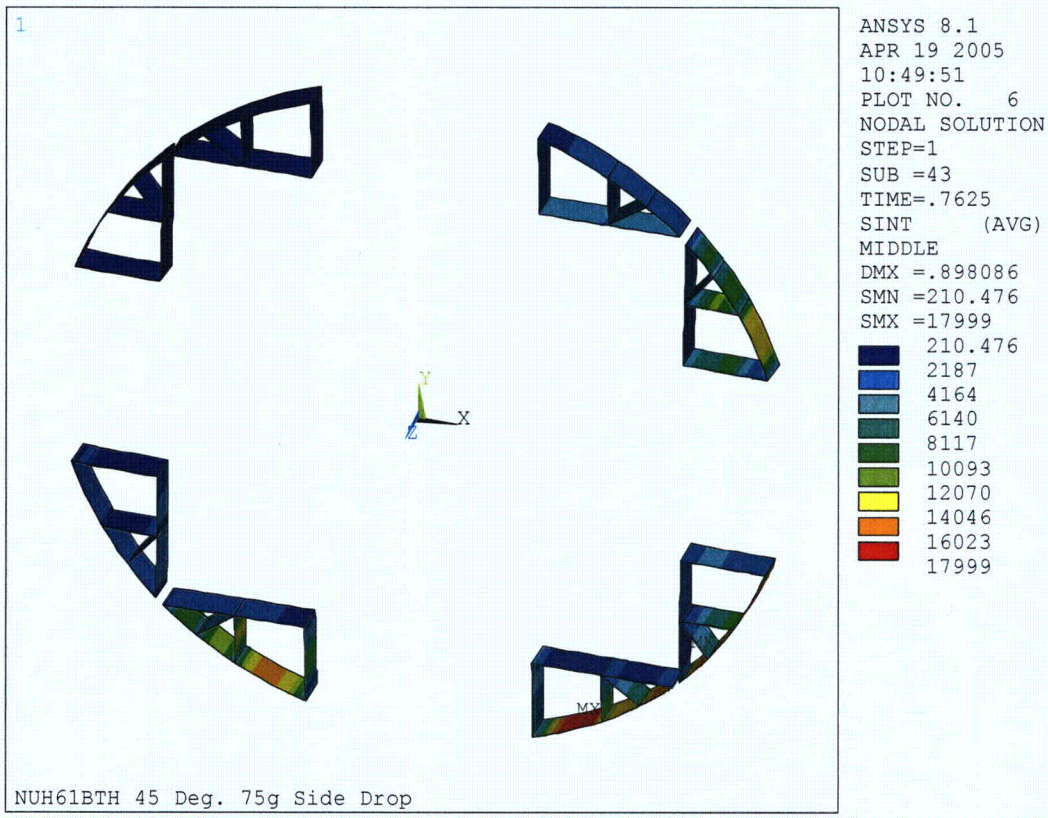

Figure T.3.7-37
45° Orientation – Type 2 Rails, P_m (76.25G)

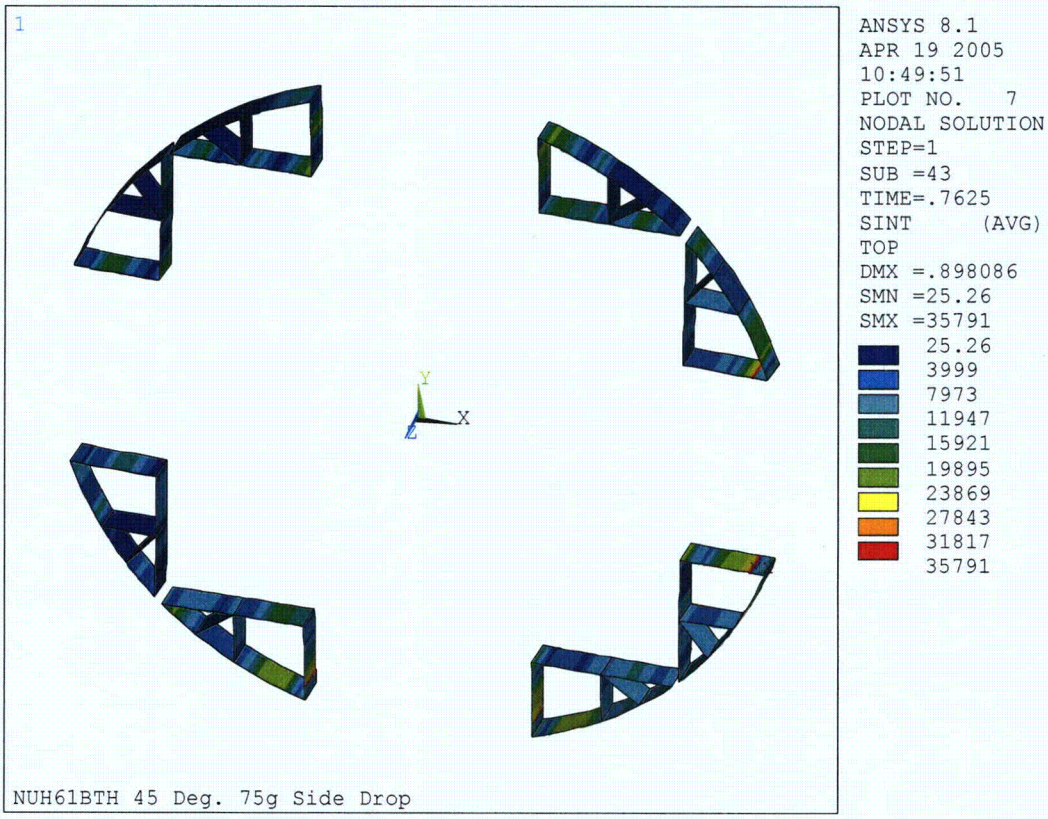

Figure T.3.7-38
45° Orientation – Type 2 Rails, $P_m + P_b$, Top (76.25G)

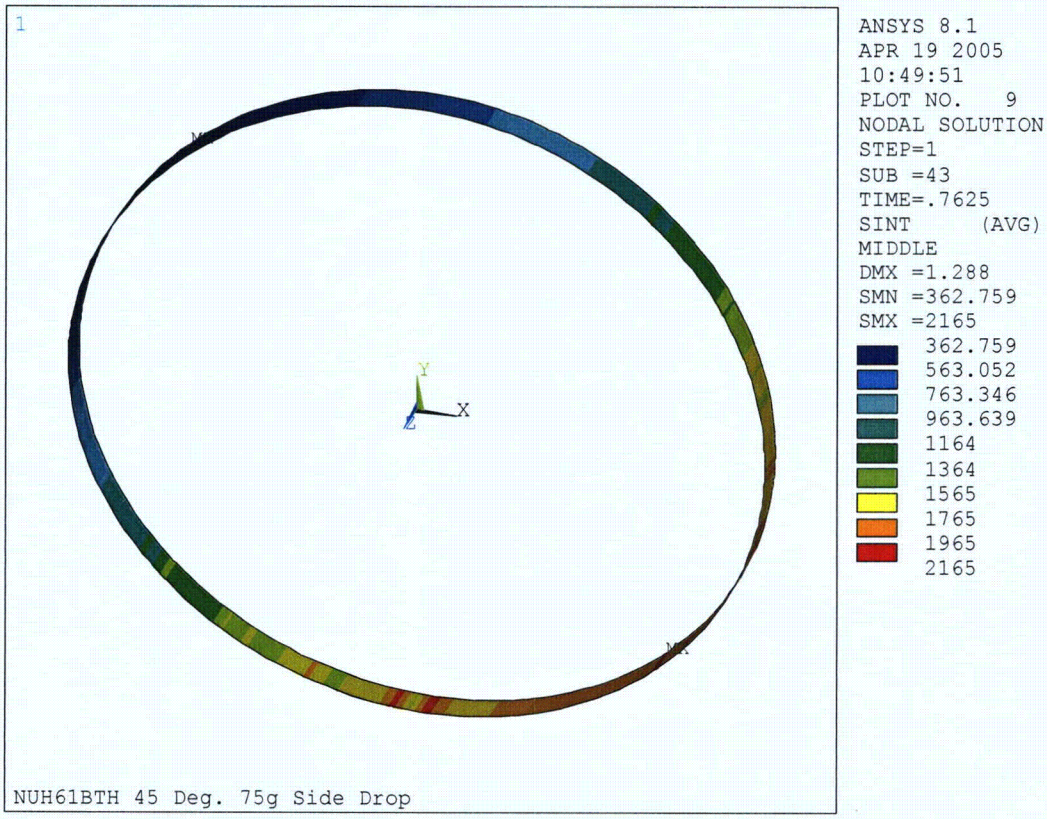

Figure T.3.7-39
45° Orientation – Type 2 Canister, P_m (76.25G)

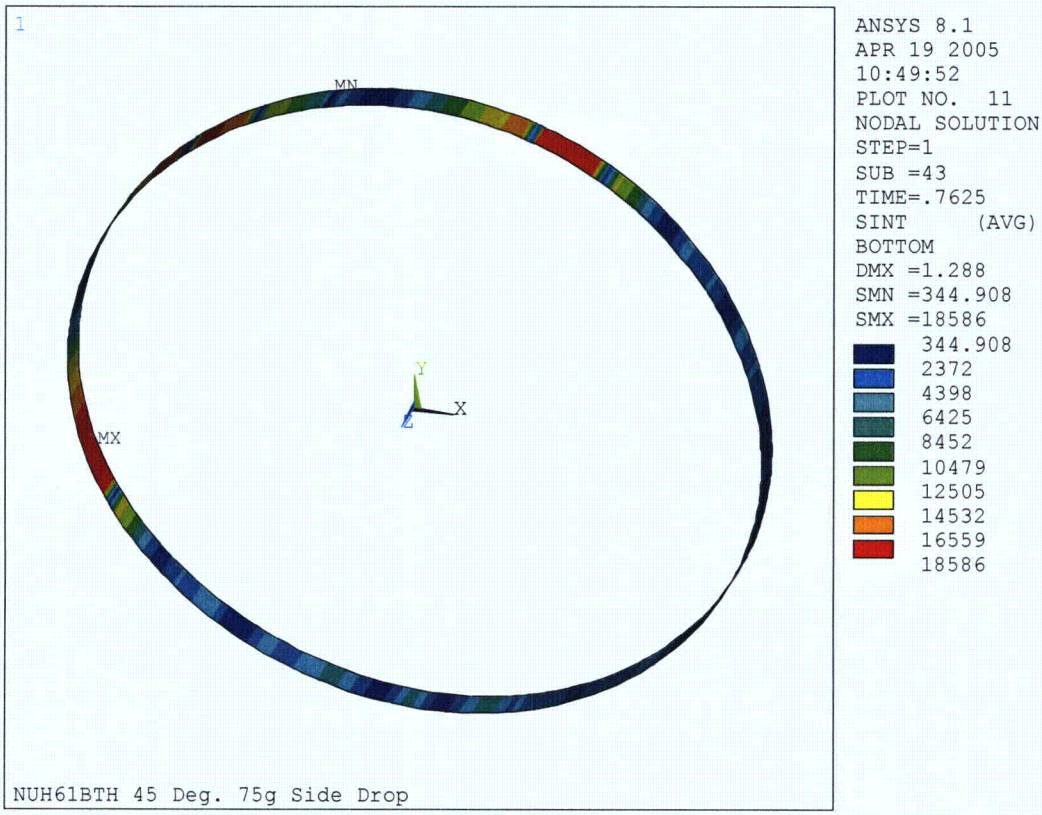

Figure T.3.7-40
45° Orientation – Type 2 Canister, $P_m + P_b$, Bottom (76.25G)

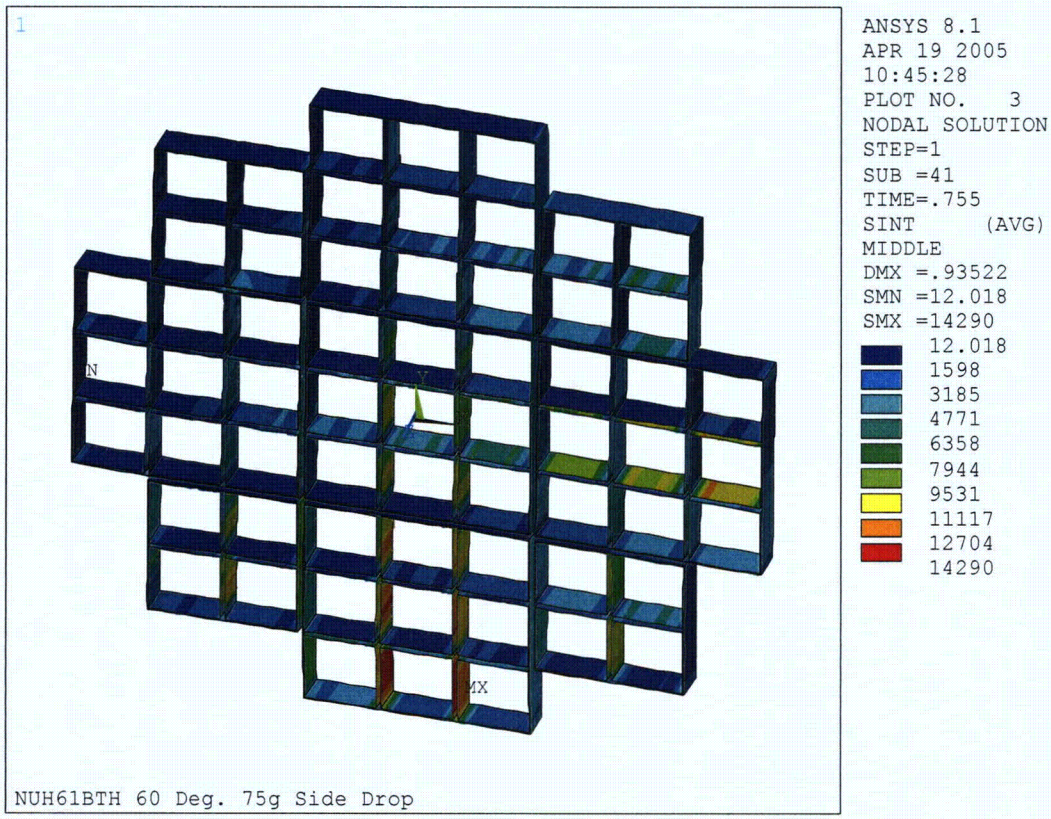

Figure T.3.7-41
60° Orientation – Type 2 Basket, P_m (75.5G)

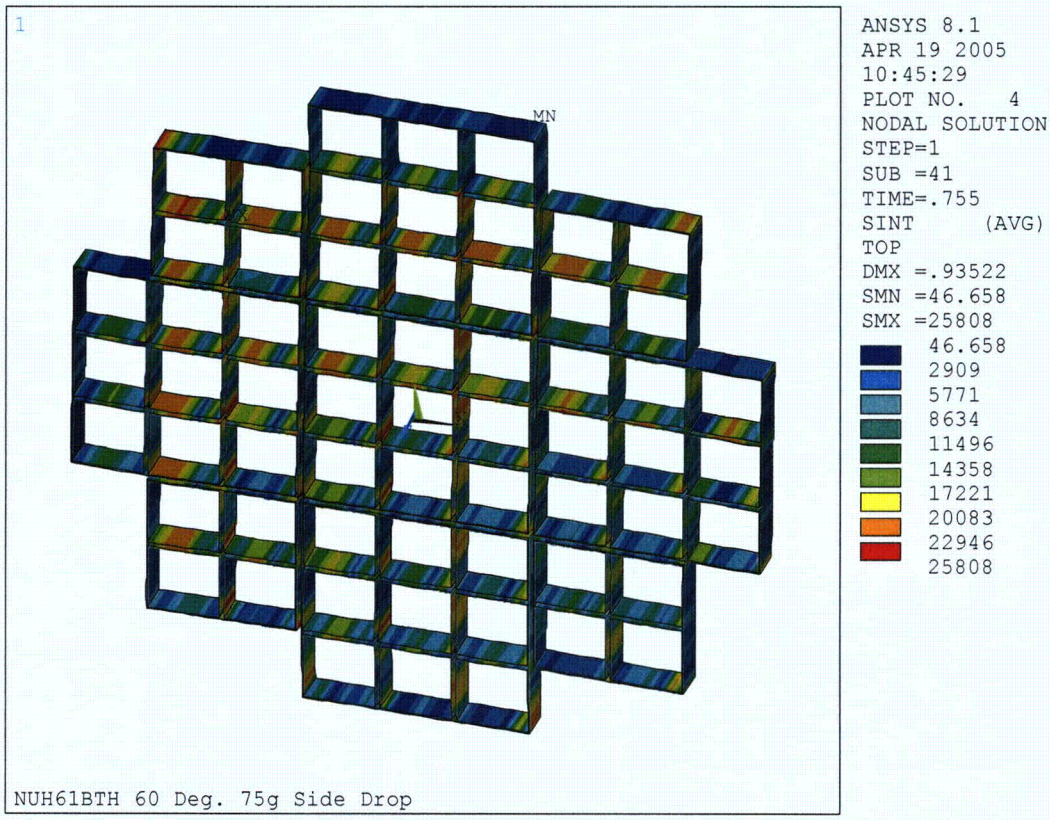

Figure T.3.7-42
60° Orientation – Type 2 Basket, $P_m + P_b$, Top (75.5G)

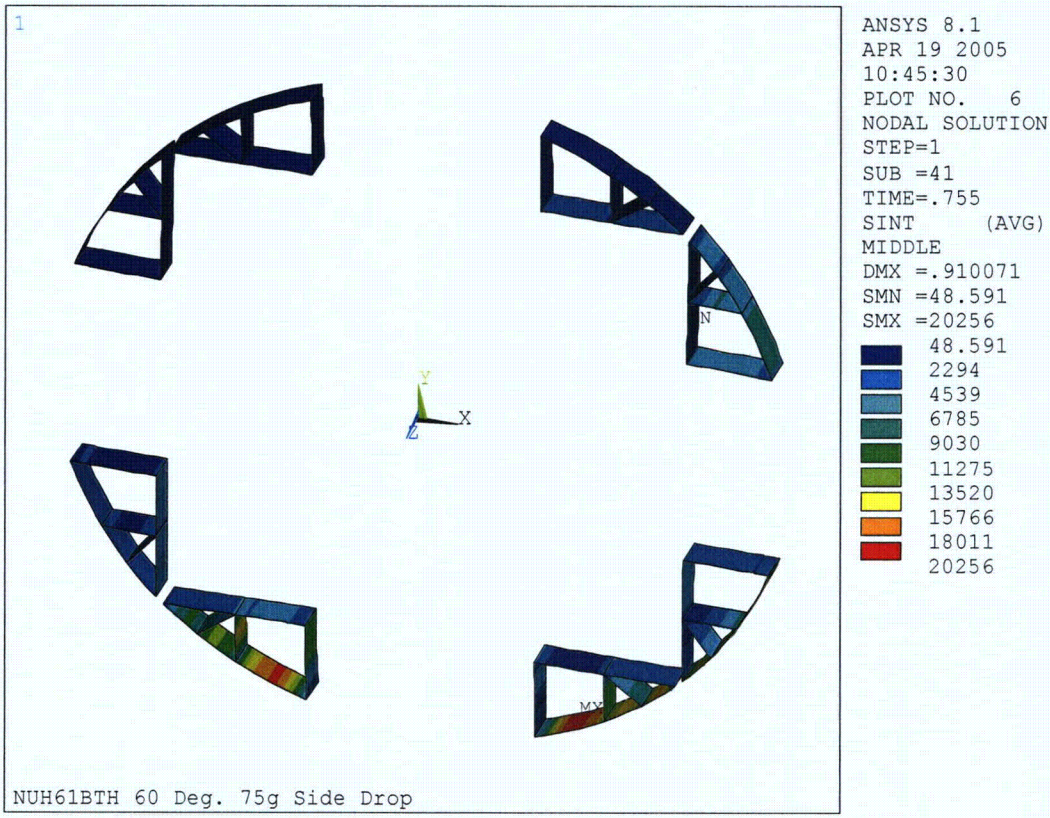

Figure T.3.7-43
60° Orientation – Type 2 Rails, P_m (75.5G)

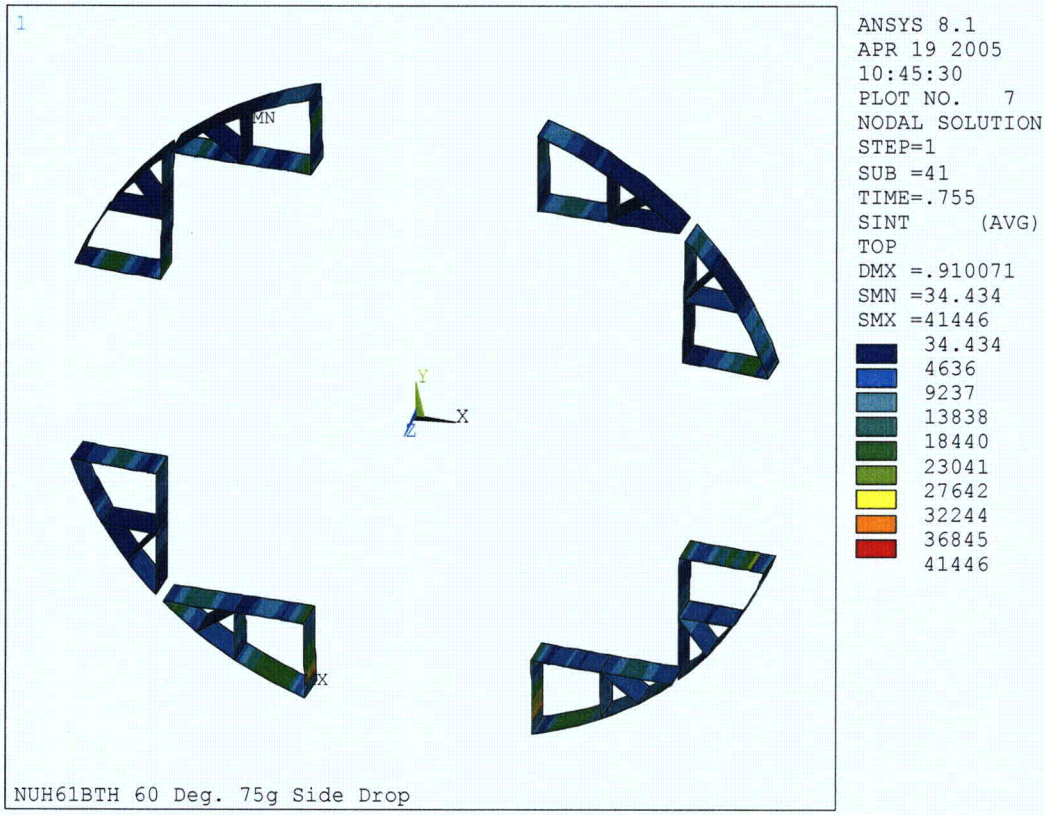

Figure T.3.7-44
60° Orientation – Type 2 Rails, $P_m + P_b$, Top (75.5G)

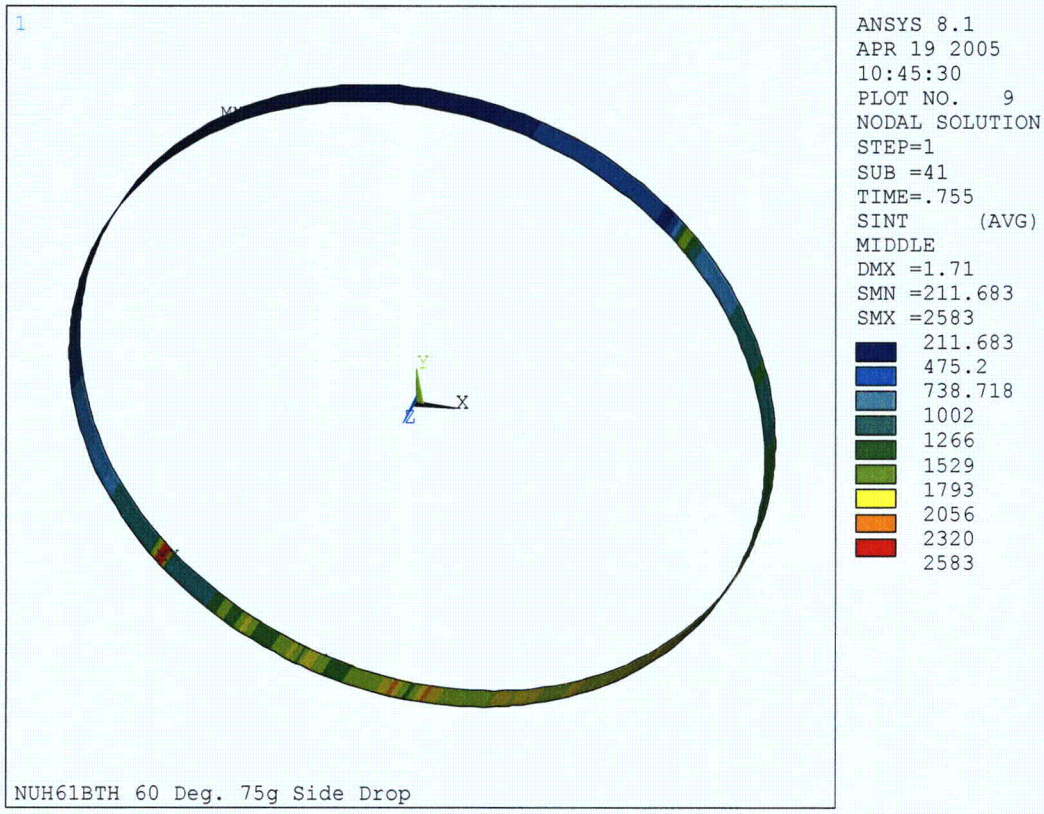

Figure T.3.7-45
60° Orientation – Type 2 Canister, P_m (75.5G)

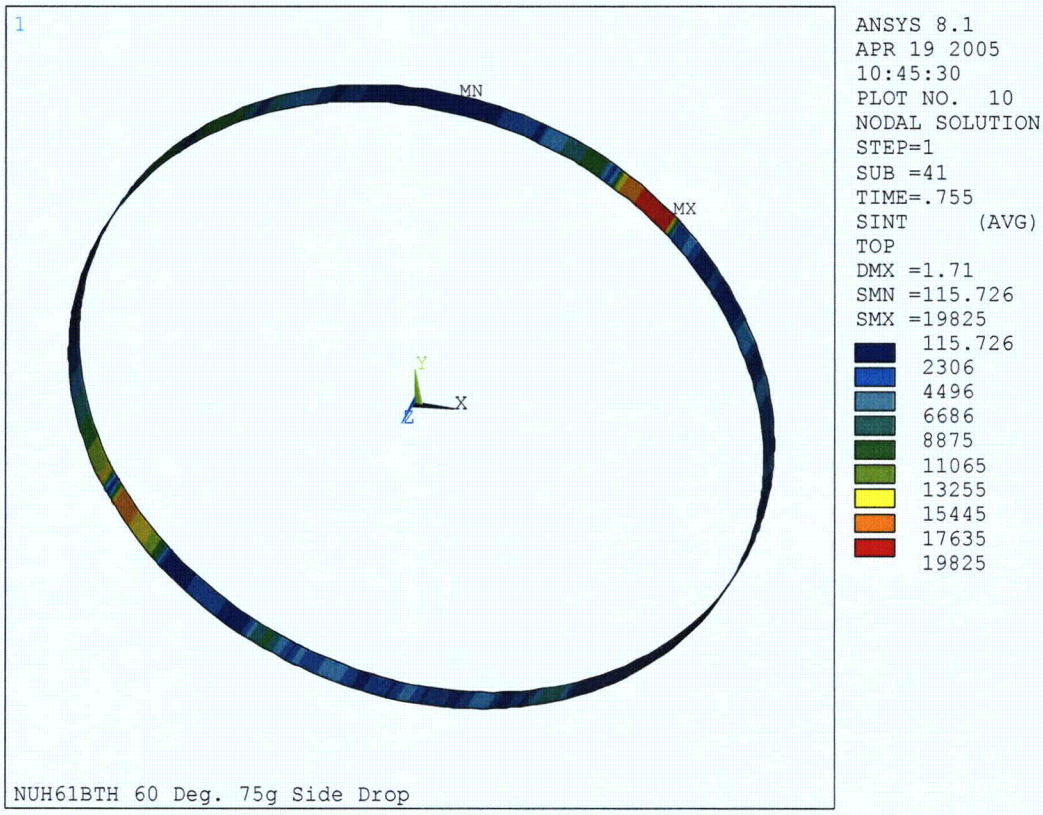

Figure T.3.7-46
60° Orientation – Type 2 Canister, $P_m + P_b$, Top (75.5G)

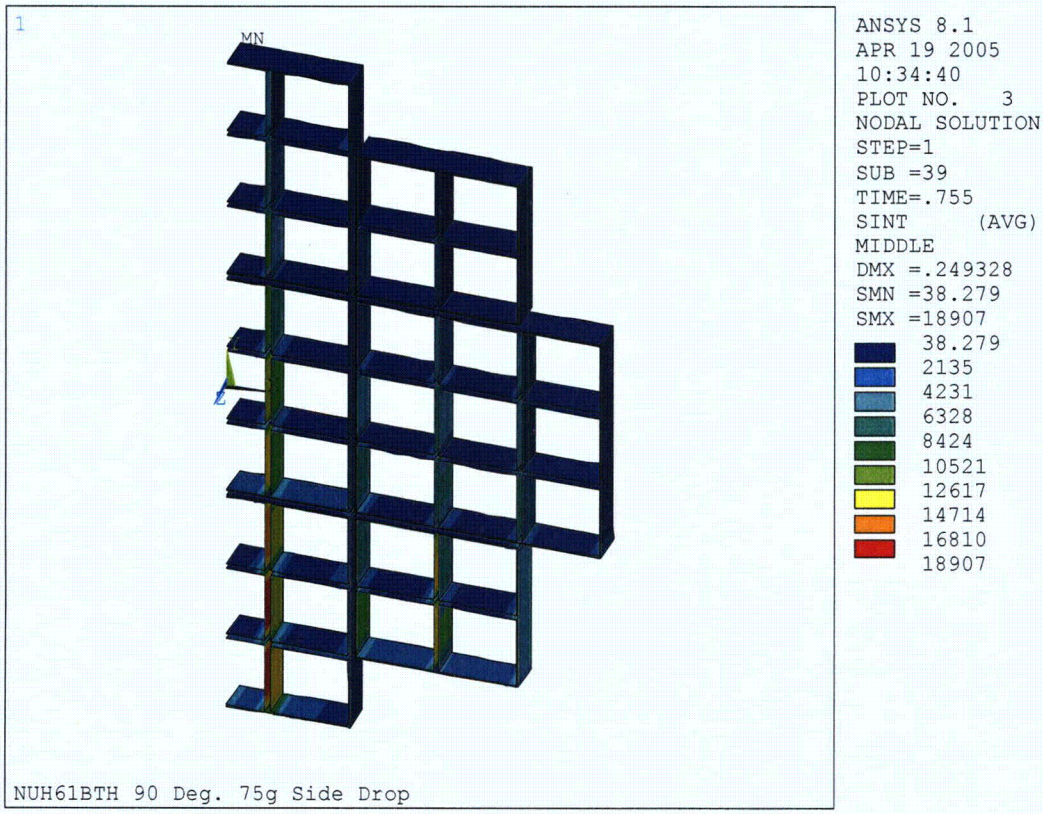

Figure T.3.7-47
90° Orientation – Type 2 Basket, P_m (75.5G)

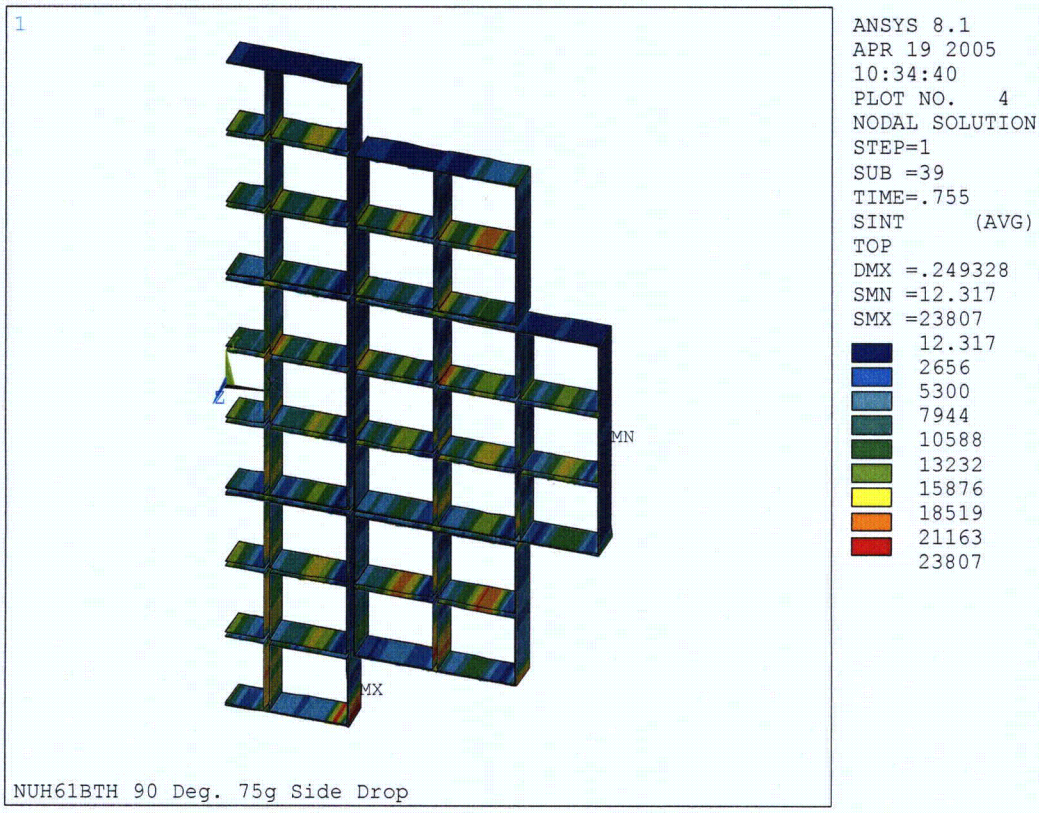

Figure T.3.7-48
90° Orientation – Type 2 Basket, $P_m + P_b$, Top (75.5G)

Figure T.3.7-49
90° Orientation – Type 2 Rails, P_m (75.5G)

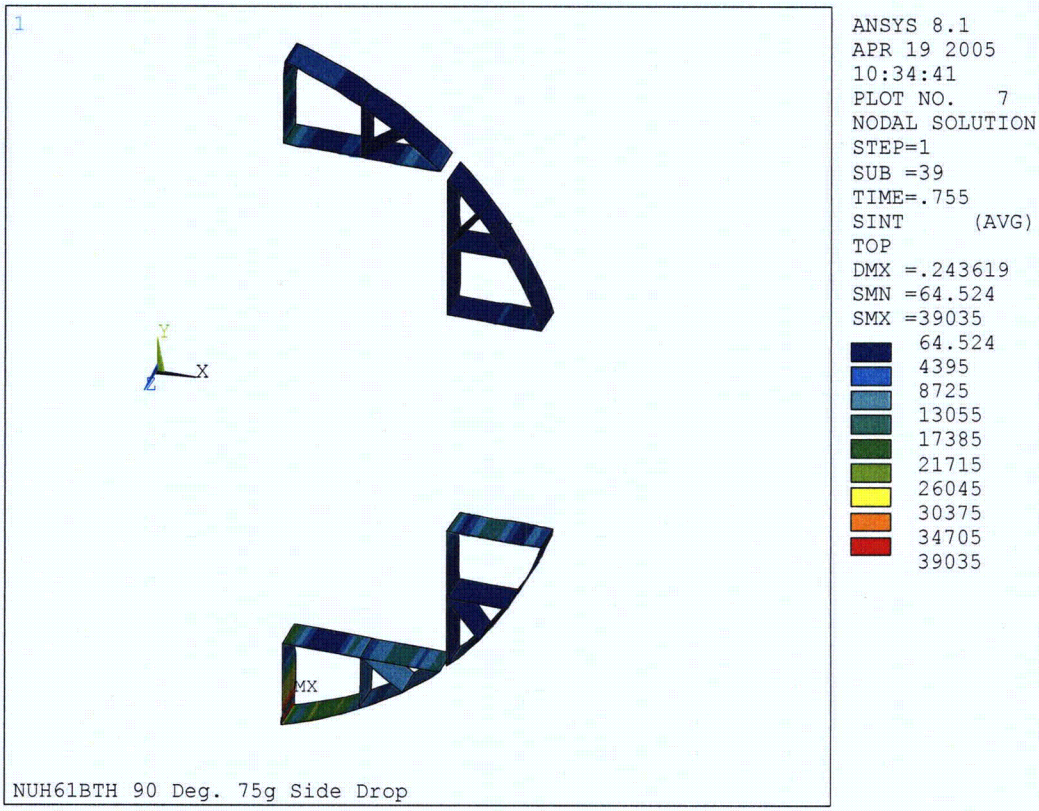

Figure T.3.7-50
90° Orientation – Type 2 Rails, $P_m + P_b$, Top (75.5G)

Figure T.3.7-51
90° Orientation – Type 2 Canister, P_m (75.5G)

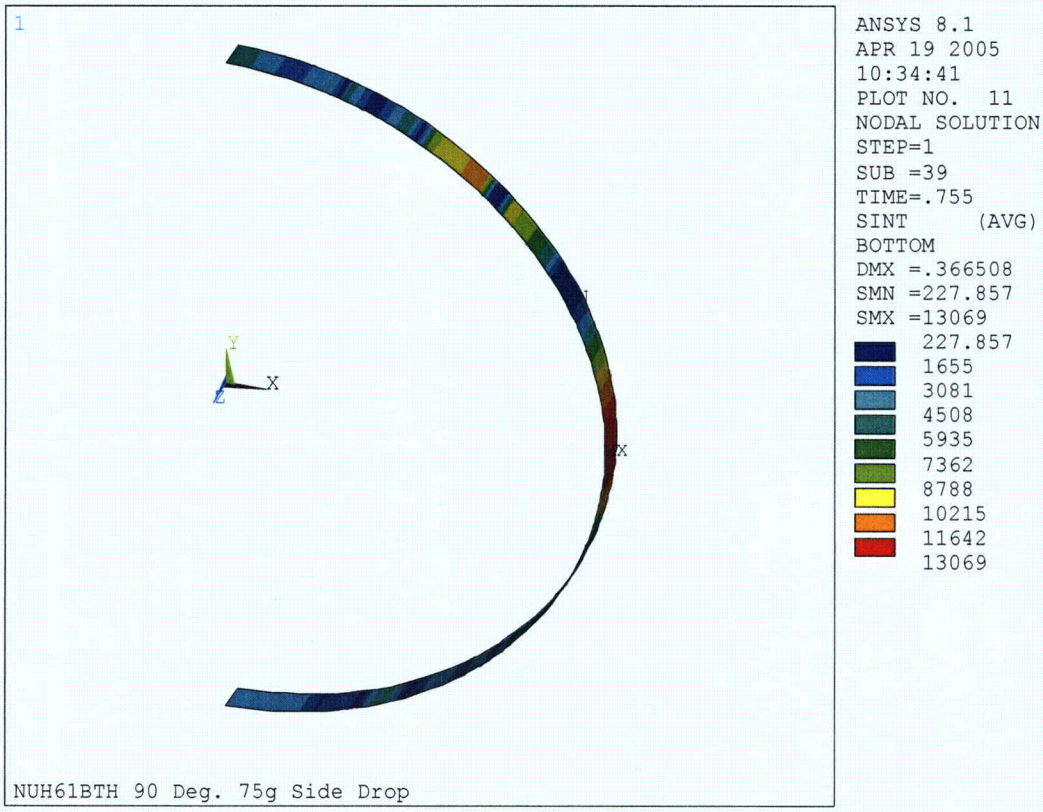

Figure T.3.7-52
90° Orientation – Type 2 Canister, $P_m + P_b$, Bottom (75.5G)

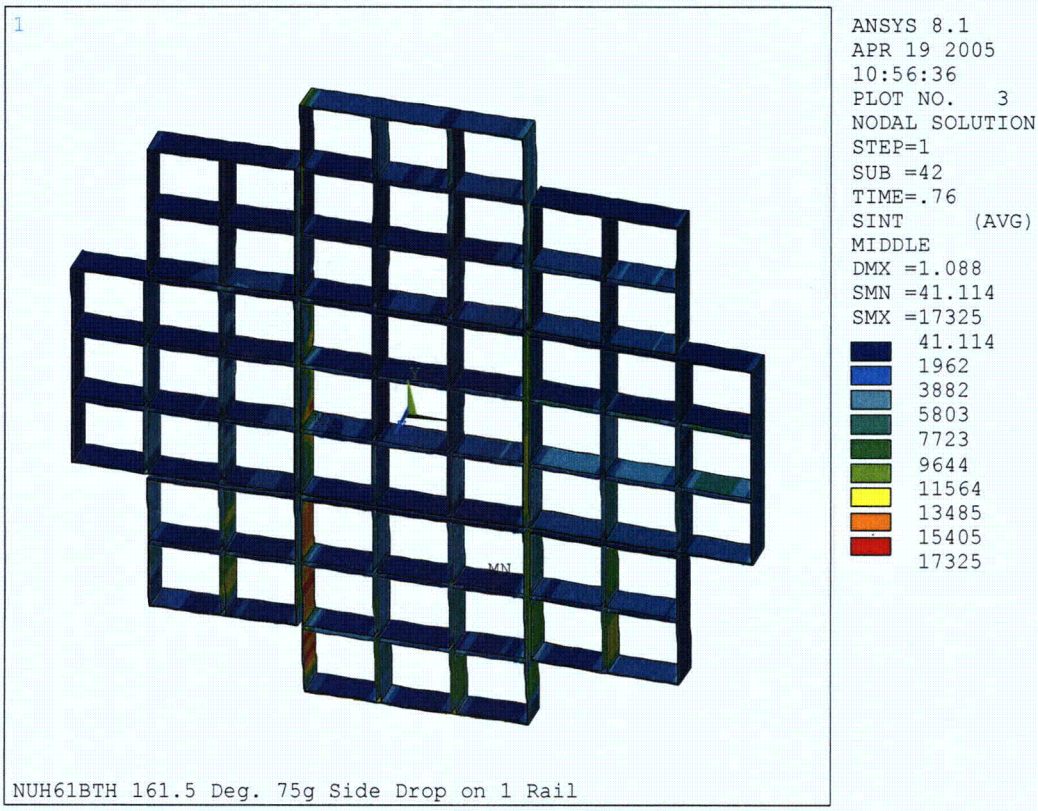

Figure T.3.7-53
161.5° Orientation – Type 2 Basket, P_m (76.0G)

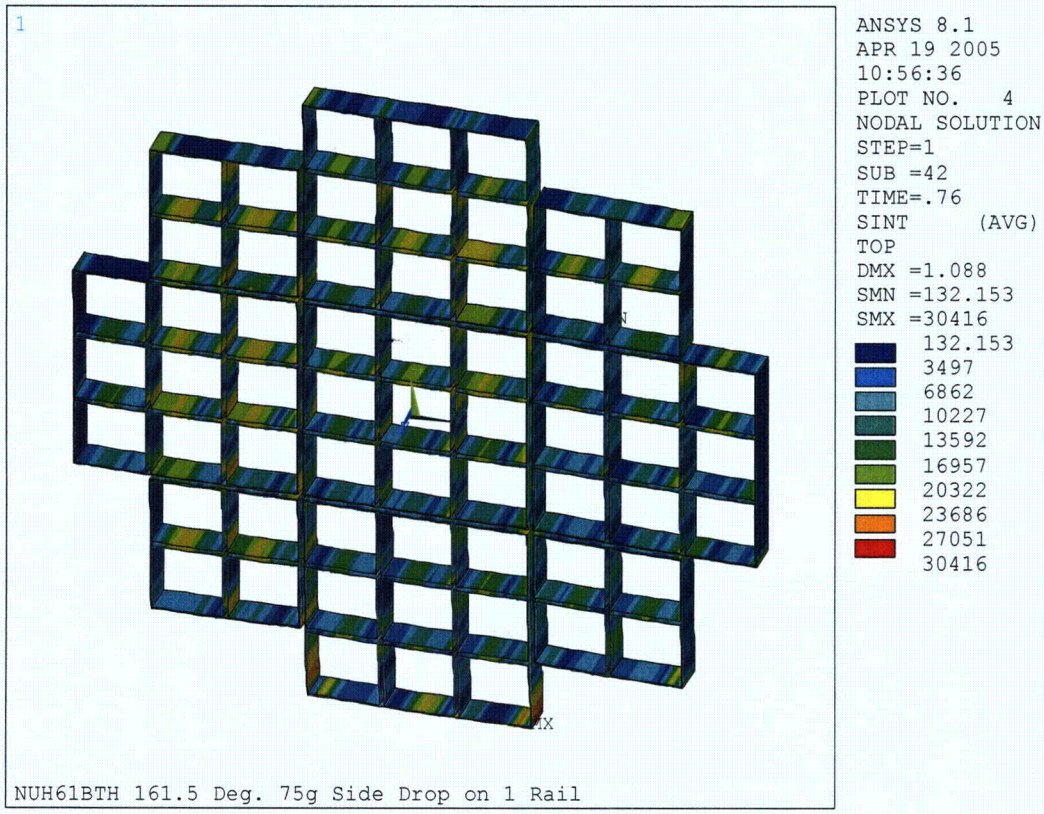

Figure T.3.7-54
161.5° Orientation – Type 2 Basket, $P_m + P_b$, Top (76.0G)

Figure T.3.7-55
161.5° Orientation – Type 2 Rails, P_m (76.0G)

Figure T.3.7-56
161.5° Orientation – Type 2 Rails, $P_m + P_b$, Top (76.0G)

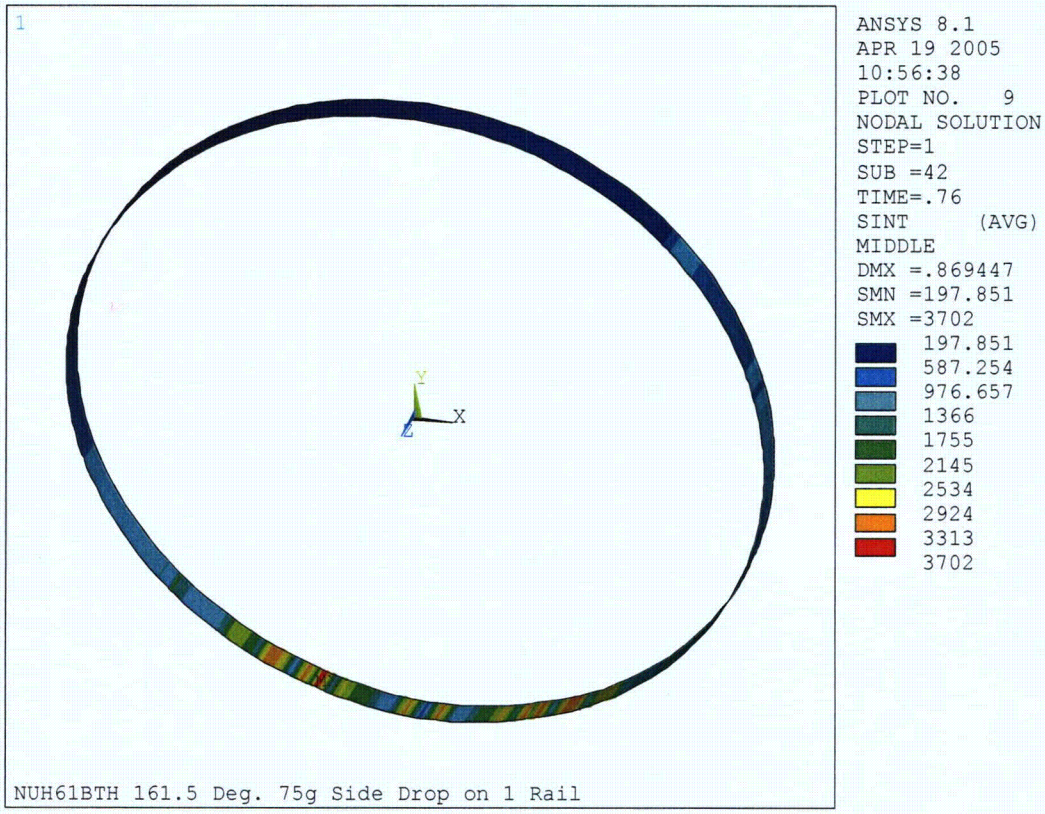

Figure T.3.7-57
161.5° Orientation – Type 2 Canister, P_m (76.0G)

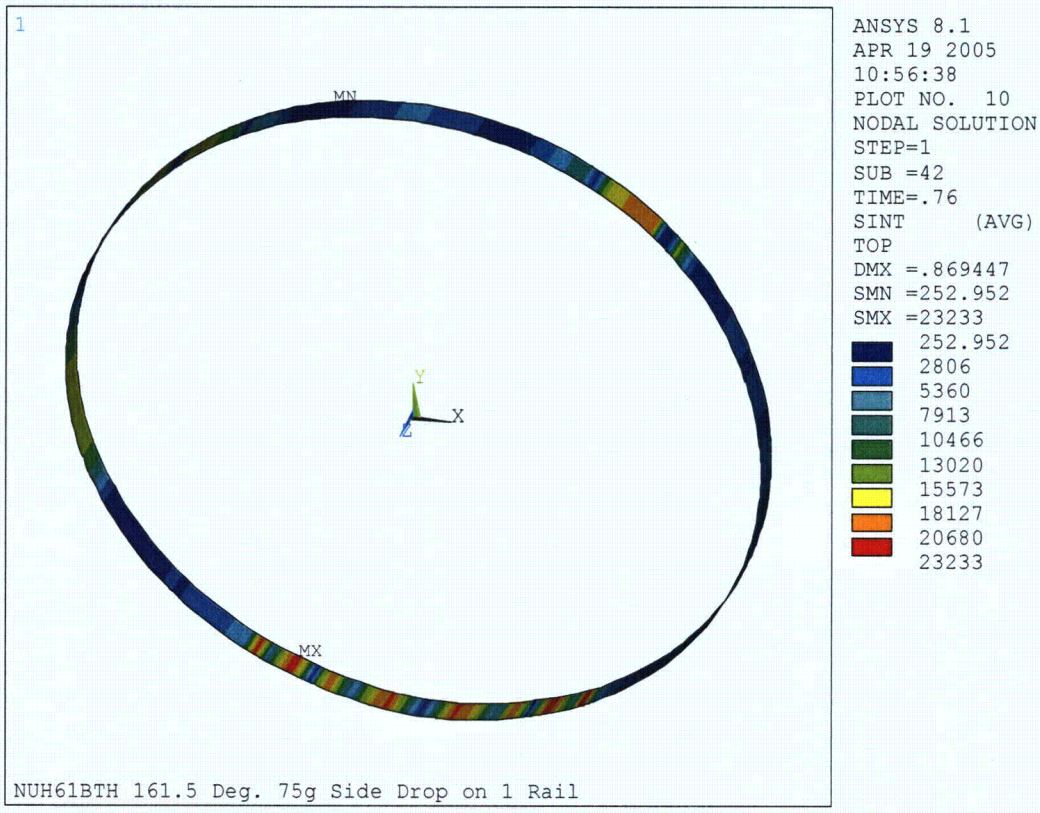

Figure T.3.7-58
161.5° Orientation – Type 2 Canister, $P_m + P_b$, Top (76.0G)

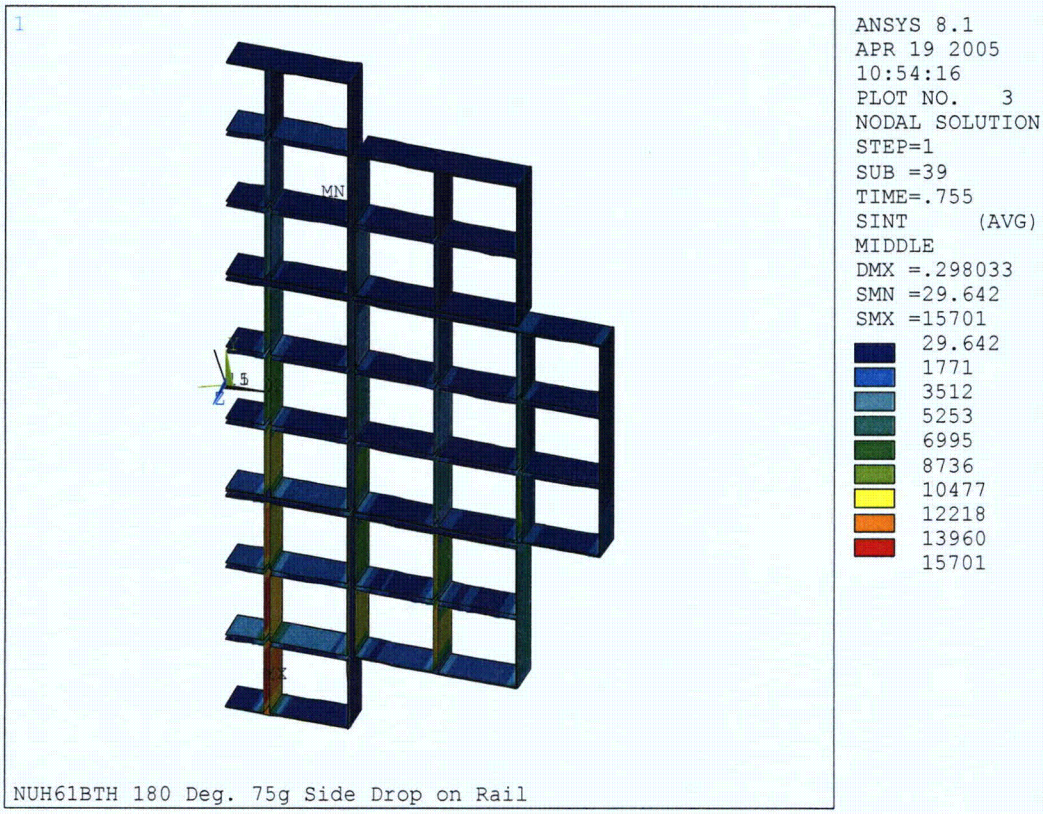

Figure T.3.7-59
180° Orientation – Type 2 Basket, P_m (75.5G)

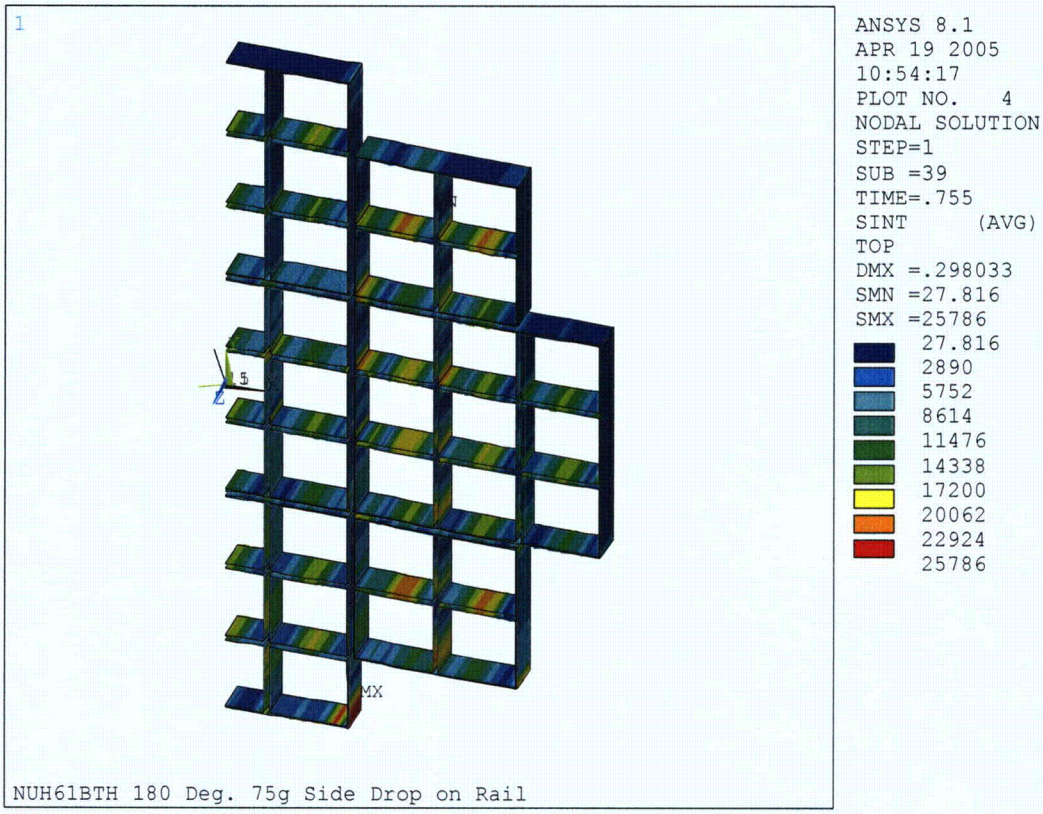

Figure T.3.7-60
180° Orientation – Type 2 Basket, $P_m + P_b$, Top (75.5G)

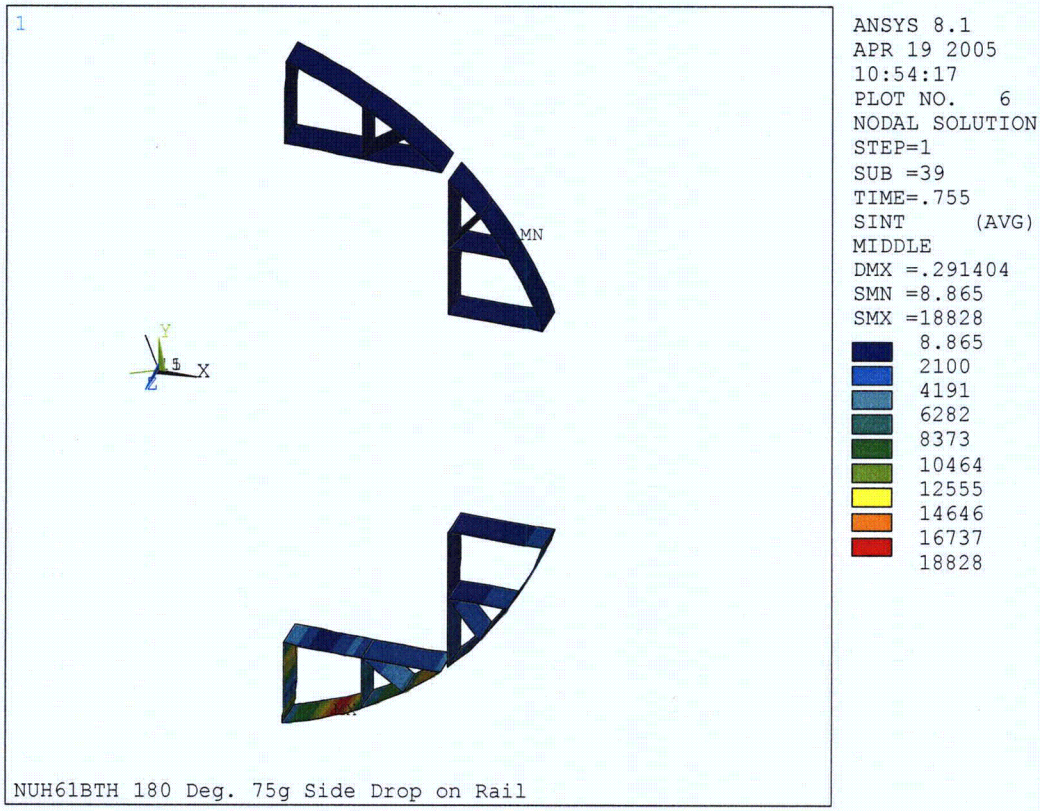

Figure T.3.7-61
180° Orientation – Type 2 Rails, P_m (75.5G)

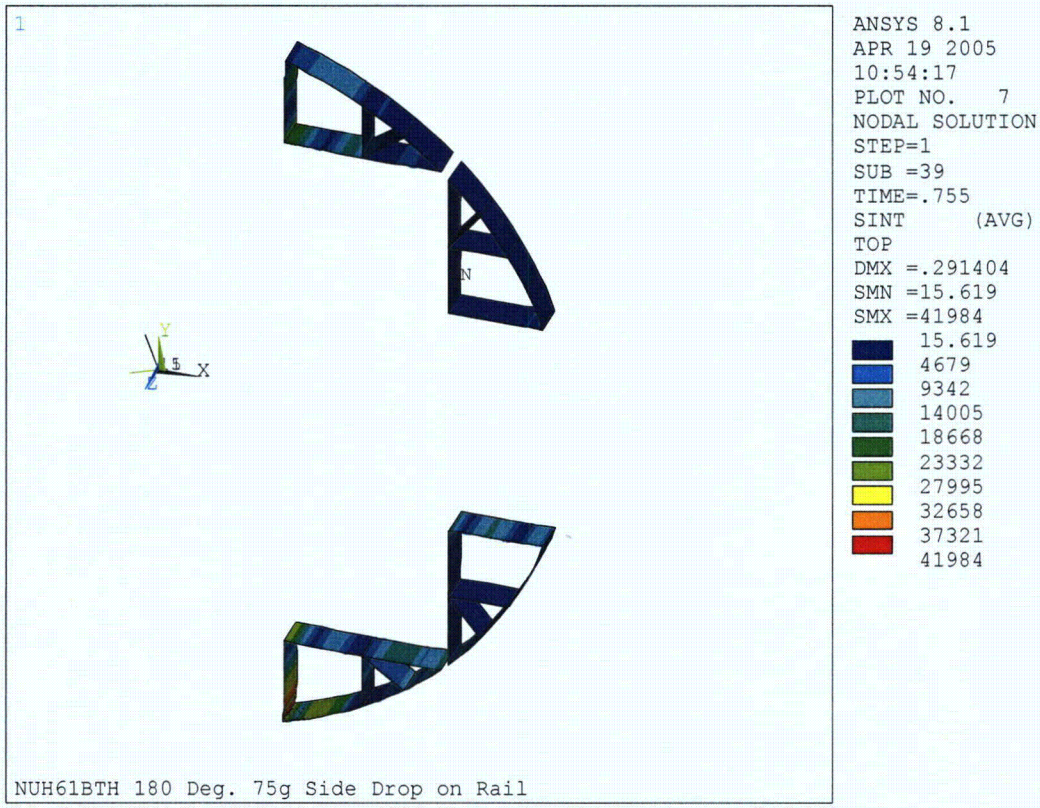

Figure T.3.7-62
180° Orientation – Type 2 Rails, $P_m + P_b$, Top (75.5G)

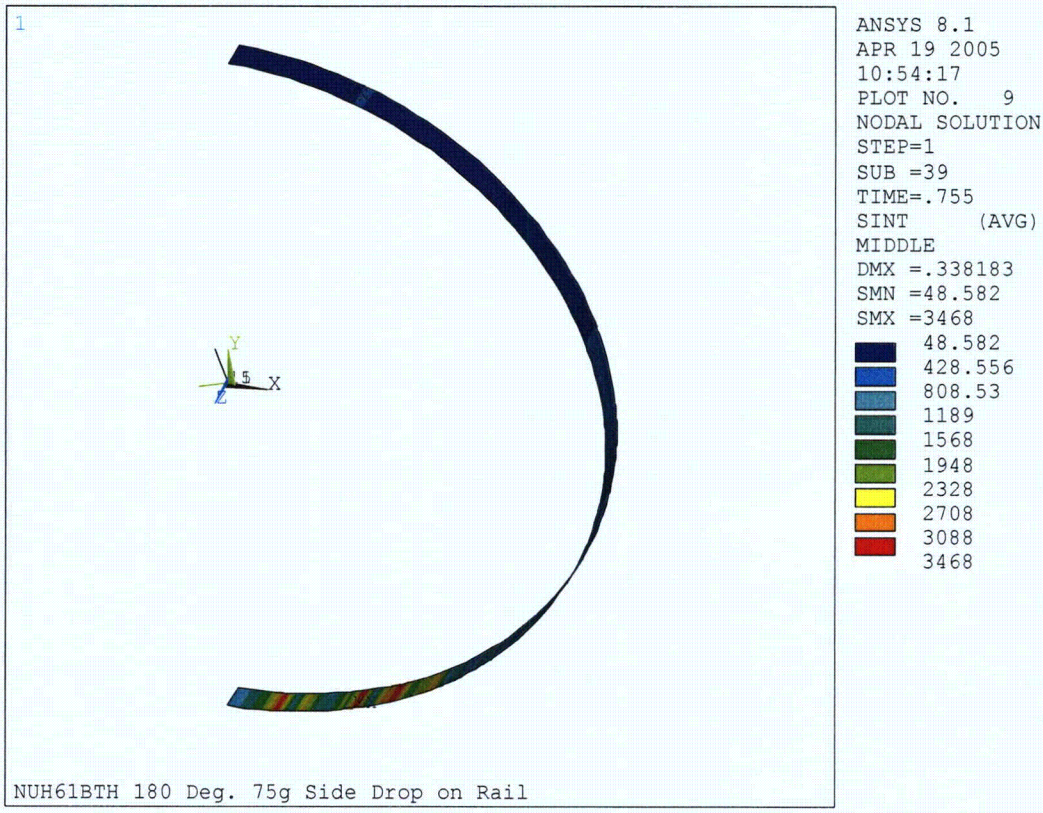

Figure T.3.7-63
180° Orientation – Type 2 Canister, P_m (75.5G)

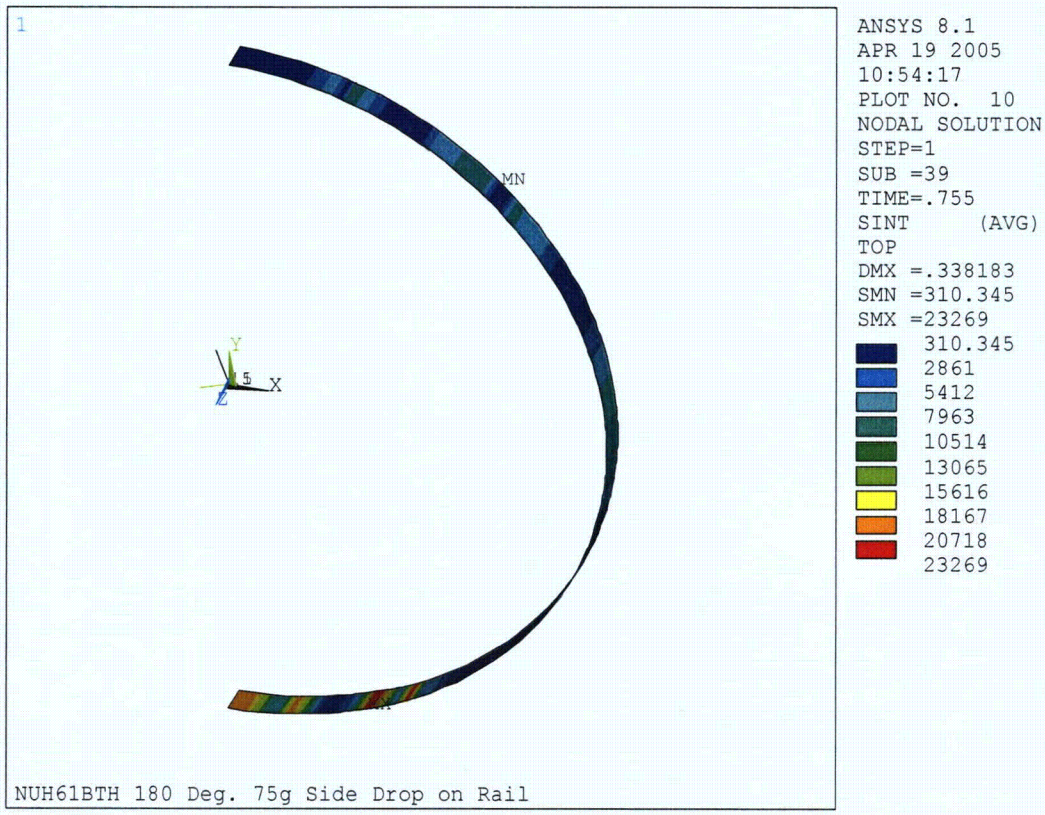

Figure T.3.7-64
180° Orientation – Type 2 Canister, $P_m + P_b$, Top (75.5G)

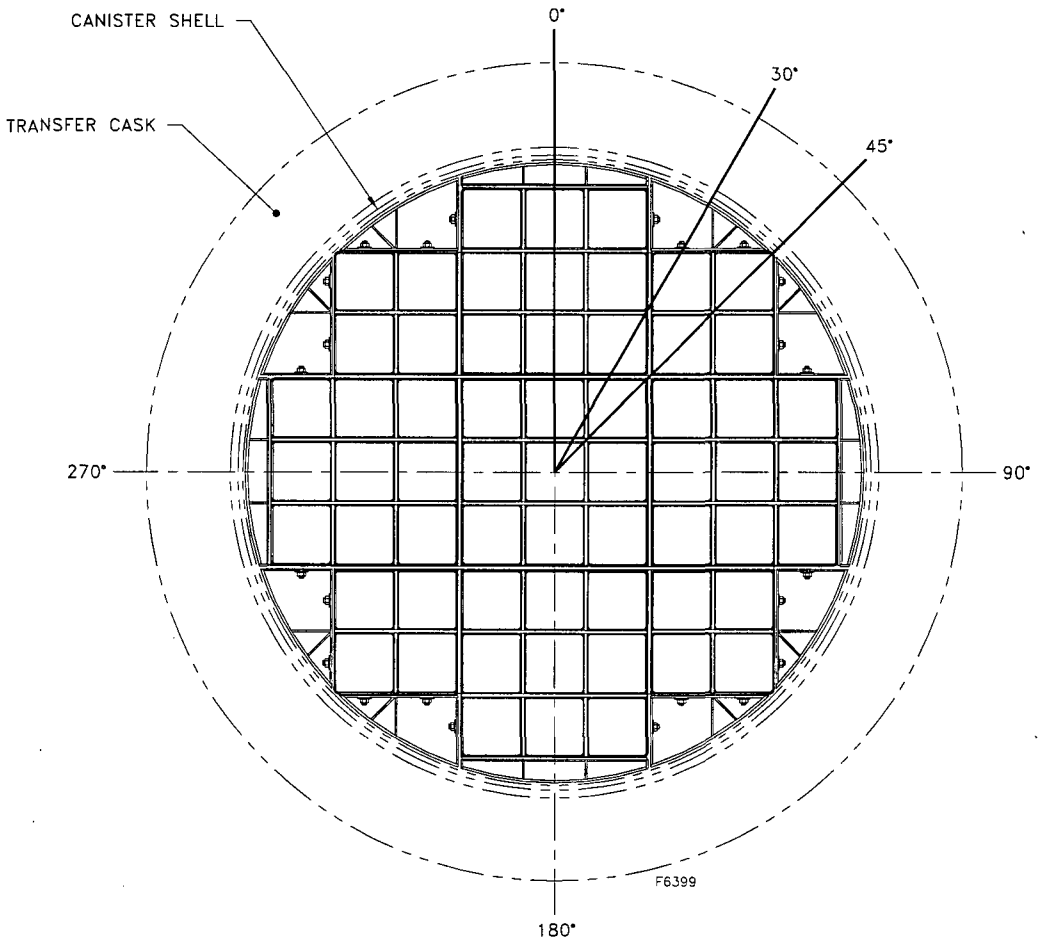

Figure T.3.7-65
NUHOMS®-61BTH Basket Drop Orientations

0°, 30°, 45°
(Type 1 shown, Type 2 is similar)

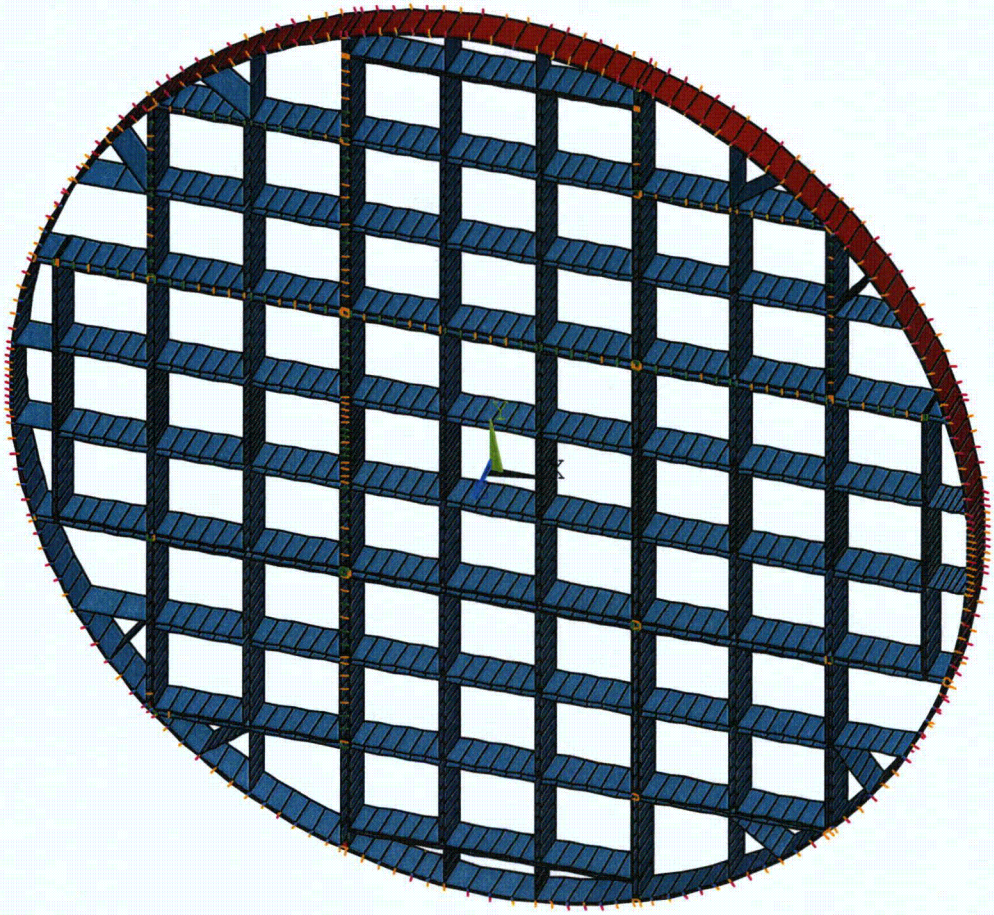

Figure T.3.7-66
Finite Element Model – Full (Type 1 Basket)

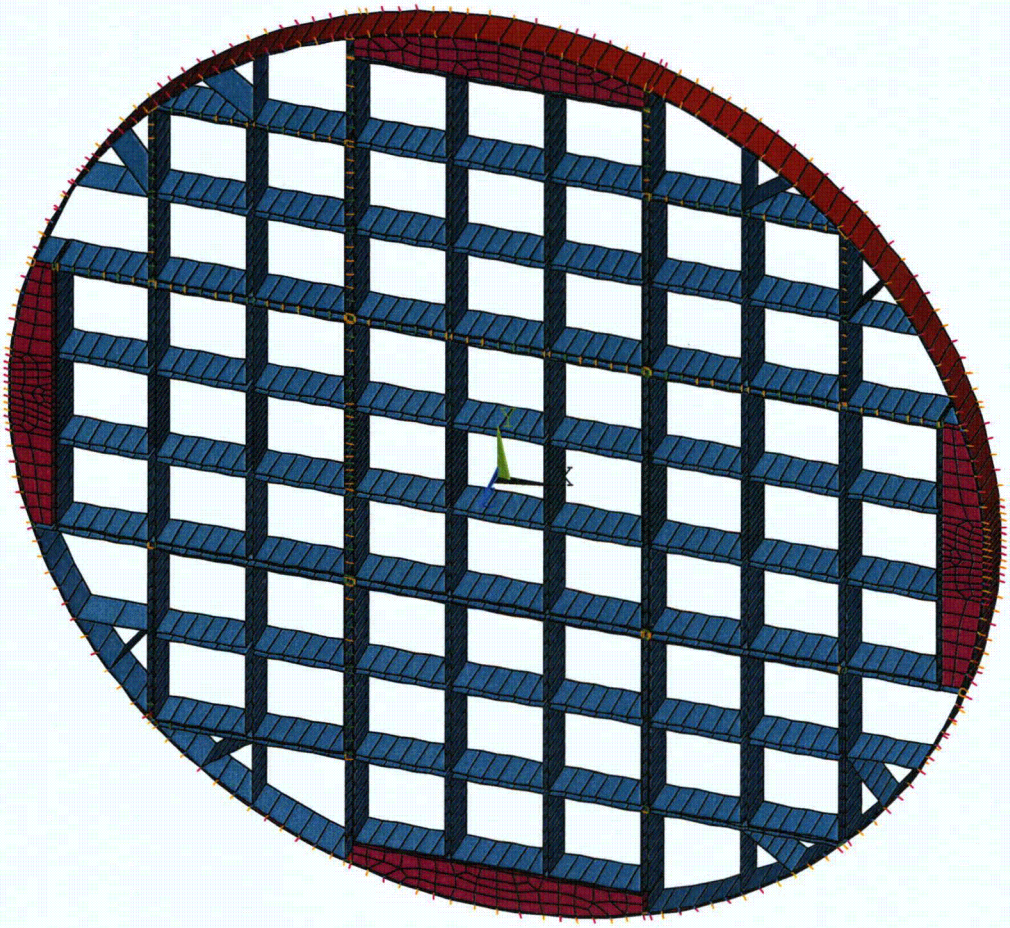

Figure T.3.7-67
Finite Element Model – Full (Type 2 Basket)

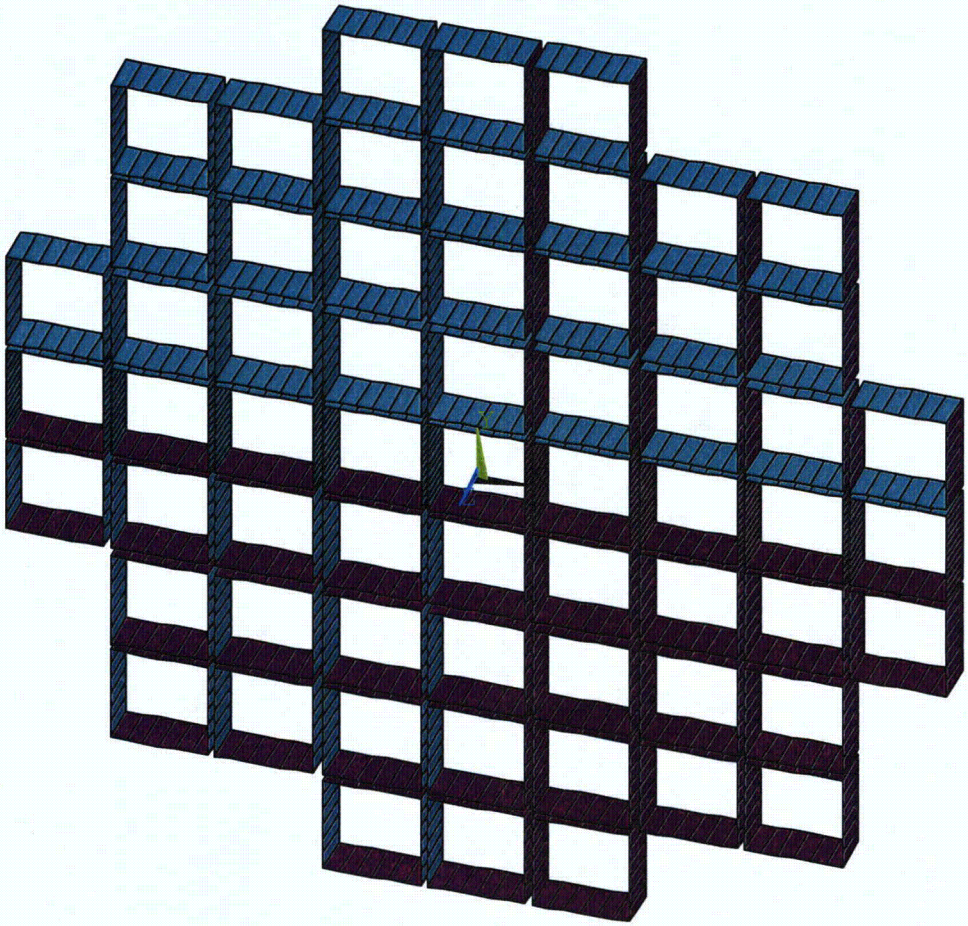

Figure T.3.7-68
Finite Element Model - Inner Boxes

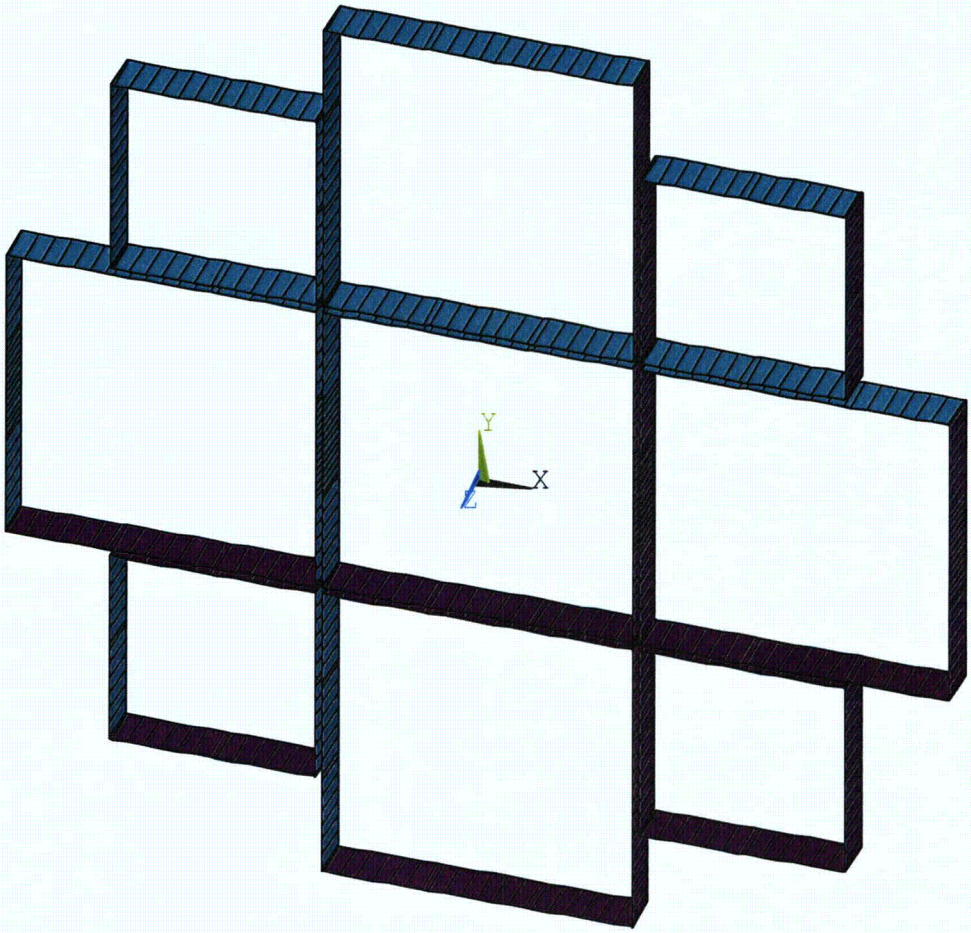

Figure T.3.7-69
Finite Element Model - Outer Boxes

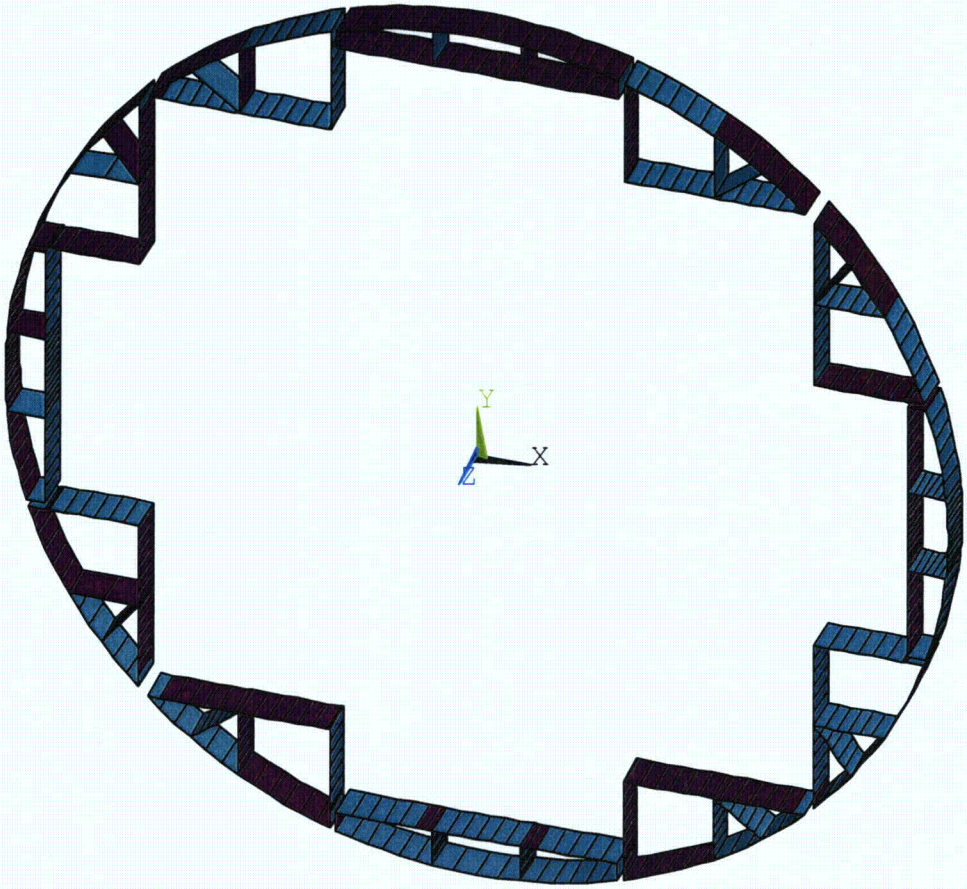

Figure T.3.7-70
Finite Element Model – Rails (Type 1 Basket)

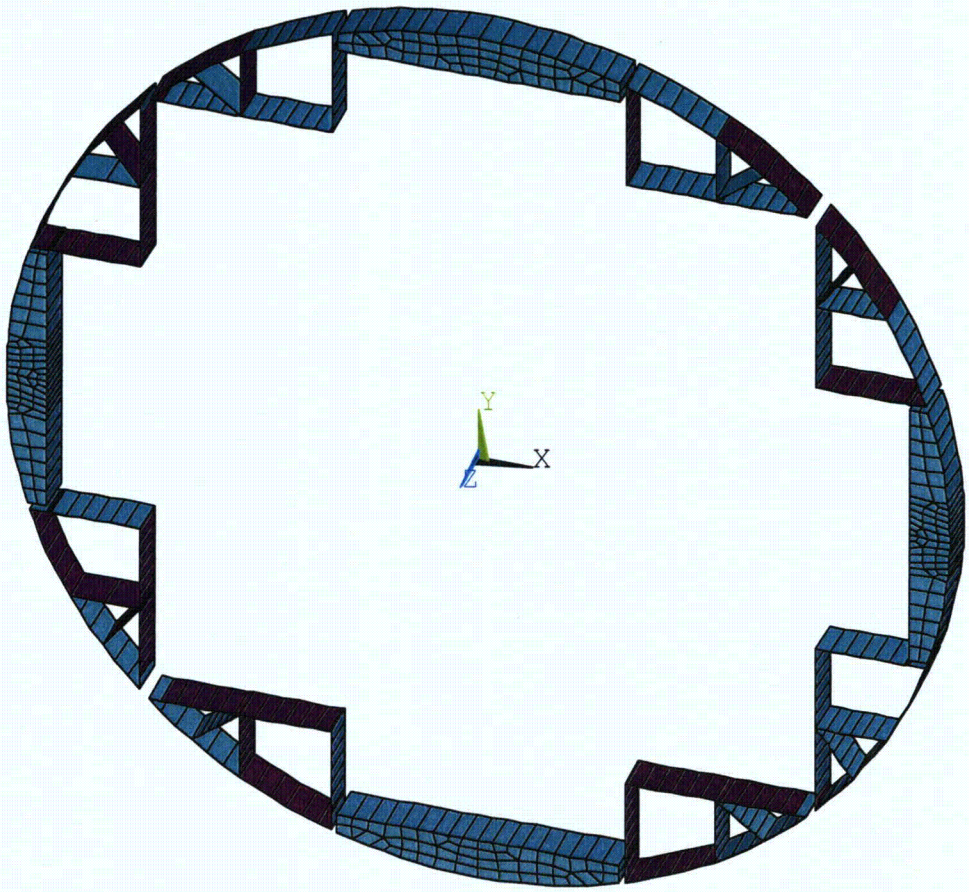

Figure T.3.7-71
Finite Element Model – Rails (Type 2 Basket)

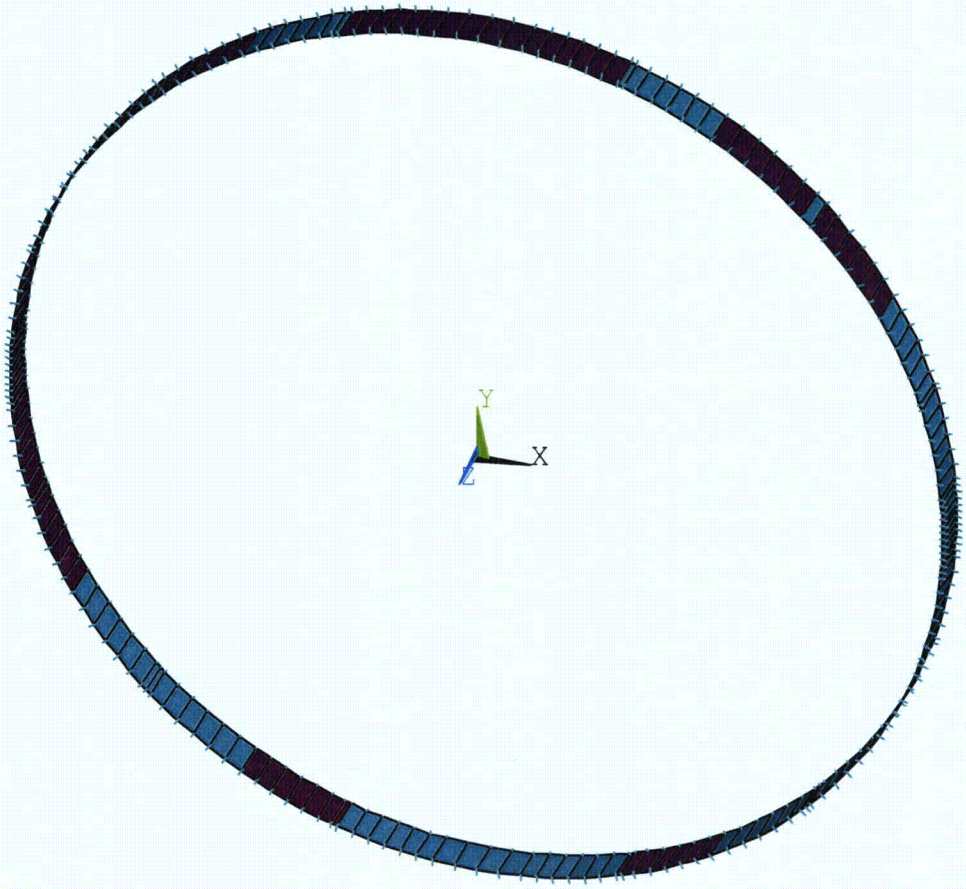

Figure T.3.7-72
Finite Element Model - Canister & Gaps

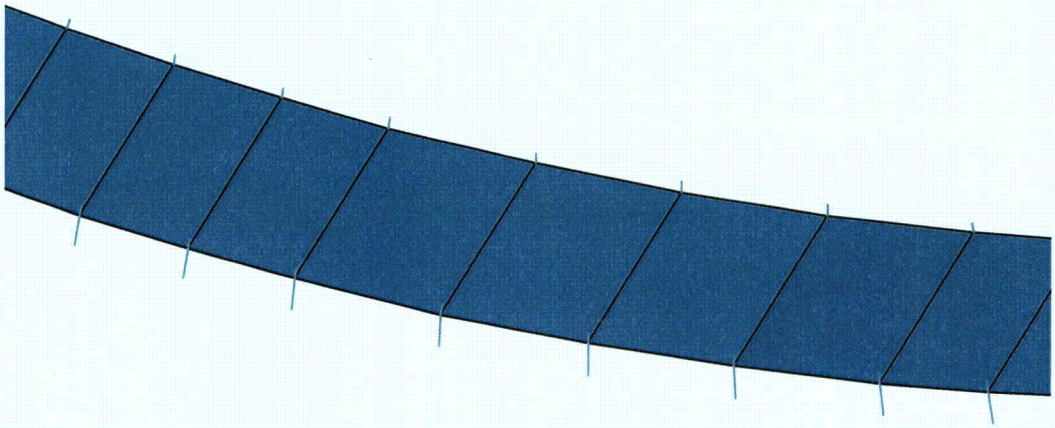

Figure T.3.7-73
Finite Element Model - Canister & Gaps (Enlarged View)

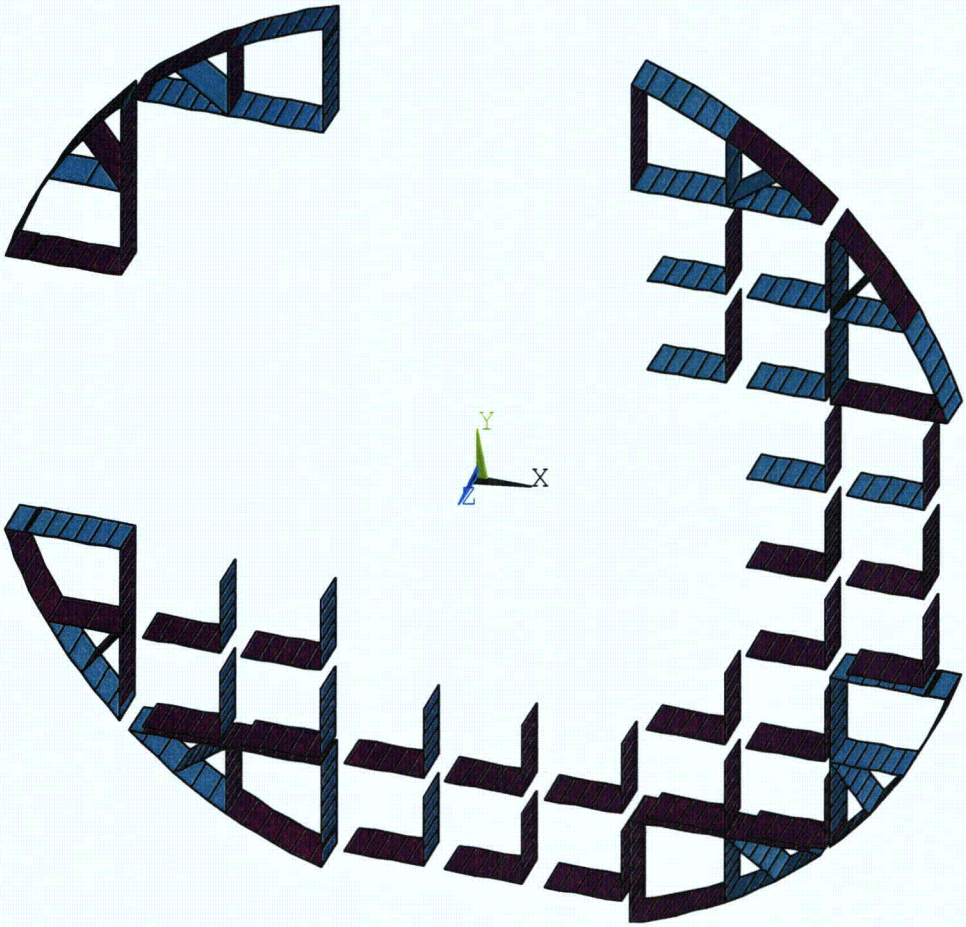

Figure T.3.7-74
Finite Element Model – Fuel Assembly Channel Plates

(Note: R45 basket rails are shown for reference only)

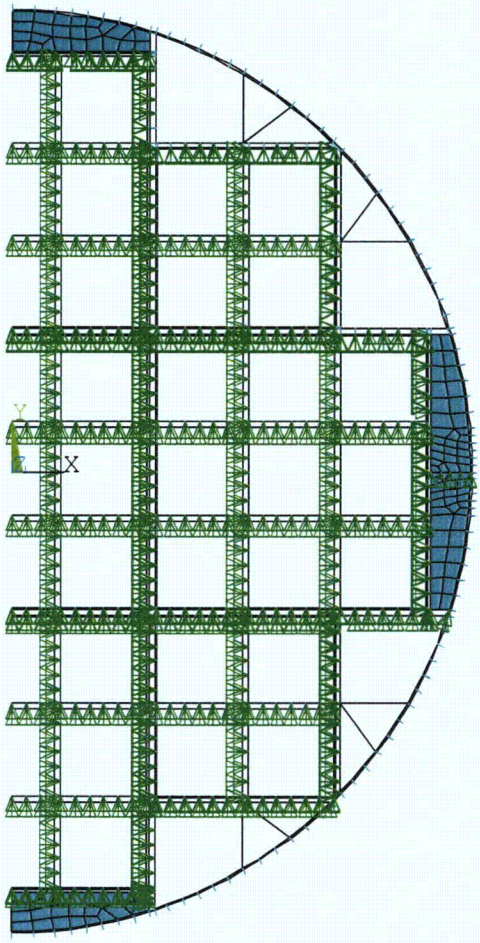

Figure T.3.7-75
0° Orientation - Couplings

(Type 2 shown, Type 1 is similar)

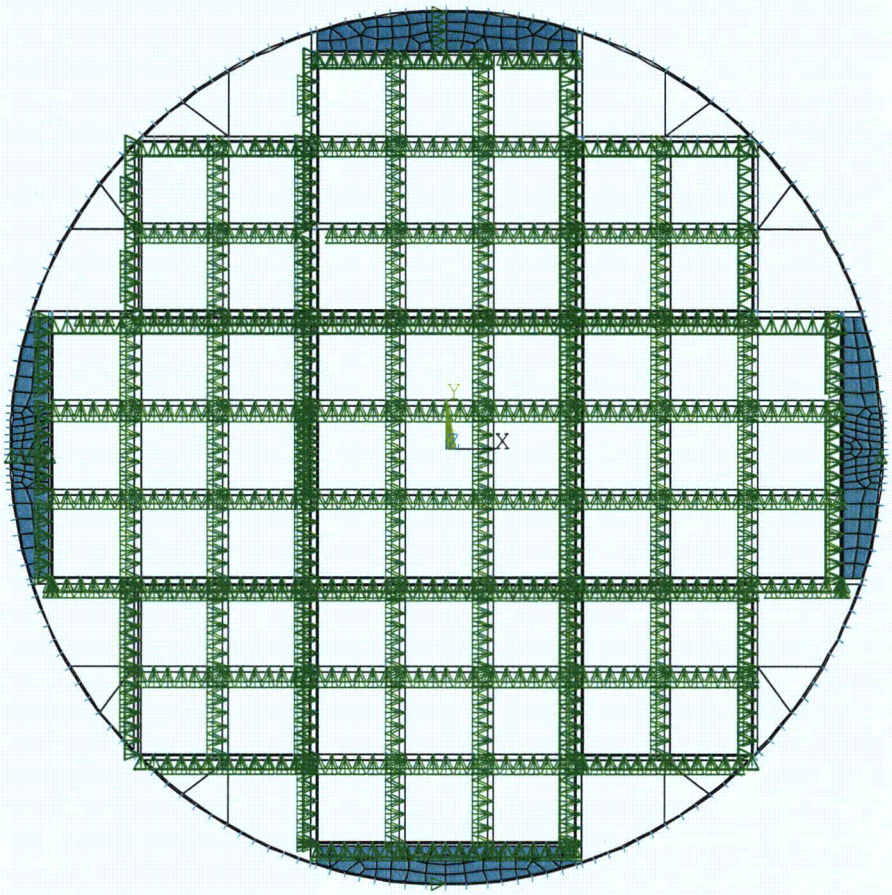

Figure T.3.7-76
30° Orientation - Couplings

(Type 2 shown, Type 1 is similar)

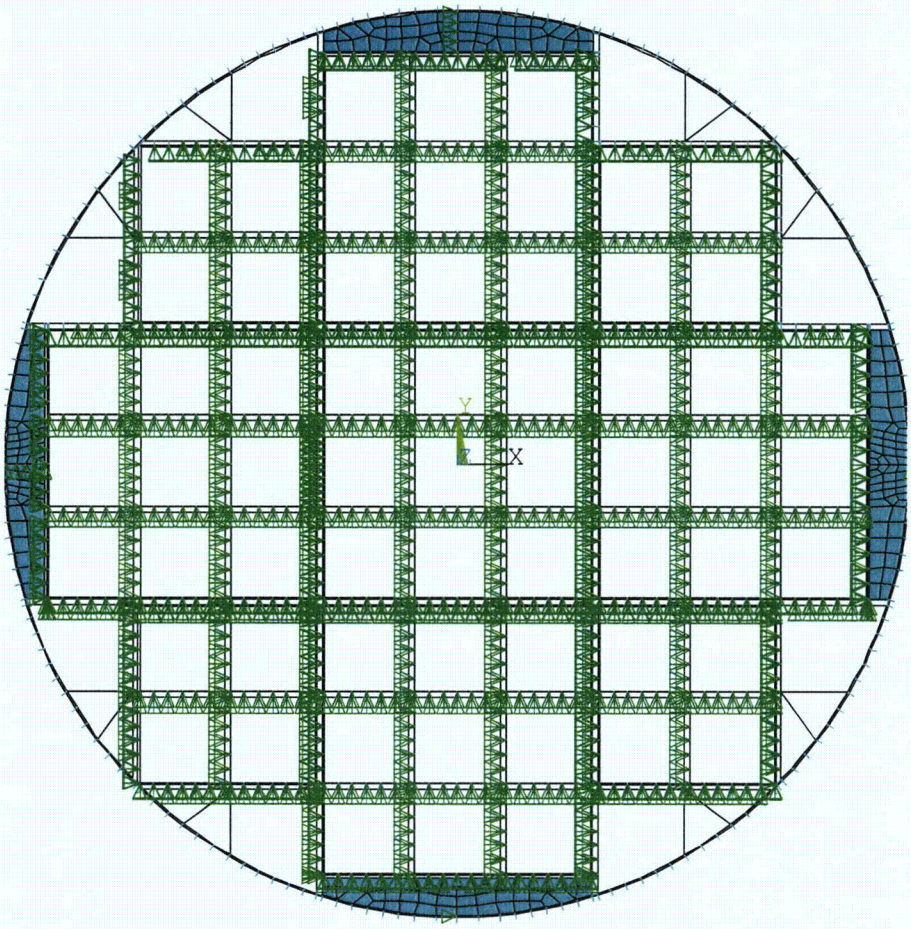

Figure T.3.7-77
45° Orientation - Couplings
(Type 2 shown, Type 1 is similar)

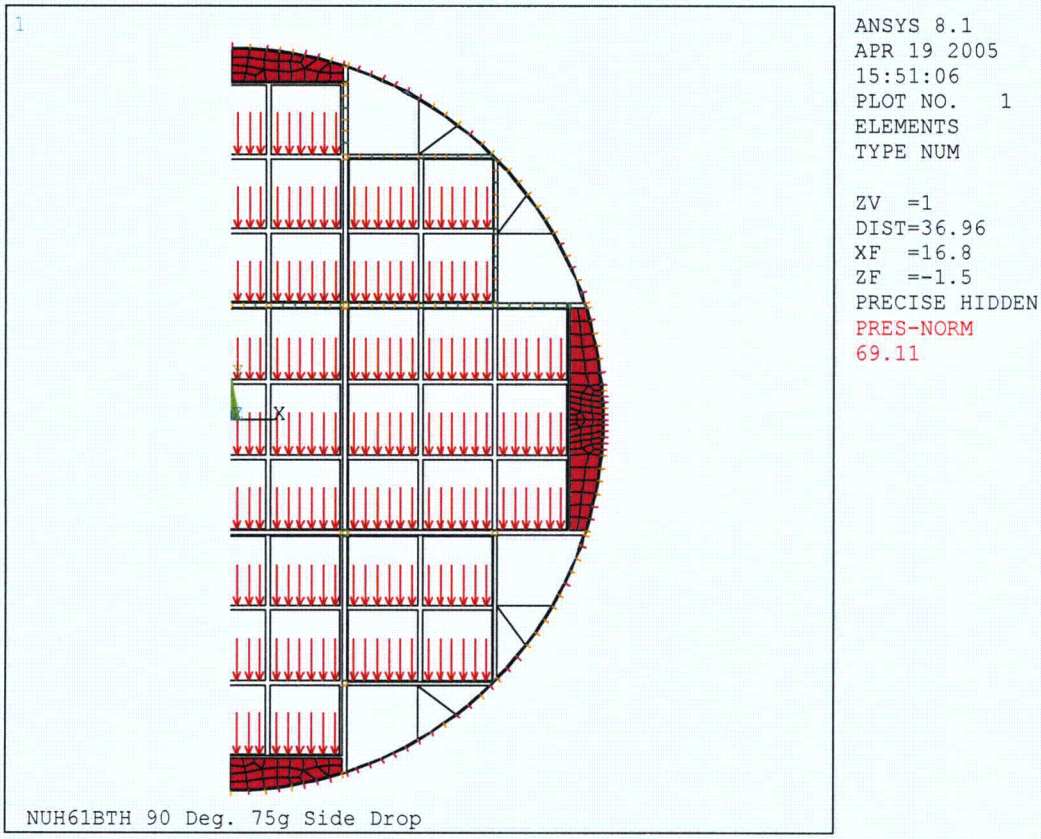

Figure T.3.7-78
0° Orientation – Loading Condition

(Type 2 shown, Type 1 is similar)

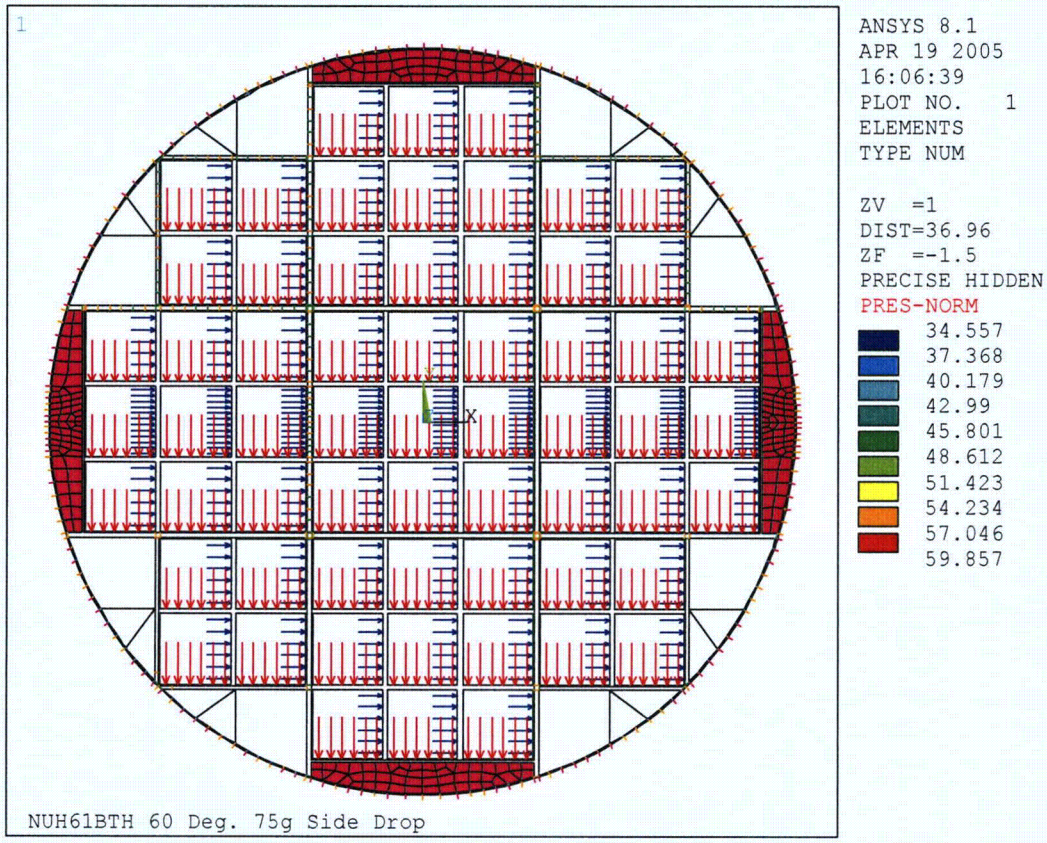

Figure T.3.7-79
30° Orientation – Loading Condition

(Type 2 shown, Type 1 is similar)

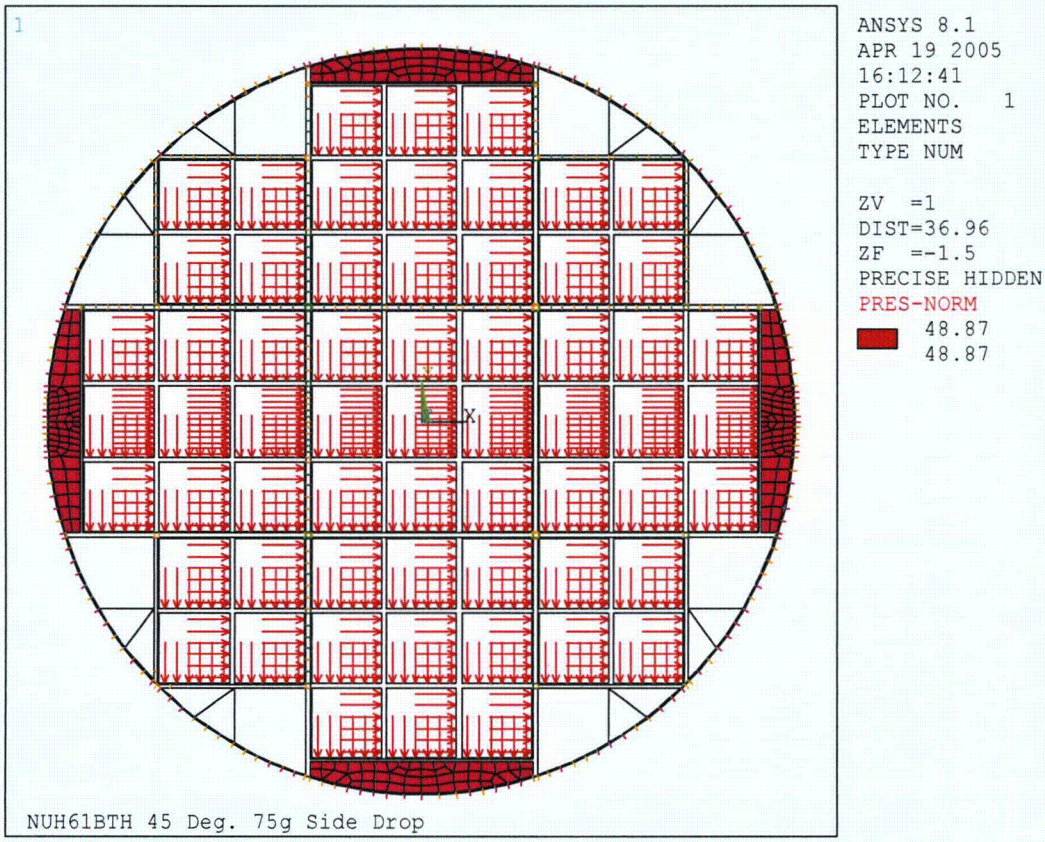

Figure T.3.7-80
45° Orientation – Loading Condition

(Type 2 shown, Type 1 is similar)

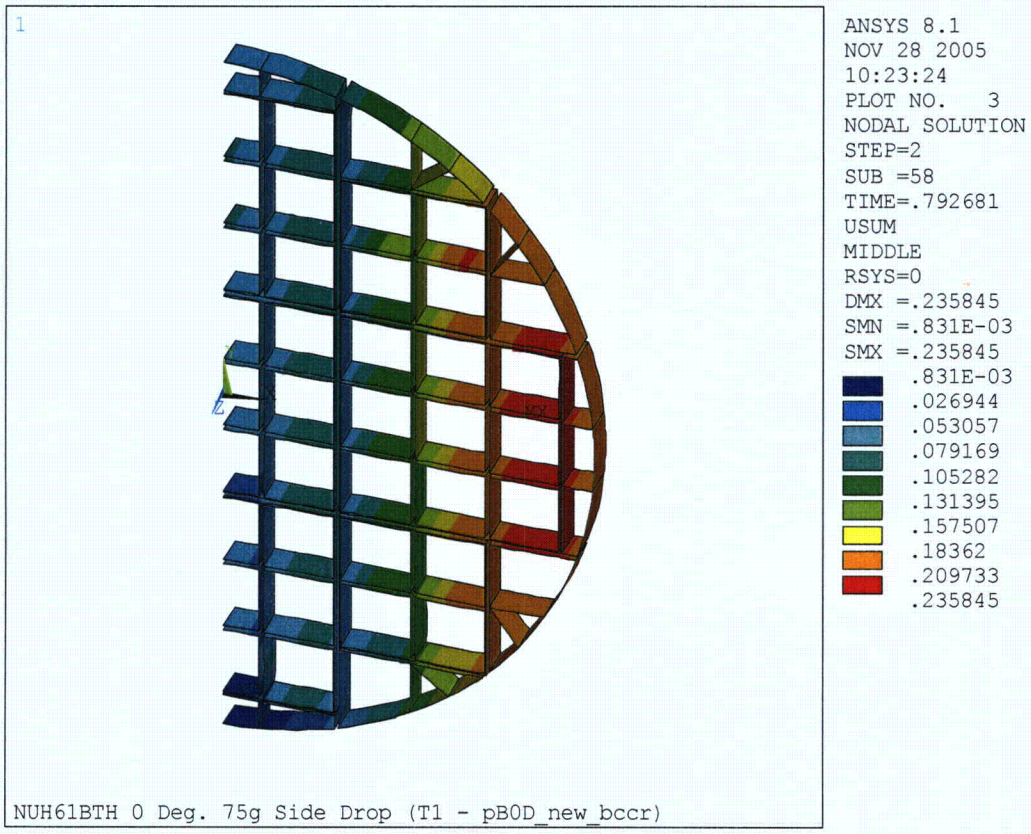

Figure T.3.7-81
Type 1 Basket 0° Side Drop – Last Converged Deformed Shape (79.27g)

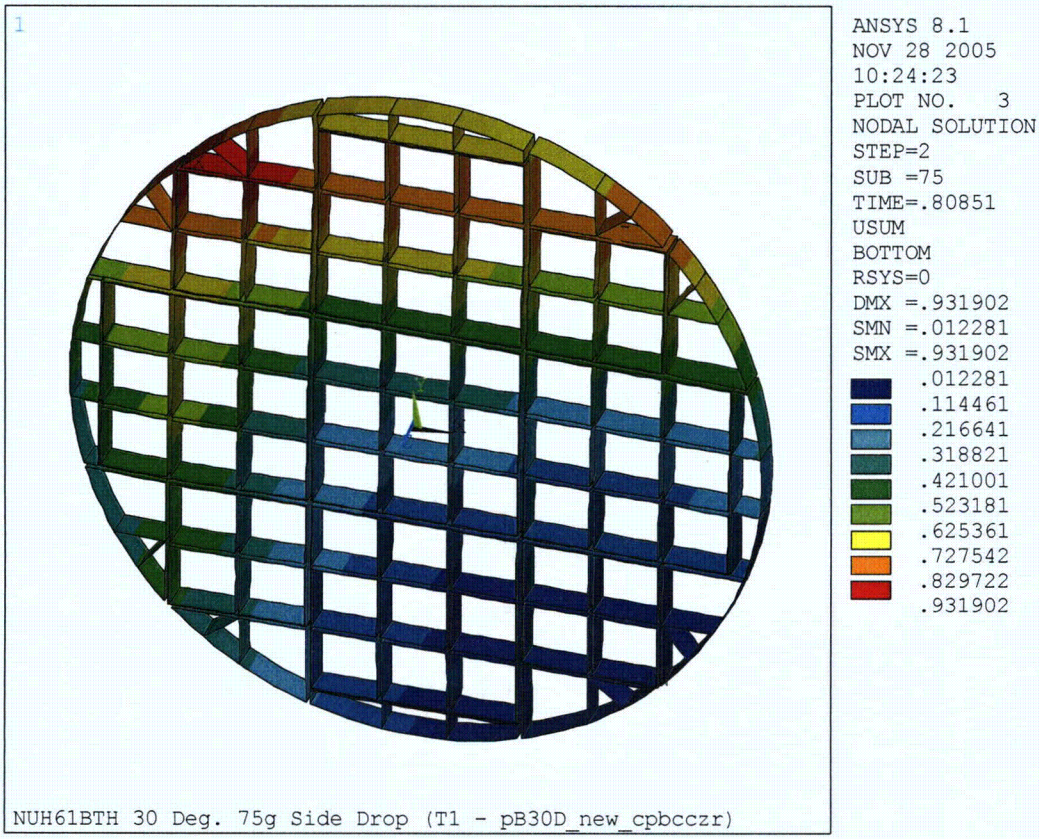

Figure T.3.7-82
Type 1 Basket 30° Side Drop – Last Converged Deformed Shape (80.85g)

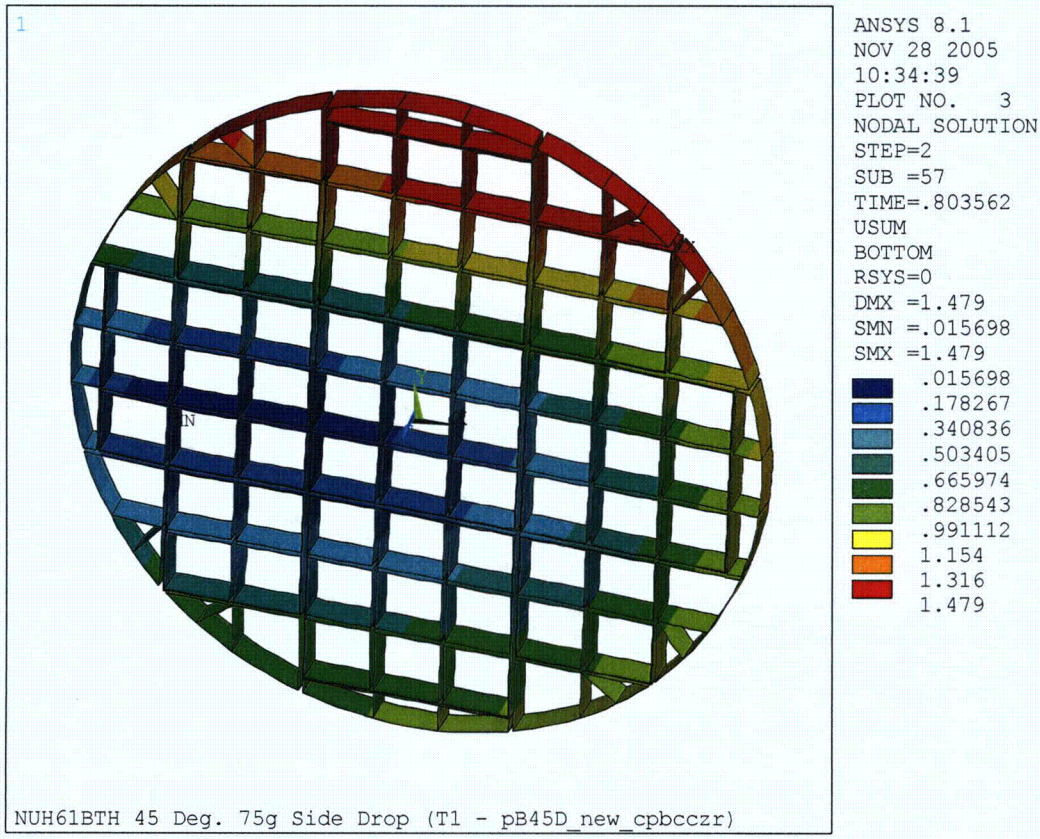

Figure T.3.7-83
Type 1 Basket 45° Side Drop – Last Converged Deformed Shape (80.36g)

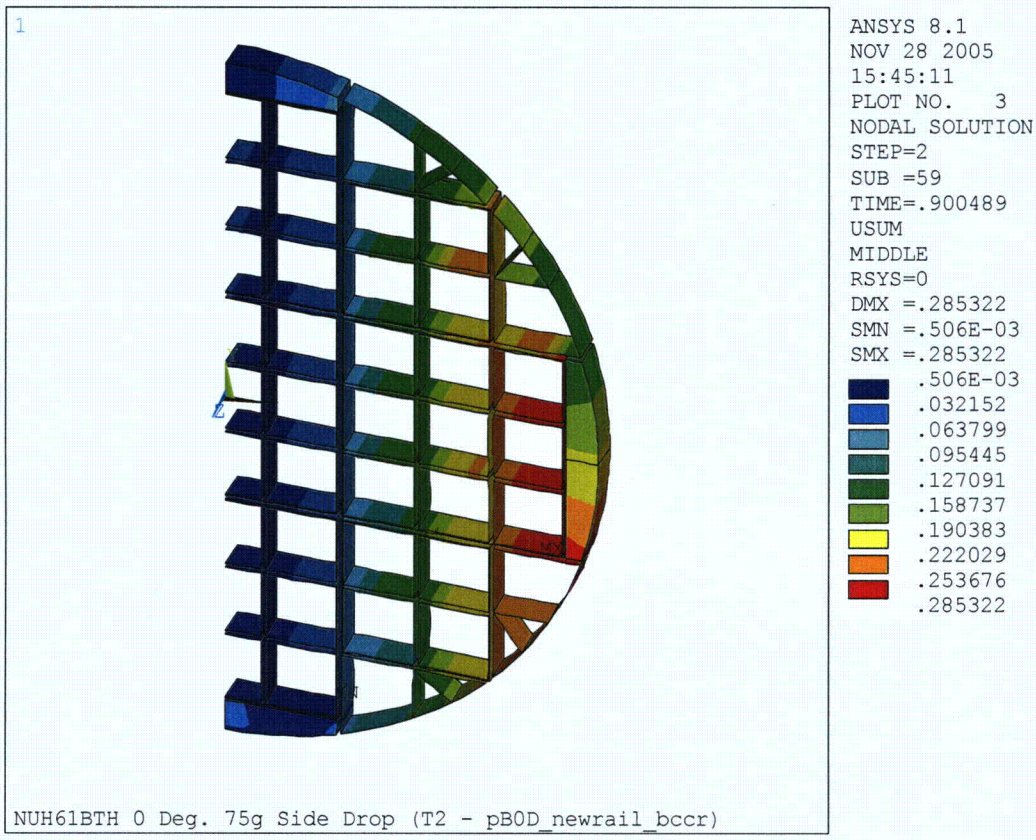

Figure T.3.7-84
Type 2 Basket 0° Side Drop – Last Converged Deformed Shape (90.05g)

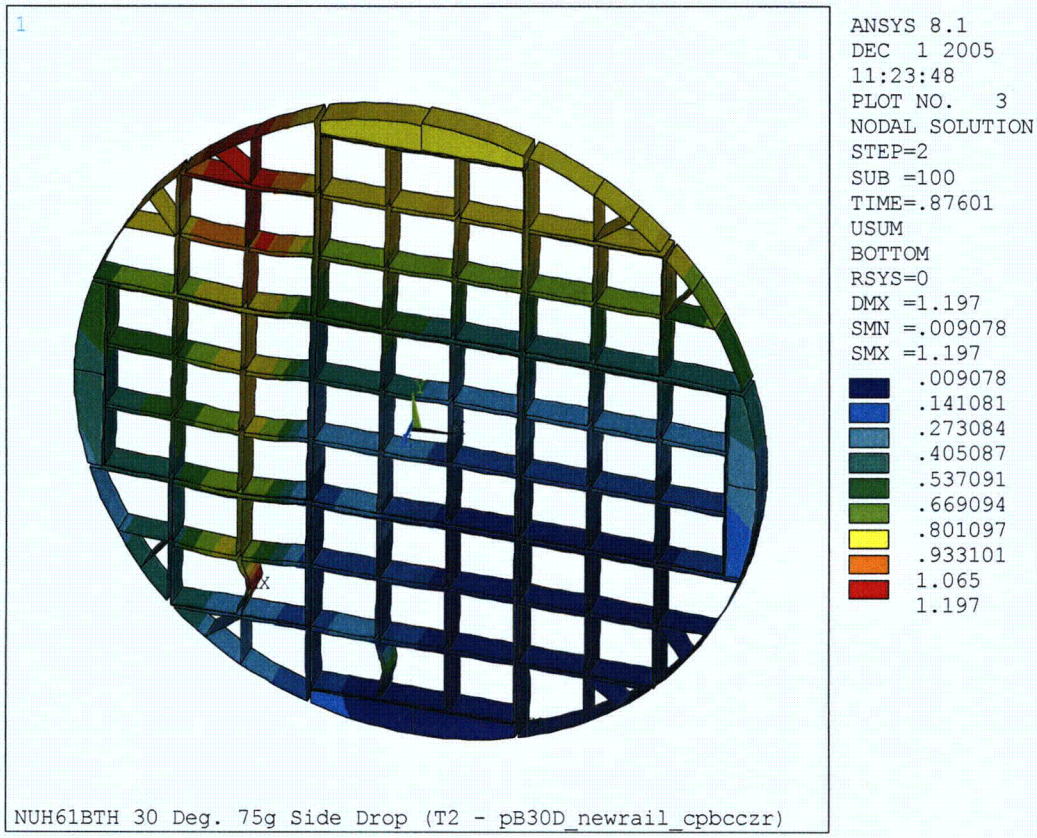

Figure T.3.7-85
Type 2 Basket 30° Side Drop – Last Converged Deformed Shape (87.60g)

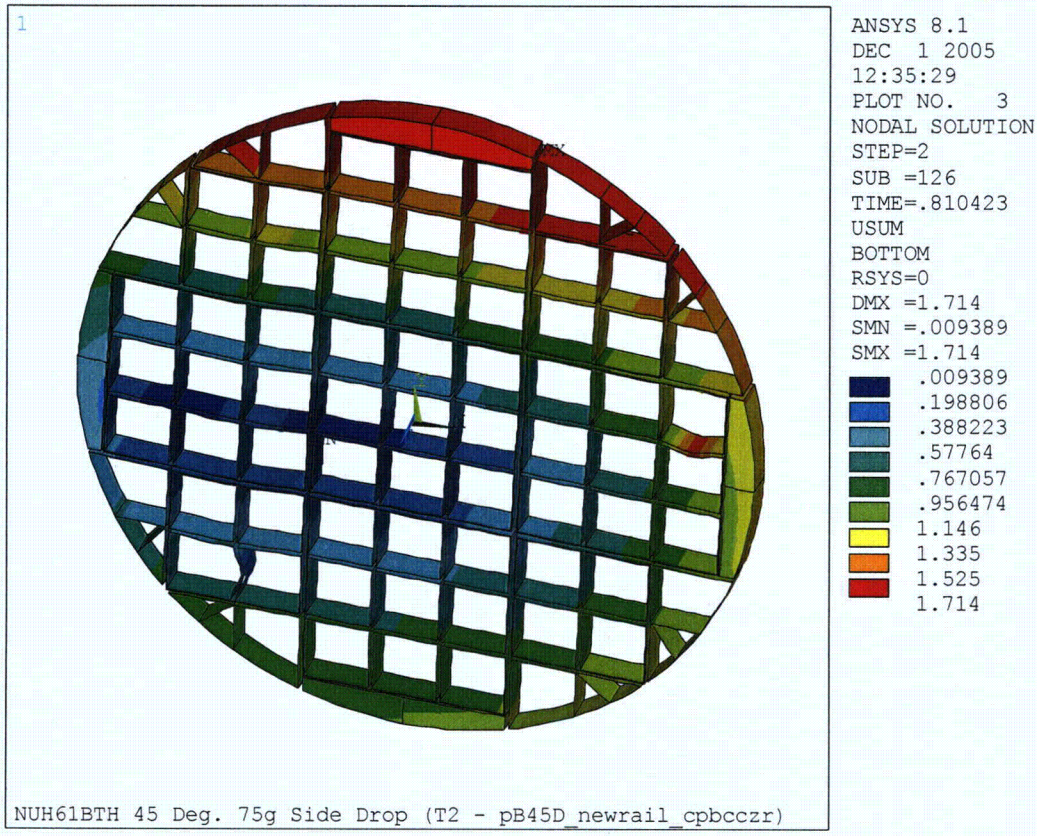

Figure T.3.7-86
Type 2 Basket 45° Side Drop – Last Converged Deformed Shape (81.04g)

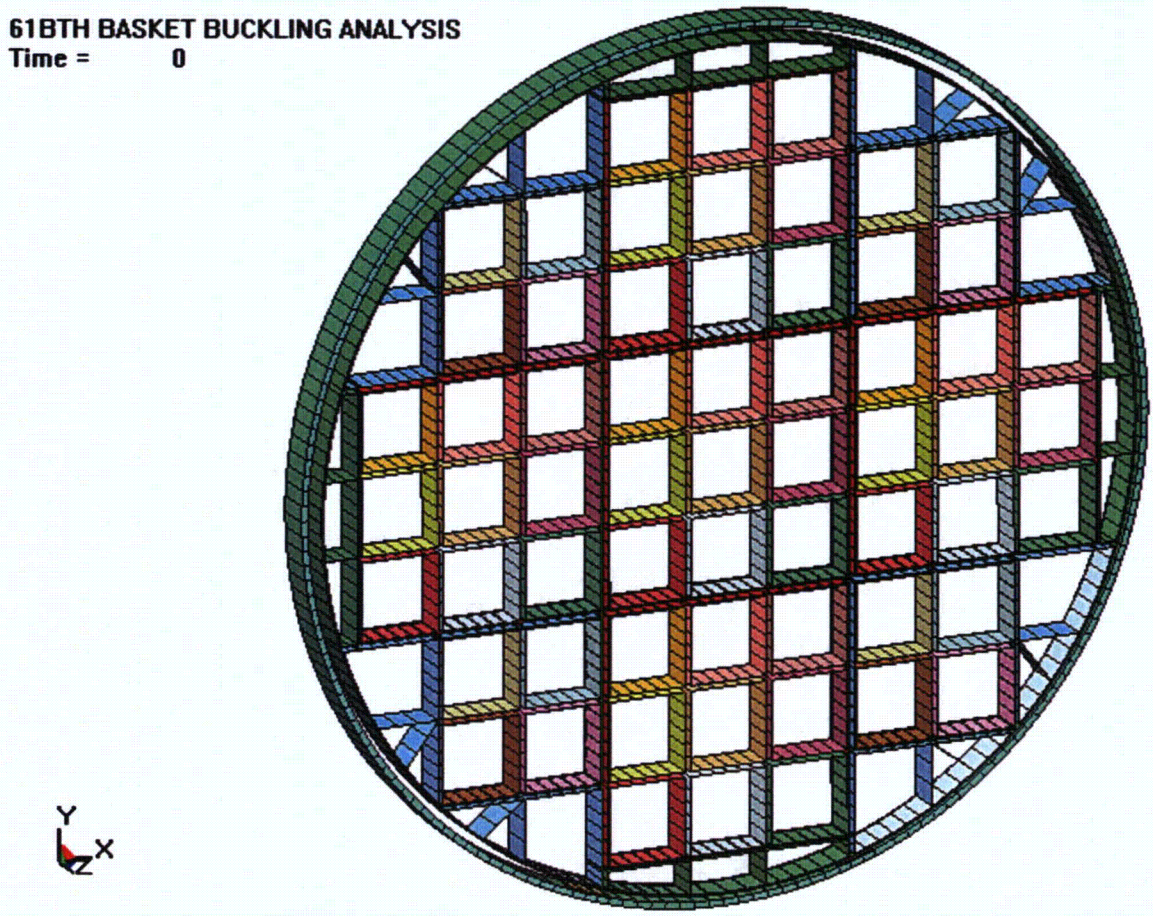

Figure T.3.7-87
NUHOMS®-61BTH, LS-DYNA Finite Element Model

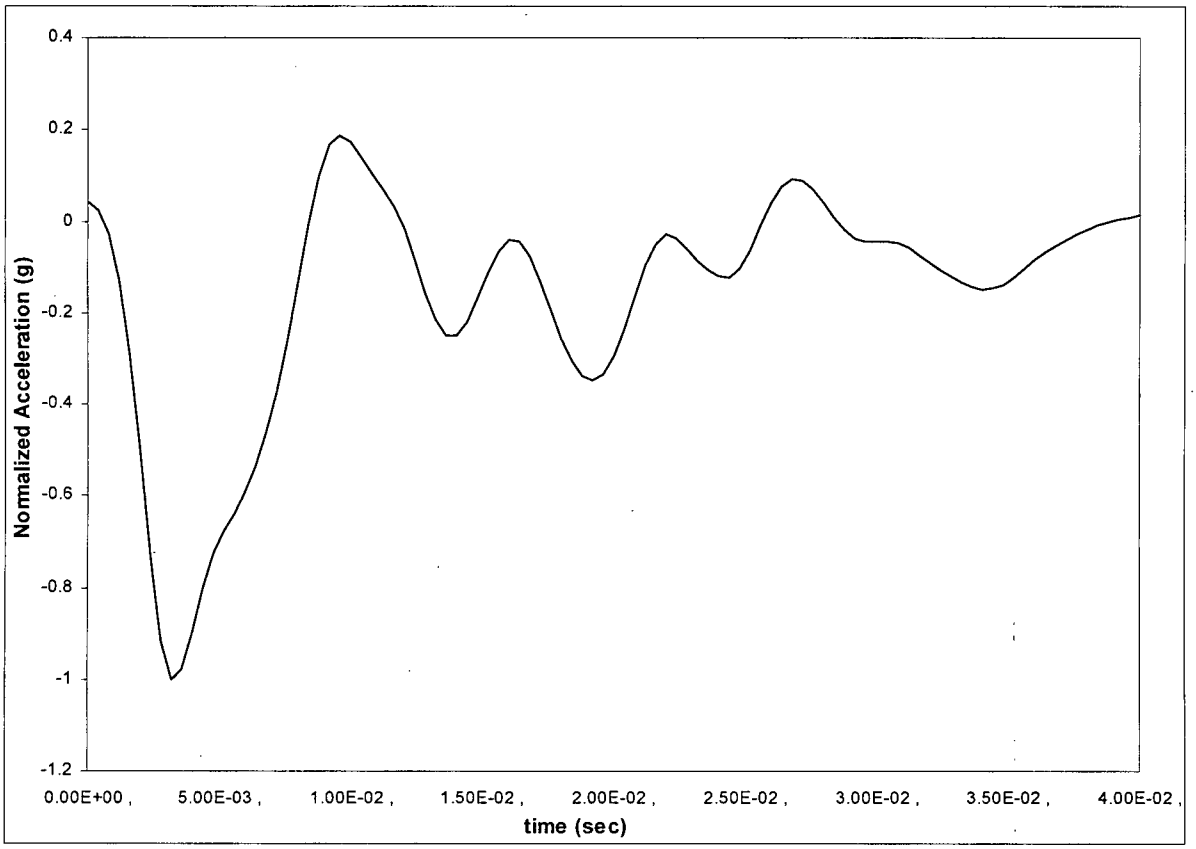

Figure T.3.7-88
Input Acceleration Time History

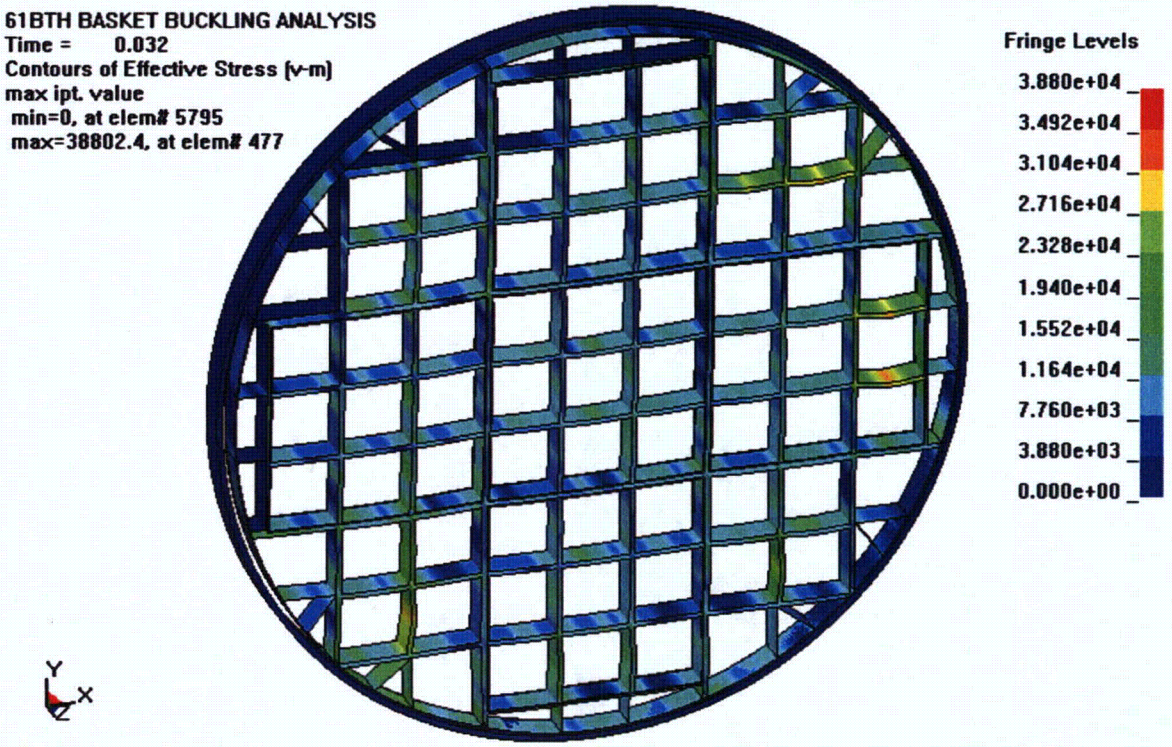

Figure T.3.7-89
Von-Mises Stress Distribution, 75g Peak Acceleration

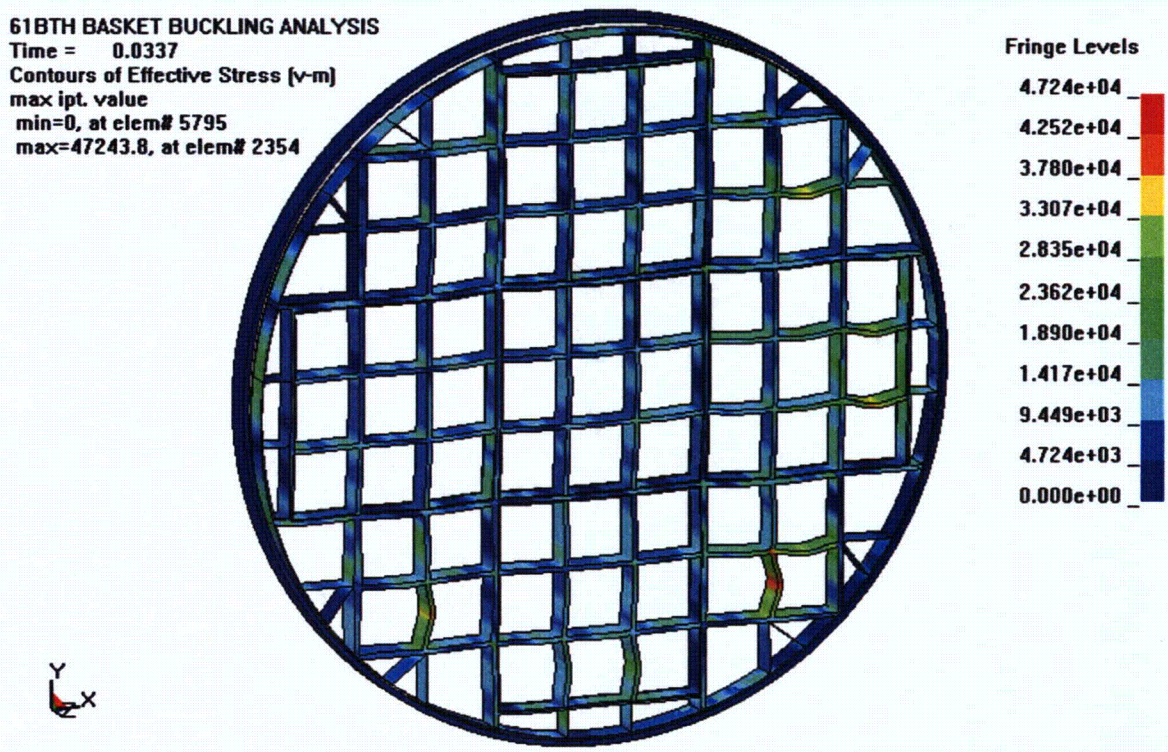

Figure T.3.7-90
Von-Mises Stress Distribution, 85g Peak Acceleration

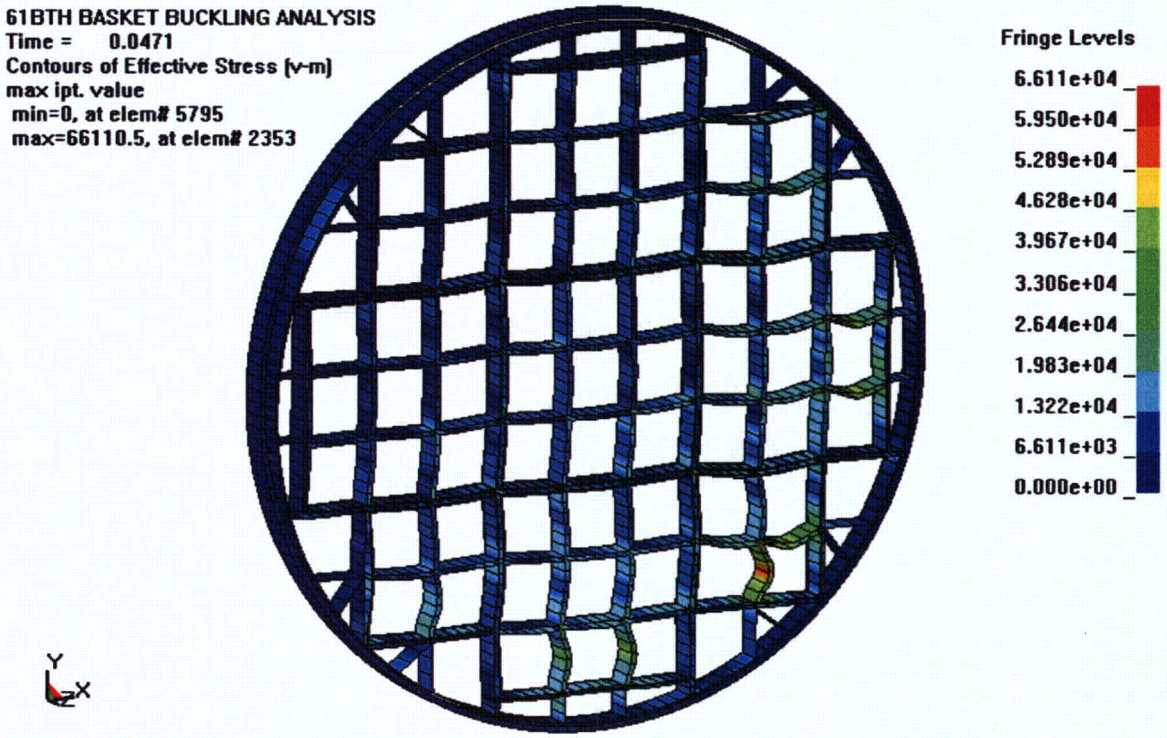

Figure T.3.7-91
Von-Mises Stress Distribution, 95g Peak Acceleration

T.3.8 References

3.1 American Society of Mechanical Engineers, ASME Boiler and Pressure Vessel Code, Section III, Subsections NB, NC, NF, NG, and Appendices 1998 Edition through 2000 Addenda.

3.2 American Society of Mechanical Engineers, ASME Boiler and Pressure Vessel Code, Section II, Part D, 1998 with 2000 Addenda.

3.3 NUREG/CR-0497, Rev. 2, "MATPRO-Version 11, A Handbook of Materials Properties for Use in the analysis of light Water Reactor Fuel Rod Behavior."

3.4 Brooks and Perkins, "Boral® Product Performance Report 624."

3.5 Pacific Northwest Laboratory Annual Report – FY 1979, "Spent Fuel and Fuel Pool Component Integrity," May 1980.

3.6 G. Wranglen, "An Introduction to Corrosion and Protection of Metals," Chapman and Hall, 1985, pp. 109-112.

3.7 A. J. McEvily, Jr., ed., "Atlas of Stress Corrosion and Corrosion Fatigue Curves," ASM Int'l, 1995, p. 185.

3.8 Baratta, et al. "Evaluation of Dimensional Stability and Corrosion Resistance of Borated Aluminum," Final Report submitted to Eagle-Pitcher Industries, Inc. by the Nuclear Engineering Department, Pennsylvania State University.

3.9 TNW letter 31-B9604-97-003 dated December 19, 1997 from Dave Dawson to Tim McGinty, NRC (Docket No. 72-1004).

3.10 "Hydrogen Generation Analysis Report for TN-68 Cask Materials," Test Report No. 61123-99N, Rev. 0, Oct 23, 1998, National Technical Systems.

3.11 ANSYS Engineering Analysis System, Users Manual for ANSYS Rev. 8.1, Swanson Analysis Systems, Inc., Houston, PA.

3.12 Roark, 5th Edition, "Formulas for Stress and Strain."

3.13 U.S. Nuclear Regulatory Commission (U.S. NRC), "Standard Format and Content for the Safety Analysis Report for an Independent Spent Fuel Storage Installation (Dry Storage)," Regulatory Guide 3.48 (Task FP-029-4), (October 1981).

3.14 American National Standard, "Design Criteria for an Independent Spent Fuel Storage Installation (Dry Storage Type)," ANSI/ANS 57.9-1984, American Nuclear Society, La Grange Park, Illinois (1984).

3.15 U.S. Atomic Energy Commission, "Damping Values for Seismic Design of Nuclear Power Plants," Regulatory Guide 1.61, (October 1973).

3.16 R. D. Blevins, "Formulas for Natural Frequency and Mode Shape," Van Nostrand Reinhold Co., New York, N.Y., (1979).

3.17 American Concrete Institute, Building Code Requirements for Reinforced Concrete (ACI 318-83) ACI, Detroit, MI (1983).

3.18 Manual of Steel Construction, American Institute of Steel Construction, 9th Edition, 1990.

3.19 NUHOMS® MP197 Transport Packaging Safety Analysis Report, USNRC Docket No. 71-9302.

3.20 W. F. Brown Jr. and J. E. Srawley, ASTM STP 410, 1966.

3.21 R. Chun, M. Witte, M. Schwartz, "Dynamic Impact Effects on Spent Fuel Assemblies", Lawrence Livermore National Laboratory, Report No. UCID-21246, October, 1987.

3.22 H. M. Chung, A. M. Garde, and T. F. Kassner, "Mechanical Properties of Zircaloy Containing Oxygen," Light-Water-Reactor Safety Research Program. Quarterly Progress Report, July-September 1975, Argonne National Laboratory, 1975, ANL 75-72, pp. 51-88.

3.23 T. J. Walker and J. N. Kass, "Variation of Zircaloy Fracture Toughness in Irradiation," Zirconium in Nuclear Applications, ASTM STP 551, ASTM, 1974, pp. 328-354.

3.24 Not used.

3.25 Spent Fuel Project Office, Interim Staff Guidance –1, "Damaged Fuel," November 2, 1998.

3.26 T. Sanders et al., A Method for Determining the Spent-Fuel Contribution to Transport Cask Containment Requirements, Sandia Report SAND90-2406, Sandia National Laboratories, Albuquerque, NM, 1992.

3.27 Methods for Impact Analysis of Shipping Containers, NUREG/CR-3966, UCID-20639, LLNL, 1987.

3.28 H. E. Adkins, Jr., B. J. Koeppel, and D. T. Tang, Spent Nuclear Fuel Structural Response when Subject to an End Impact Accident, PVP2004, San Diego, CA, July 25-29 2004.

3.29 K. J. Geelhood and C. E. Beyer, PNNL Stress/Strain Correlation for Zircaloy, March 2005.

3.30 Not Used.

3.31 L. F. Van Swam, A. A. Strasser, J. D. Cook, and J. M. Burger, Behavior of Zircaloy-4 and Zirconium Linear Zircaloy-4 Cladding at High Burnup, Proceedings of the 1997 International Topical Meeting on LWR Fuel Performance, Portland, Oregon March 2-6, 1997.

3.32 A. B. Johnson, Jr., E.R. Gilbert, Technical Basis for Storage of Zircaloy-Clad Spent Fuel in Inert Gases, PNL-4835, September 1983.

3.33 SCALE: A Modular Code System for Performing Standardized Computer Analyses for Licensing Evaluation, Vols. I-III, NUREG/CR-0200, Rev. 5 (ORNL/NUREG/CSD-2/R5), March 1997 (Standard Composition Library, Table M8.2.4).

3.34 R. W. Hertzberg, "Deformation and Fracture Mechanics of Engineering Material," John Wiley & Sons, New York, 1976.

3.35 Light-Water Reactor Safety Research Program: Quarterly Progress Report, July-September 1976, Section III, "Mechanical Properties of Zircaloy Containing Oxygen," Figures III-29—III-32, ANL 75-72, September 1975.

3.36 Chung, H. M., Yagger, F. L., and Kassner, T. F., "Fracture Behavior and Micro Structural Characteristics of Irradiated Zircaloy Cladding," Zirconium in the Nuclear Industry Seventh International Symposium, ASTM STP 939, R. B. Anderson and L. F. P. Van Swan, Eds., American Society for Testing and Materials, Philadelphia, 1987.

3.37 ANSI N14.5-1997, "Leakage Tests on Packages for Shipment."

3.38 NUHOMS® HD - Safety Analysis Report, CoC 1030

3.39 Fuketa, T., Sasajima, H., Mori, Y. and Ishijima, K., "Fuel Failure and Fission Gas Release in High Burnup PWR Fuels under RIA Conditions," Journal of Nuclear Material, 248, 1997.

3.40 Chung, H. M. and Kassner, T. F., "Cladding Metallurgy and Fracture Behavior During Reactivity-Initiated Accidents at High Burnup," Nuclear Engineering and Design, 186, 1998.

3.41 Edsigner, K., Davies, J. H. and Adamson, R. B., "Degraded Fuel Cladding Fractorgraphy and Fracture Behavior," Zirconium in the Nuclear Industry: Twelfth International Symposium, ASTM STP 1354, G. P. Sobal and G. D. Moan, Eds., American Society for Testing and Materials, West Conshohocken, PA., 2000.

3.42 Garde, A. M., "Effect of Irradiation and Hydriding on the Mechanical Properties of Zircaloy- 4 at High Fluence," Zirconium in the Nuclear Industry: Eighth International Symposium, ASTM STP 1023, L. F. P. Van Swam and C. M. Eucken, Eds., American Society for Testing and Materials, Philadelphia, 1989.

3.43 Erbacher, F. J. and Leistikow, S., "Zircaloy Fuel Cladding Behavior in a Loss-of – Coolant Accident, A Review," Zirconium in the Nuclear Industry: Seventh International

Symposium, ASTM STP 939, R. B. Adamson and L. F. P. Swam, Eds., American Society for Testing and Materials, Philadelphia, 1987.

3.44 Kuroda, M., et al., "Influence of Precipitated Hydride on the Fracture Behavior of Zircaloy Fuel Cladding Tube," Journal of Nuclear Science and Technology, Vol. 37, No. 8, August 2000.

3.45 "The Stress Analysis of Cracks Handbook" Third Edition by Hiroshi Tada et al., ASME press.

3.46 A. Machiels, EPRI Report, "Fracture Toughness Data for Zirconium Alloys Application to Spent Fuel Cladding in Dry Storage", 1001281, January 2001.

3.47 R. W. Hertzberg," Deformation and Fracture Mechanics of Engineering Material" John Wiley & Sons, New York, 1976.